

# Lawrence Berkeley National Laboratory

## Recent Work

### Title

NONLINEAR OPTICS OF SURFACES AND ADSORBATES

### Permalink

<https://escholarship.org/uc/item/5kg6g9n1>

### Author

Heinz, T.F.

### Publication Date

1982-11-01

e.2



# Lawrence Berkeley Laboratory

UNIVERSITY OF CALIFORNIA

## Materials & Molecular Research Division

NONLINEAR OPTICS OF SURFACES AND ADSORBATES

Tony F. Heinz  
(Ph.D. Thesis)

November 1982

RECEIVED  
LAWRENCE  
BERKELEY LABORATORY

FEB 9 1983

LIBRARY AND  
DOCUMENTS SECTION

### TWO-WEEK LOAN COPY

*This is a Library Circulating Copy  
which may be borrowed for two weeks.  
For a personal retention copy, call  
Tech. Info. Division, Ext. 6782.*



LBL-15255  
e.2

## DISCLAIMER

This document was prepared as an account of work sponsored by the United States Government. While this document is believed to contain correct information, neither the United States Government nor any agency thereof, nor the Regents of the University of California, nor any of their employees, makes any warranty, express or implied, or assumes any legal responsibility for the accuracy, completeness, or usefulness of any information, apparatus, product, or process disclosed, or represents that its use would not infringe privately owned rights. Reference herein to any specific commercial product, process, or service by its trade name, trademark, manufacturer, or otherwise, does not necessarily constitute or imply its endorsement, recommendation, or favoring by the United States Government or any agency thereof, or the Regents of the University of California. The views and opinions of authors expressed herein do not necessarily state or reflect those of the United States Government or any agency thereof or the Regents of the University of California.

NONLINEAR OPTICS OF SURFACES AND ADSORBATES

Tony F. Heinz

Department of Physics  
University of California  
Berkeley, California 94720

and

Materials and Molecular Research Division  
Lawrence Berkeley Laboratory  
Berkeley, California 94720

NOVEMBER 1982

Ph. D. Thesis

This work is partially supported by the Director, Office of Energy Research, Office of Basic Energy Sciences, Materials Sciences Division of the U.S. Department of Energy under Contract Number DE-AC03-76SF00098.

# NONLINEAR OPTICS OF SURFACES AND ADSORBATES

Tony Frederick Heinz

## ABSTRACT

In any material possessing a center of inversion, the process of optical second-harmonic generation (SHG) is forbidden within the electric-dipole approximation. As a consequence, the second-harmonic (SH) radiation produced by the excitation of two adjoining centrosymmetric media can arise largely from the few atomic layers of the interfacial region where the symmetry prevailing in the bulk is broken. This thesis presents a series of experiments exploring the influence of molecular adsorbates on SHG from such interfaces and evaluating the potential of this process as a surface-specific optical probe.

Studies have been conducted on adsorption onto both metallic and insulating substrates. Formation of the first monolayer of AgCl on a silver electrode induced a 20-fold increase in SH output. Similar results have been observed for adsorbed pyridine and pyrazine molecules. Consideration is given to the origin of these nonlinearities, particularly that associated with the adsorption of the centrosymmetric pyrazine species. In situ measurements of the equilibrium and transient behavior of pyridine adsorption on silver in an electrochemical environment have been made by means of SHG. The roughened silver samples used in these investigations produce unusually strong SH signals. A general formalism for treating the enhancement in the local electromagnetic fields found at such surfaces is elaborated and a comparison with experimental results is presented.

For the case of molecules adsorbed on smooth, insulating substrates,

the SHG technique has been extended along two lines, taking advantage of the spectral and tensorial properties of the nonlinearity of the interface. The former yields spectroscopic data on the adsorbate; the latter gives information on the adsorbate orientation. With a tunable pump laser, the position and lineshape of the  $S_0 \rightarrow S_2$  electronic transition in rhodamine dye molecules adsorbed on fused silica have been recorded. The polarization dependences, which are specified by the tensor elements of the nonlinear susceptibility, proved helpful in the construction of a model of adsorption geometry. By a more refined experimental procedure and theoretical analysis, the orientation of p-nitrobenzoic acid adsorbed at a solid/liquid interface has also been determined from measurements of the SHG.

L. R. J. van

## ACKNOWLEDGEMENTS

I am indebted to my advisor, Professor Y. R. Shen, for his guidance and support during the course of my thesis research. He has set for me a high standard of clarity of thought and expression, as well as of graciousness in unhesitatingly putting aside his own work to help to solve any problem troubling me.

It is a pleasure to express my gratitude to three very able and amiable collaborators. Chenson Chen and Daniel Ricard kindly let me join their on-going effort and provided me with a model of organization and proper experimental technique. More recently, Harry Tom has been an active, innovative, and thoroughly enjoyable coworker of mine.

All of the members of Professor Shen's group have been generous in sharing both their knowledge and their equipment with me. I should particularly like to mention Ralph Page and Steve Durbin, each of whom has provided an unreasonably large amount of quite unreciprocated aid. I have also benefited from discussions of certain theoretical questions with visiting Professors Peixian Ye and Jose Leite.

My heartfelt thanks are extended to Rita Jones. Rita has contributed to this thesis not only through her impeccable typing, but also through her enduring good cheer.

My progress in graduate school has been furthered by fellowships from the National Science Foundation and from the IBM Corporation, which I gratefully acknowledge. This work was partially supported by the Director, Office of Energy Research, Office of Basic Energy Sciences, Materials Sciences Division of the U.S. Department of Energy under Contract Number DE-AC03-76SF00098.

## TABLE OF CONTENTS

	PAGE
I. Introduction	1
References	6
II. Second-Harmonic Generation at Surfaces	8
A. General Considerations	8
B. Models of the Nonlinear Response	15
C. Experimental Work	21
References	24
Figure Captions	26
Figures	27
III. Second-Harmonic Generation of Adsorbates on Metal Surfaces	29
A. Detection of Molecular Monolayers by Second-Harmonic Generation	29
B. Application: Equilibrium and Transient Study of Pyridine Adsorption	39
C. Centrosymmetric Adsorbate: Pyrazine	44
References	50
Figure Captions	53
Figures	56
IV. Second-Harmonic Generation of Adsorbates on Insulating Surfaces	68
A. Theoretical Considerations	68
B. Study of Rhodamine Dyes Adsorbed on Fused Silica	72
C. Study of p-Nitrobenzoic Acid Adsorbed on Fused Silica	81
References	97



	Page
Tables	99
Figure Captions	101
Figures	102
V. Conclusion and Extensions	110
Appendix I: Electrodynamics of a Polarized Sheet	113
A. Boundary Conditions	113
B. Radiated Fields	116
Figure Caption	118
Figure	119
Appendix II: Surface Enhancement and Local-Field Effects	120
A. Introduction	120
B. Theory of Local-Field Enhancement	121
C. Surface Enhancement of Raman Scattering and SHG	133
D. Concluding Remarks	138
References	142
Figure Caption	146
Figure	147
Appendix III: Counting Statistics	148

## I. INTRODUCTION

Optical techniques have certain features that make them very desirable as probes of the physics and chemistry of interfaces. With modern laser technology, one can obtain energy resolution down to a fraction of a  $\mu\text{eV}$  and temporal resolution on the scale of a psec. Furthermore, in contrast to most of the commonly used methods for the study of surfaces in ultrahigh vacuum, optical processes can generally be employed for interfaces between two dense media. This property permits the investigation of a wide class of interesting and important problems which are difficult to approach by other means.<sup>1</sup>

The relatively weak interaction of light with the materials systems that allows one to probe interfaces between two dense media tends, however, to entail a low sensitivity to the few layers of atoms or of molecules comprising the interface itself. Various schemes have been devised for augmenting the signal from the interface in optical scattering processes. In order to set the stage for a treatment of second-order optical nonlinearities at interfaces, the subject of this thesis, we shall consider briefly other developments in the application of optical probes to the study of interfaces. The most straightforward approach to enhancing the signal from the interface is simply to increase the effective surface area available. Dispersed systems, which are, in fact, of considerable industrial significance, may provide sufficient surface area for direct infrared absorption measurements of the vibrational spectra of adsorbates.<sup>2</sup> For metallic surfaces, multiple reflections between two parallel sample planes can serve a similar purpose.<sup>3</sup> The interaction of a laser beam with a surface can also be increased by

arranging for the light to fall on the sample at grazing incidence. In certain cases, this permits one to obtain vibrational spectra of adsorbed species from a single flat interface.<sup>4</sup> Surface plasmons<sup>5</sup> at interfaces with a metal and other types of guided waves<sup>6</sup> in appropriate dielectric media have proved helpful in obtaining large surface signals as well. Such surface waves can increase both the intensity of the electromagnetic fields and the length of the interaction region.

A different task consists in concentrating on decreasing the background signal from the bulk media, thus highlighting the weaker surface signal. This idea is embodied in the widely applied method of ellipsometry.<sup>7</sup> The technique can be viewed as a means of canceling the signal from the bulk by a crossed polarizer and can provide a high degree of sensitivity for behavior at the interface. Ellipsometry, which finds particular use in the study of thin films, is suitable only for optically flat interfaces. The difficulties associated with the strong reflections from metal substrates in absorption measurements of vibrational spectra can be circumvented by monitoring not the reflected light from an external source, but the blackbody radiation from the sample itself. This method of emission spectroscopy is still in the early stages of development.<sup>8</sup> Hybrid optical techniques, such as optoacoustic spectroscopy<sup>9</sup> and bolometry,<sup>10</sup> also show promise as surface probes.

During the past few years, researchers have begun to exploit nonlinear optical processes for the study of interfaces. The majority of the work has been concerned with the third-order or Raman-type nonlinearity. As a rule, the signals arising from spontaneous Raman scattering by adsorbates in low dispersion systems are too weak to be useful.

For certain systems, most notably those with a roughened silver surface, the local electric fields at the interface can, however, be amplified. This phenomenon of surface-enhanced Raman scattering can lead to an increase in the intensity of Raman-scattered light by several orders of magnitude, greatly facilitating detection. In the absence of any special surface-enhancement mechanism, the intrinsic Raman cross-section can be increased by means of excitation in resonance with electronic transitions in the molecule. Such resonant Raman scattering has been applied to study adsorption at interfaces in electrochemical environments.<sup>11</sup> A different scheme for increasing Raman signals is based on stimulating the scattering process by exposing the scatterer to light at both the pump and Raman-shifted frequencies. While the technique of Raman-gain spectroscopy<sup>12,13</sup> requires sophisticated equipment and is subject to problems of spurious signals, it does have adequate sensitivity for measurements of vibrational spectra of adsorbates at monolayer coverages.<sup>14,15</sup> Moreover, this coherent scattering process presents attractive possibilities for time-resolved measurements.<sup>16,17</sup> An alternative method of obtaining vibrational spectra is to detect the coherent anti-Stokes Raman scattering under the same type of excitation. Although potential problems from background signals and laser-induced damage remain, this widely used form of nonlinear spectroscopy<sup>18</sup> appears to have adequate sensitivity for studies of adsorbed monolayers.<sup>19</sup>

The subject of this thesis is the physics of the second-order non-linearity at interfaces and its applications as a probe of interfacial structure, composition, and behavior. In contradistinction to the optical probes enumerated above (all of which are based on linear or on

third-order nonlinear effects), scattering by a second-order nonlinearity can exhibit a remarkable intrinsic sensitivity to the interface itself. The origin of this surface sensitivity lies in the property that second-order nonlinear processes are (dipole) forbidden in media possessing a center of inversion. Thus, for the case of an interface between two centrosymmetric media, the signals from second-order nonlinearities may arise predominantly from the narrow boundary region in which the symmetry of the bulk media is broken. For this reason, the second-order nonlinear optical effects of sum- and difference-frequency generation may share the high degree of surface sensitivity of the probes relying on the emission, absorption or scattering of massive particles, the standard tools for studies of surfaces in ultrahigh vacuum.<sup>20</sup>

The work presented in this dissertation deals primarily with the influence of molecular adsorbates on the second-harmonic generation (SHG) process at an interface. Following a general discussion of SHG at surfaces of centrosymmetric media (Ch. II), we consider SHG by metallic surfaces in the presence of adsorbates. A series of experiments investigating molecular adsorption on a roughened silver sample in an electrochemical cell have been performed. Chapter III, Sec. A presents experimental results on SHG by the silver surface overlaid by noncentrosymmetric adsorbates. In particular, the easily discernible second-harmonic (SH) signal from adsorbed pyridine permitted a study of the dynamical and equilibrium behavior of the adsorption process (Sec. B). We have also investigated the change in SHG induced by the adsorption of a centrosymmetric species. As described in Sec. C, adsorbed pyrazine strongly affects the SHG by the interface, indicative of a symme-

try-lifting pyrazine/silver interaction. In all of these measurements on roughened silver surfaces, an enhancement of a few orders of magnitude in the SH intensity relative to that of a smooth surface was observed. This effect can be understood as the consequence of the strong electric fields present near resonant protrusion on the silver surface. A general analysis of this phenomenon and its effect for various optical processes is given in Appendix II. Experimental results are compared with the predictions of model calculations.

The studies of adsorption on silver surfaces underscore the surface sensitivity of SHG. In the fourth chapter, the potential of SHG as a surface probe is further developed. It is shown that with a transparent substrate exhibiting no particular surface enhancement, SHG by molecular adsorbates (even at submonolayer coverages) is readily detectable. In the experiment of Sec. B on monolayers of adsorbed rhodamine dyes, spectroscopic information is obtained by scanning the input at the fundamental frequency so as to pass through a resonance with a molecular transition at the harmonic frequency. At resonance the nonlinear polarizability tensor of the adsorbate assumes a particularly simple form and partial specification of the orientation of the adsorbed species can be inferred from the polarization dependences of the SHG process. In the following section, the orientation of a p-nitrobenzoic acid adsorbed on a fused silica substrate is deduced by a more refined application of the SHG technique. The concluding chapter is a brief review of the work and presents some direct extensions thereof.

## References:

1. The macroscopic methods of physical chemistry can be applied to the study of such interfaces. See A. W. Adamson, Physical Chemistry of Surfaces, 3rd ed. (Wiley, New York, 1976).
2. L. H. Little, Infrared Spectra of Adsorbed Molecules (Academic Press, New York, 1966).
3. R. G. Greenler, J. Chem. Phys. 50, 1963 (1969).
4. R. G. Greenler, J. Chem. Phys. 44, 310 (1966).
5. Y. J. Chabal and A. J. Sievers, Phys. Rev. Lett. 44, 944 (1980).
6. J. F. Raboit, R. Santo, N. E. Schlotter, and J. D. Swalen, IBM J. Res. Develop. 26, 209 (1982).
7. R. M. A. Azzam and N. M. Bashara, Ellipsometry and Polarized Light (North Holland, Amsterdam, 1972).
8. D. L. Allara, D. Teicher, and J. F. Durana, Chem. Phys. Lett. 84, 20 (1981).
9. F. Träger, T. J. Chuang, and H. Coufal, "Surface Photoacoustic Spectroscopy," presented at the Third International Conference on Vibrations at Surfaces (1982).
10. R. B. Barley, T. Iri, and P. L. Richards, Surf. Sci. 100, 626 (1980).
11. R. P. Van Duyne, J. Physique 38 C5, 239 (1977).
12. A. Owyong, IEEE J. Quantum Electron. QE-14, 192 (1978).
13. B. F. Levine, C. V. Shank, and J. P. Heritage, IEEE J. Quantum Electron. QE-15, 1418 (1979).
14. J. P. Heritage and D. L. Allara, Chem. Phys. Lett. 74, 507 (1980).
15. B. F. Levine, C. G. Bethea, A. R. Tretola, and M. Korngor, Appl. Phys. Lett. 37, 595 (1980).

16. J. P. Heritage, Appl. Phys. Lett. 34, 470 (1979).
17. J. P. Heritage, J. G. Bergman, A. Pinczuk, and J. M. Worlock, Chem. Phys. Lett. 67, 229 (1979).
18. P. D. Maker and R. W. Terhune, Phys. Rev. 137, A801 (1965); R. F. Begley, A. B. Harvey, and R. L. Byer, Appl. Phys. Lett. 25, 387 (1974).
19. C. K. Chen, A. R. B. de Castro, Y. R. Shen, and F. DeMartini, Phys. Rev. Lett. 43, 946 (1979).
20. G. A. Somorjai, Chemistry in Two Dimensions: Surfaces (Cornell Univ. Press, Ithaca, 1981), Ch.2.



## II. SECOND-HARMONIC GENERATION AT SURFACES

### A. General Considerations

#### 1. Nonlinear Source Polarization

In the presence of strong optical fields of a laser, the nonlinear response of the material system to the electromagnetic waves can be significant. Characterizing the linear response of the medium by a local, isotropic dielectric constant  $\epsilon$  and a magnetic permeability  $\mu = 1$ , we can write the wave equation including a (generalized) nonlinear source polarization  $\vec{P}^{\text{NLS}}$  as<sup>1</sup>

$$\vec{\nabla} \times \vec{\nabla} \times \vec{E}(\vec{r}, \omega_i) - \epsilon(\omega_i) (\omega_i/c)^2 \vec{E}(\vec{r}, \omega_i) = 4\pi (\omega_i/c)^2 \vec{P}^{\text{NLS}}(\vec{r}, \omega_i), \quad (1a)$$

subject to

$$\nabla \cdot \epsilon(\omega_i) \vec{E}(\vec{r}, \omega_i) = -4\pi \vec{\nabla} \cdot \vec{P}^{\text{NLS}}(\vec{r}, \omega_i). \quad (1b)$$

These relations apply for each Fourier component at angular frequency  $\omega_i$ . Appropriate boundary conditions at interfaces can be determined by a careful integration of these equations at the discontinuity. Just as is the case for most problems in linear optics, we usually need only consider a local relation between the nonlinear polarization  $\vec{P}^{\text{NLS}}$  and the electric fields of the various waves. For the second-order nonlinearity, the source polarization at frequency  $\omega$  then takes the form:<sup>2</sup>

$$\vec{P}^{\text{NLS}}(\omega) = \chi^{(2)}(\omega = \omega_1 + \omega_2) : \vec{E}(\omega_1) \vec{E}(\omega_2), \quad (2)$$

with an implicit summation over all frequencies  $\omega_1$  and  $\omega_2$  satisfying  $\omega_1 + \omega_2 = \omega$ . The numerical value of the second-order nonlinear susceptibility  $\chi^{(2)}$  depends on the exact relation between the Fourier amplitudes and the real, time-dependent quantities. Here the convention  $\vec{E}(t) = \vec{E}(\omega)e^{-i\omega t} + \vec{E}^*(\omega)e^{+i\omega t}$  will be adopted. Higher-order nonlinearities can, of course, be expressed by successive terms in an expansion analogous to that of Eq. (2).

Inspection of Eq. (2) reveals that the second-order nonlinear susceptibility  $\chi^{(2)}$  must be a third-rank tensor with even parity under inversion. Consequently, in a medium with a center of inversion,  $\chi^{(2)} = 0$  obtains.<sup>3</sup> The assumption of a local response of the nonlinear polarization to the applied fields is only an approximation. The lowest-order correction to include nonlocal behavior can be expressed quite generally as

$$P_i^{\text{NLS}}(\omega) = \chi_{\text{nonloc}}^{(2)}(\omega = \omega_1 + \omega_2) : \vec{E}(\omega_1) \vec{\nabla} \vec{E}(\omega_2). \quad (3)$$

The coefficient  $\chi_{\text{nonloc}}^{(2)}$  representing this nonlocal quadratic nonlinearity of the medium is now a fourth-rank tensor. For centrosymmetric media, it is no longer the case that the nonlinear response vanishes in this approximation. If we consider a centrosymmetric medium which also has cubic symmetry, we readily deduce that  $\chi_{\text{nonloc}}^{(2)}$  has just four independent elements for SHG. The  $i$ -th component of the nonlinear polarization takes the form:

$$P_i^{\text{NLS}}(2\omega) = (\delta - \beta - 2\gamma) [\vec{E}(\omega) \cdot \vec{\nabla}] E_i(\omega) + \beta E_i(\omega) [\vec{\nabla} \cdot \vec{E}(\omega)]$$

$$+ \gamma \nabla_{\mathbf{i}} [\vec{E}(\omega) \cdot \vec{E}(\omega)] + \zeta E_{\mathbf{i}}(\omega) \nabla_{\mathbf{i}} E_{\mathbf{i}}(\omega). \quad (4a)$$

$\beta$ ,  $\gamma$ ,  $\delta$ , and  $\zeta$  are (frequency-dependent) parameters characterizing the medium. By application of Maxwell's equations, we can transform the previous expression into

$$\begin{aligned} P_{\mathbf{i}}^{\text{NLS}}(2\omega) = & (\delta - \beta) [\vec{E}(\omega) \cdot \vec{\nabla}] E_{\mathbf{i}}(\omega) + \beta E_{\mathbf{i}}(\omega) [\nabla \cdot \vec{E}(\omega)] \\ & + (2i\omega/c) \gamma [\vec{E}(\omega) \times \vec{B}(\omega)]_{\mathbf{i}} + \zeta E_{\mathbf{i}}(\omega) \nabla_{\mathbf{i}} E_{\mathbf{i}}(\omega). \end{aligned} \quad (4b)$$

Only the last term in these expressions is not compatible with isotropy, since it clearly does not transform as a vector under an arbitrary rotation. Thus, for this higher symmetry, we can write the nonlinear source polarization as

$$\begin{aligned} \vec{P}^{\text{NLS}}(2\omega) = & (\delta - \beta) [\vec{E}(\omega) \cdot \vec{\nabla}] \vec{E}(\omega) + \beta \vec{E}(\omega) [\vec{\nabla} \cdot \vec{E}(\omega)] \\ & + (2i\omega/c) \gamma [\vec{E}(\omega) \times \vec{B}(\omega)]. \end{aligned} \quad (5)$$

In fact, no experiment has yet been performed on a centrosymmetric material medium with cubic symmetry for which the additional anisotropic behavior of the  $\zeta$  term in Eq. (4) has been identified.<sup>4</sup>

Let us discuss briefly the nature of the various contributions to the nonlinear polarization of Eq. (5). For an arbitrary excitation of an inhomogeneous medium, all of the terms should be significant. In a homogeneous medium, however, the second term,  $\vec{E}(\omega) [\vec{\nabla} \cdot \vec{E}(\omega)]$ , must always vanish by Gauss's law. The first member of the equation will van-

ish as well under excitation by a single plane wave  $[\vec{E}(\omega) \propto e^{i\vec{k}\cdot\vec{r}}]$ .

The third term still survives, but the induced polarization is oriented along the propagation direction of the fundamental wave. Such a longitudinal polarization cannot produce a growing, propagating wave in the medium, but at the discontinuity of a surface it can radiate. In a homogeneous, isotropic medium with inversion symmetry, this magnetic-dipole term will be the only contribution to the bulk polarization for excitation by a plane wave. Under a general excitation, say by two plane waves, both the  $\vec{E} \times \vec{B}$  and  $[\vec{E} \cdot \vec{\nabla}]\vec{E}$  sources can be present.

The lowest-order nonlocal terms for the polarization are typically suppressed relative to the local response (if not symmetry-forbidden) by a factor of  $ka$ , where  $k$  is the wavevector of the light and  $a$  is an atomic dimension. For optical excitation, this implies that the SHG of a single layer of atoms with broken inversion symmetry should be comparable to the bulk signal from  $\sim 10^3$  unperturbed layers. It is therefore important to consider the behavior of the surface region carefully in order to understand the SHG process fully. The situation for SH reflection contrasts markedly with that for linear reflection, for which the response of the surface atoms is overwhelmed by the (dipole-allowed) polarization in the bulk.

The inversion symmetry of the bulk must of necessity be lifted at the surface of the medium or at the interface between two media. For this interfacial region, we then expect an electric-dipole contribution to the second-order nonlinearity. We can define a surface susceptibility tensor to relate the electric fields (either just inside or just outside of the medium) to the total source polarization of the surface. For SHG by the surface of cubic or higher symmetry, the three indepen-

dent components of this third-rank tensor  $S_{\chi}^{\leftrightarrow(2)}$  are  $S_{\chi_{\perp\parallel\parallel}}^{(2)}$ ,  $S_{\chi_{\parallel\perp\parallel}}^{(2)} = S_{\chi_{\parallel\parallel\perp}}^{(2)}$ , and  $S_{\chi_{\perp\perp\perp}}^{(2)}$ . We expect to experience very rapidly changing electric fields at the interface. In classical optics, for example, one models the normal component of the electric field as changing discontinuously to preserve the continuity of  $\epsilon E_{\perp}$ . It then follows that nonlocal contributions to the surface current will be significant for variations perpendicular to the surface.<sup>5</sup> We can, nonetheless, incorporate all of the contributions to the surface current in the coefficient  $S_{\chi}^{\leftrightarrow(2)}$ . We thereby neglect the nonlocality in the transverse direction, a reasonable approximation for optical excitation.

In summary, let us consider the description of two adjoining centrosymmetric materials. We can divide the system into two parts: an interfacial zone and the remaining bulk media. The interfacial zone is taken to be sufficiently large to include all of the material in which the inversion symmetry is broken, as well as the entire region in which strong field gradients are present. Since this transition zone is still far less thick than an optical wavelength, we are justified in treating the induced nonlinear polarization as a sheet. In this case, the nonlinearity can be described by the surface susceptibility tensor  $S_{\chi}^{\leftrightarrow(2)}$ . Away from the boundary, the lowest-order nonlocal terms are sufficient to characterize the nonlinear response. Thus, for two neighboring media that are homogeneous, isotropic, and centrosymmetric in the bulk, we can express the nonlinear source polarization as<sup>6</sup>

$$\begin{aligned} \vec{P}^{\text{NLS}}(2\omega) = & S_{\chi}^{\leftrightarrow(2)} : \vec{E}(\omega) \vec{E}(\omega) \delta(z) + (\delta_1 - \beta_1 - 2\gamma_1) (\vec{E}(\omega) \cdot \vec{\nabla}) \vec{E}(\omega) \\ & \times \theta(-z) + \gamma_1 \vec{\nabla} [\vec{E}(\omega) \cdot \vec{E}(\omega)] \theta(-z) + (\delta_2 - \beta_2 - 2\gamma_2) \end{aligned}$$

$$\times (\vec{E}(\omega) \cdot \vec{\nabla}) \vec{E}(\omega) \theta(z) + \gamma_2 \vec{\nabla} [\vec{E}(\omega) \cdot \vec{E}(\omega)] \theta(z). \quad (6)$$

In this relation, subscripts 1 and 2 refer to the two different media; their boundary defines the plane of  $z = 0$ .  $\delta(z)$  and  $\theta(z)$  denote the usual delta and step functions.

## 2. Radiated Fields

Having established the form of the nonlinear source polarization for the system of interest, we can proceed to derive the SH radiation fields from Maxwell's equations. We first solve for the fields at the fundamental frequency, overlooking the weak effect of nonlinearities. The source terms for the harmonic polarization are then determined by Eq. (6), and the SH fields follow from the wave equation of formula (1). The excitation of a semi-infinite nonlinear medium by a plane wave causes reflected and transmitted harmonic beams to be created. If  $\vec{k}_{\parallel}(\omega)$  represents the transverse component of the wavevector of the pump wave, the two harmonic beams have directions specified by  $\vec{k}_{\parallel}(2\omega) = 2\vec{k}_{\parallel}(\omega)$ . In general, the dispersion in the linear dielectric constants implies that the SH waves will not propagate in the same directions as the transmitted and reflected waves at the fundamental frequency. This effect is minimal for experiments conducted in air, but can be significant in more highly dispersive materials.

We give here an explicit expression for the SH radiation produced in medium 1 by the nonlinear source polarization of Eq. (6). Media 1 and 2 have linear dielectric constants of  $\epsilon_1$  and  $\epsilon_2$ , while the interfacial layer is assigned a dielectric constant of  $\epsilon'$ . For a system excited by the linearly polarized plane wave  $\vec{E}(\omega)e^{i\vec{k}^{(1)} \cdot \vec{x}}$ , we obtain harmonic fields:

$$\begin{aligned}
E_p(2\omega) = & i32\pi E^2(\omega)\epsilon_1(\omega)k^{(1)}(2\omega)k_x(\omega)[k_z^{(1)}(\omega)]^2B^{-2}(\omega)B^{-1}(2\omega)\cos^2\phi \times \\
& \times \left\{ [k_x^2(\omega)k_o^{-2}(\omega)][a_2^2(\omega)a_2(2\omega)S_{\chi_{\perp\perp\perp}}(2) - a_2(2\omega)S_{\chi_{\perp\parallel\parallel}}(2) + a_1^{-1}(2\omega) \times \right. \\
& \times (a_1^{-2}(\omega) - 1)\gamma_1] + [\epsilon_2(\omega) + \epsilon_1^{-1}(\omega)A^{-2}(\omega)B^2(\omega)\tan^2\phi][a_2(2\omega) \times \\
& \times S_{\chi_{\perp\parallel\parallel}}(2) + a_1^{-1}(2\omega)\gamma_1 - a_2^{-1}(2\omega)\gamma_2] - [k_z^{(2)}(\omega)k_z^{(2)}(2\omega)k_o^{-2}(\omega)] \times \\
& \times [a_2(\omega)S_{\chi_{\parallel\perp\perp}}(2)] \tag{7a}
\end{aligned}$$

$$\begin{aligned}
E_s(2\omega) = & i128\pi E^2(\omega)k^{(1)}(\omega)k_x(\omega)[k_z^{(1)}(\omega)]^2A^{-1}(\omega)B^{-1}(\omega)A^{-1}(2\omega)\cos\phi \sin\phi \times \\
& \times [a_2(\omega)S_{\chi_{\parallel\perp\perp}}(2)] , \tag{7b}
\end{aligned}$$

with

$$a_1(\Omega) = \epsilon_1(\Omega)/\epsilon_2(\Omega), \quad a_2(\Omega) = \epsilon_2(\Omega)/\epsilon'(\Omega)$$

$$A(\Omega) = k_z^{(1)}(\Omega) + k_z^{(2)}(\Omega)$$

$$B(\Omega) = \epsilon_2(\Omega)k_z^{(1)}(\Omega) + \epsilon_1(\Omega)k_z^{(2)}(\Omega). \tag{7c}$$

In this formula, it is assumed that the only distinct nonvanishing elements of  $S_{\chi}^{**}(2)$  are  $S_{\chi_{\perp\perp\perp}}(2)$ ,  $S_{\chi_{\perp\parallel\parallel}}(2)$ , and  $S_{\chi_{\parallel\perp\perp}}(2) = S_{\chi_{\parallel\parallel\perp}}(2)$ . The second term of Eq. (6) can produce a bulk polarization from the interference of the incident and reflected beams at the fundamental frequency. Its contribution has been neglected. The formula does, however, account correctly

for both the direct and interference terms generated by the source polarization  $\gamma_1 \vec{\nabla}[\vec{E}(\omega) \cdot \vec{E}(\omega)]$ . The sign conventions adopted for the component of the SH radiation lying in the plane of incidence  $[\vec{E}_p(2\omega)]$  and for the component normal to the plane of incidence  $[\vec{E}_s(2\omega)]$  are indicated in Fig. 1. The figure also shows the azimuthal angle,  $\phi$ , of the electric field of the pump.  $\vec{k}^{(i)}(\omega) = k_x(\omega)\hat{x} + k_z^{(i)}(\omega)\hat{z}$  denotes the wavevector of the pump radiation in medium  $i = 1$  or  $2$ , with  $k_x\hat{x}$  being the common transverse component. The dispersion relation, of course, requires that  $[k^{(i)}(\omega)]^2 = \epsilon_i(\omega)k_o^2(\omega) = \epsilon_i(\omega)(\omega/c)^2$ . The wavevectors for the harmonic fields are given by  $\vec{k}^{(i)}(2\omega) = 2k_x(\omega)\hat{x} + k_z^{(i)}(2\omega)\hat{z} = 2k_x(\omega)\hat{x} + 2[\epsilon_i(2\omega)k_o^2(\omega) - k_x^2(\omega)]^{1/2}\hat{z}$ .

The derivation of Eq. (7) is not difficult. Because of the highly singular nature of the dipole sheet, the value of  $E_1$  within the sheet may be infinite. Failure to realize this fact has introduced some errors in the literature. The correct boundary conditions for a sheet of polarization are presented in Appendix I.

## B. Models of the Nonlinear Response

### 1. The Multipole Expansion and the Bulk Terms

The basis of all quantum-mechanical calculations of the second-order nonlinearity is a computation of the induced current in second-order time-dependent perturbation theory under the interaction Hamiltonian for the classical pump fields and the material system. This induced nonlinear current is linked to the (generalized) nonlinear source polarization of Eq. (1) by  $\vec{P}^{\text{NLS}}(2\omega) = (i/2\omega)\vec{J}(2\omega)$ . The quadratic relationship between the pump electric fields and  $\vec{P}^{\text{NLS}}$  then yields an expression for the second-order nonlinear susceptibility. Formulas derived in this



manner<sup>1</sup> exhibit all degrees of nonlocal behavior and can, in principle, be used in any calculation of SH response. The second-order nonlinear susceptibility is given as a weighted sum of products of matrix elements in the form of  $\langle g | \mathcal{H}_{\text{int}} | n' \rangle \langle n' | \mathcal{H}_{\text{int}} | n \rangle \langle n | \vec{J} | g \rangle$ . In practice, it is often possible to simplify these expressions by use of a multipole expansion, a development in terms of successively more nonlocal character. Good convergence is assured provided that the motion of each electron is confined to a region much smaller than that over which the variation of the optical field is appreciable ( $ka \ll 1$ ).

The multipole expansion can be derived by performing a canonical transformation under which the interaction Hamiltonian and the current are expressed as follows:<sup>7</sup>

$$\mathcal{H}_{\text{int}} = - \vec{P} \cdot \vec{E}(\vec{r}, t) - \vec{M} \cdot \mathbf{B}(\vec{r}, t) - \vec{Q} : \vec{\nabla}_{\vec{r}} \vec{E}(\vec{r}, t) - \dots$$

$$\vec{J} = N \left[ \frac{\partial}{\partial t} \langle \vec{P} \rangle + c \vec{\nabla}_{\vec{r}} \times \langle \vec{M} \rangle - \frac{\partial}{\partial t} \vec{\nabla}_{\vec{r}} \cdot \langle \vec{Q} \rangle + \dots \right]. \quad (8a)$$

The multiple moment operators for an electron of charge  $-e$  and mass  $m$  are

$$\vec{P} = - e \vec{x}$$

$$\vec{M} = - (e/2mc)$$

$$\vec{Q} = - (e/2) \vec{x} \vec{x}. \quad (8b)$$

$\vec{r}$  denotes the coordinate of the localized unit under consideration, and

$N$  is their density in the medium. The local response results from using only the first term in the expansions of  $\mathcal{H}_{\text{int}}$  and  $\vec{J}$ . The lowest-order nonlocal response is obtained by selecting one of the other terms for one application of the interaction Hamiltonian or in the expansion of the current. In a centrosymmetric medium the local response vanishes. The magnetic-dipole and electric-quadrupole terms then lead (assuming also isotropy) to a nonlinear source polarization of the form of Eq. (5) [Ref. 8]. The magnetic dipole generates a polarization proportional to  $\vec{E} \times \vec{B}$ , while the electric quadrupole gives rise to terms proportional to  $(\vec{\nabla} \cdot \vec{E})\vec{E}$  and to  $2(\vec{E} \cdot \vec{\nabla})\vec{E} + (i\omega/c)\vec{E} \times \vec{B}$ . (In component form, the last expression can be written as  $P_i^{\text{NLS}} = E_j \nabla_j E_i + E_j \nabla_i E_j$ .) Such an expansion is clearly appropriate for the bound electrons in the bulk of the medium (where the spatial variation of the fields occurs over the scale of an optical wavelength). In the low-frequency limit, Bloembergen et al.<sup>9</sup> have derived an approximate expression for the quadrupolar contribution. In the notation of Eq. (5), their result is

$$\beta = -2\gamma \approx 3(4n_b e)^{-1} [\chi^{(1)}(\omega)]^2, \quad \delta = 0 \quad (9)$$

with a total bound-electron density  $n_b$  and an associated linear susceptibility  $\chi^{(1)}(\omega)$ .

For metals, the response of the conduction electrons must also be considered. If the excitation energy lies below that required for interband transitions, a free-electron model of the conduction electrons may be a good approximation. The second-order nonlinear response of a free, noninteracting electron gas has been calculated through classical<sup>10</sup> and quantum mechanics.<sup>11-13</sup> In the bulk of the material, the dis-

tance an electron travels during a period of the optical excitation is much less than the distance over which the optical field varies spatially ( $kv_{\text{Fermi}} \ll \omega$ ); hence, the lowest-order approximation to the nonlocality is adequate:

$$\vec{P}^{\text{NLS}}(2\omega) = (n_c e^3 / 8m^2 \omega^4) \nabla [\vec{E}(\omega) \cdot \vec{E}(\omega)]. \quad (10)$$

In this formula  $m$  represents the effective mass of the conduction electrons and  $n_c$  is their density. For the bulk of the material, generalizations to include the effects of the exact band structure in intra- and interband transitions can be found in the literature.<sup>11,13-15</sup> Of course, the evaluation of such expressions requires a knowledge of the matrix elements of the true eigenstates.

## 2. Surface Terms

The theory of second-order nonlinear optical effects in the bulk of centrosymmetric media is, as we have seen, relatively well understood. The response can be computed accurately by consideration of the lowest-order nonlocal terms. If the exact forms of the wavefunctions are not available, good approximations can be made for insulating materials or for materials with a free-electron behavior. As a consequence of the weakness of the bulk nonlinearity, it is, however, also necessary to consider the surface contribution in detail. Here we are faced with considerably more difficulties in the theory. From a fundamental point of view, the problems stem from a poorer knowledge of the electronic states at the surface. At the least, one must construct some sort of model for the behavior of the electrons at the surface. The second principal complication arises from the possible invalidity of the multi-

pole expansion at the boundary. Because of the abrupt change in the material properties, we expect a significant variation in the fields to occur over a short distance. As an example, let us consider the case of a free-electron gas. The criterion for the dominance of the lowest-order nonlocal terms requires  $v_{\text{Fermi}} k \ll \omega$ . At the surface,  $k$  should be interpreted as the wavevector corresponding to the screening of the normal component of the electric field experienced in entering the material. For the electron gas, we may take  $k \sim k_s = 6\pi n e^2 / E_{\text{Fermi}}$ , the Thomas-Fermi wavevector.<sup>16</sup> The stipulation then becomes  $\omega \gg \omega_p = (4\pi n e^2 / m)^{1/2}$ . In the experiment work on metals, this relation has not been satisfied.

Despite the inaccuracies attendant upon a local (i.e., lowest-order nonlocal) analysis, this forms the basis of essentially all of the quantitative models.<sup>17</sup> Only in the work of Rudnick and Stern<sup>13</sup> is a complete nonlocal calculation performed. They found that the local approximation for a free-electron gas is adequate for the transverse component of the surface current, but introduces a substantial error for the part normal to the surface. The usual procedure<sup>9</sup> relies on computing the polarization induced by the surface discontinuity in the first two terms of Eq. (5). The intrinsic nonlinearity (represented by coefficients  $\beta$  and  $\delta$ ) is determined by the response in the bulk media. Approximate values for these coefficients are given by Eq. (9) for insulators. The result of Eq. (10) for a homogeneous free-electron gas must be augmented by a term arising from the change in electron density at the surface:<sup>9</sup>

$$\beta = e/8\pi m \omega^2, \quad \gamma = n e^3 / 8\pi m \omega^4, \quad \delta = \beta + 2\gamma. \quad (10)$$

The surface currents produced by such a polarization can be included in the surface nonlinear susceptibility  $\chi^{(2)}$ .

Since the surface lacks inversion symmetry, a direct dipole contribution to the nonlinearity should also be considered. It has been speculated that this dipole term acting on the asymmetrically distorted core electrons in the first atomic layer could substantially augment SHG.<sup>18</sup> This mechanism should be particularly important for materials with relatively small dielectric constants. At interfaces of such materials, we expect to find comparatively weak field gradients, making the nonlocal terms proportional to  $\partial E_z / \partial z$  less significant. In fact, the SHG exhibited by transparent solids and liquids<sup>9,19,20</sup> does not agree in detail with the predictions of Eq. (9). Our studies of SHG by adsorbate-covered surfaces can, for the most part, be interpreted in terms of the dipole contribution to the nonlinearity from the aligned adsorbate molecules.

A different mechanism leading to SHG is possible in the presence of strong dc fields. Such an effect has been observed clearly in calcite subjected to an external field<sup>21</sup> and can be attributed to the third-order process with a nonlinear polarization of  $\chi^{(3)} : \vec{E}_{dc} \vec{E}(\omega) \vec{E}(\omega)$ . Third-order nonlinear processes are, of course, dipole allowed in centrosymmetric media. The most direct evidence of this behavior for surfaces comes from the pronounced changes in SHG efficiency of silver and silicon samples held under bias in an electrochemical cell.<sup>22</sup> The double charge layer formed above the solid samples can lead to very large electric fields. In the case of silver, this field is screened in the first few Angstroms of the metal, and the bias dependence (if not from dc-induced SHG in the electrolyte) must be associated with the surface. It

has also been suggested<sup>20</sup> that in some materials, such as liquids and polar crystals, sufficiently strong dc fields may be present to make the  $\chi^{(3)}$  process operative for SHG. Terms originating in this fashion can also be included in the surface nonlinearity  $S_{\chi}^{(2)}$  provided that the dc fields do not penetrate far into the bulk.

### C. Experimental Work

#### 1. Clean Surfaces

SHG by reflection from a centrosymmetric medium was first observed for a silver sample,<sup>23</sup> which remains the most extensively studied material.<sup>9,13,19,24-27</sup> Other measurements of SHG have been carried out for gold,<sup>9</sup> for alkali metals,<sup>28</sup> for semiconductors,<sup>12</sup> for alkali-halide crystals and other insulating materials,<sup>9,19,20</sup> and for some liquids.<sup>20</sup> As a rule, the nonlinearity of the metals exceeded that of the semiconductors by an order of magnitude, and the nonlinearity of transparent materials was smaller by a further order of magnitude.

For our later discussion, it will prove useful to determine the dominant terms in the nonlinearity of silver. In Fig. 2, the data of Bloembergen et al.<sup>9</sup> are given for SHG by a p-polarized input beam as a function of the angle of incidence of the pump  $\theta$ . This angular dependence agrees with that of Sonnenberg and Heffner.<sup>24</sup> If we now try to fit this variation to the forms predicted by Eq. (7a) with  $\epsilon_1 = 1$  and  $\epsilon' = \epsilon_2$ , we find that only a very small admixture of the first term is possible; that is,  $S_{\chi_{\perp\perp\perp}}^{(2)} - S_{\chi_{\perp\parallel\parallel}}^{(2)}$  can be neglected. This fact was previously not apparent because of the omission of the factor of  $\sin^2\theta$  in the angular dependence of this term. The relative magnitude of the two remaining independent components of  $S_{\chi}^{(2)}$  can be found most directly by

comparing the p-polarized output for an s-polarized input (yielding  $S_{\chi_{\perp\parallel\parallel}}^{(2)} - \gamma$ ) with the s-polarized component of the SH for excitation with a pump of mixed polarization (yielding  $S_{\chi_{\parallel\perp\parallel}}^{(2)}$ ). Wang and Duminski<sup>19</sup> have performed such a measurement and have deduced comparable contributions to the SH generated by a p-polarized pump from these two sources.

## 2. Influence of Adsorbates

The question of the influence of adsorbates on SHG by surfaces has received only scant attention in the literature and has been studied in a controlled fashion in just a single case. In the early work the issue was simply overlooked, although Brown et al.<sup>23</sup> observed the same SHG by an evaporated silver film exposed to air for a few seconds as for a sample exposed for several hours. Bloembergen et al.<sup>9</sup> noted the same independence of SHG as a function of the age of the sample. They suggested that this result was theoretically tenable, since the nonlinearity of adsorbates was expected to be relatively small compared with that of metal surfaces. For the case of liquid surfaces, Wang<sup>20</sup> could not always obtain reproducible results, a fact which he attributed to surface contamination of these materials of lesser intrinsic nonlinearity. Brown and Matsuoka,<sup>25</sup> however, tried to test explicitly the claimed independence of the SHG by silver to the condition of its surface. They observed a drop by a factor of 4 in SHG by an evaporated film held under a vacuum of  $10^{-7}$  Torr upon exposure to air at atmospheric pressure. Since the nature of the adsorbates was unknown, it was difficult to devise a detailed theory. The authors believed that the most probably explanation for the effect was a SH polarization in the metal induced by a dc electric field associated with the adsorbates. Rudnick and Stern,<sup>13</sup> on the other hand, report an increase in SHG by a silver film upon breaking

a better vacuum. It was proposed that the change in SH could be attributed to scattering of the parallel surface current. Only in the experiment of Chen et al.<sup>29</sup> was the surface altered in a controlled fashion while monitoring the SH signal. The system studied consisted of a clean germanium surface overlaid by up to a monolayer of sodium atoms maintained in an ultrahigh vacuum. At full monolayer coverage of the surface by the adsorbate, the SH signal was several times larger than that of the bare surface. Chen and coworkers felt that the surface nonlinearity of sodium was sufficiently strong to cause the increased SHG.



## References

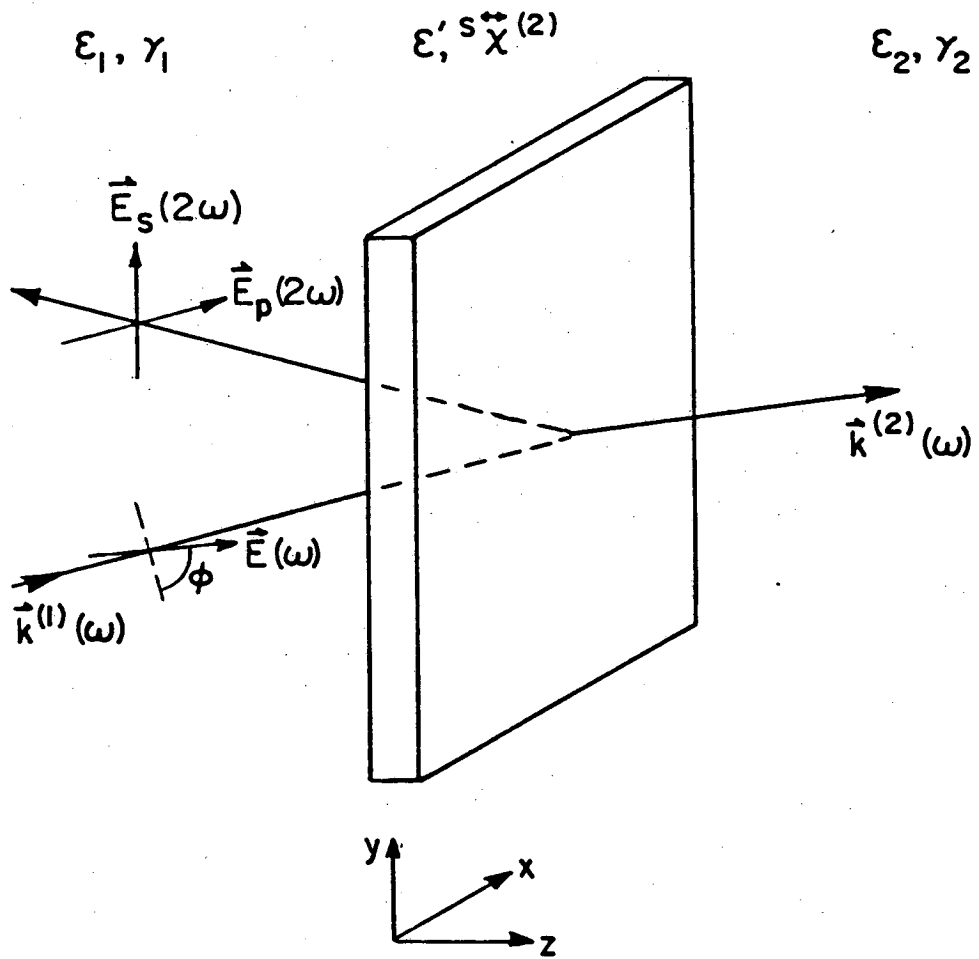
1. J. A. Armstrong, N. Bloembergen, J. Ducuing, and P. S. Pershan, Phys. Rev. 127, 1918 (1962).
2. Terms for the difference frequency have the form  $\overset{\leftrightarrow}{\chi}^{(2)}(\omega = \omega_2 - \omega_1): \vec{E}(\omega_2)\vec{E}^*(\omega_1)$ .
3. For the case of SHG, the relation  $\overset{\leftrightarrow}{\chi}^{(2)} = 0$  also holds for any isotropic medium. See D. S. Chemla, J. L. Oudar, and J. Perhpagnon, Phys. Rev. B 12, 4534 (1975).
4. For excitation of a homogeneous medium by a single plane wave, only this anisotropic term is capable of inducing a transverse (i.e., radiating) polarization.
5. See discussion of Sec. B.
6. The last four terms are to be evaluated in the bulk only; all surface contributions are to be incorporated in the third term.
7. This form neglects spin-related terms. See N. Bloembergen and Y. R. Shen, Phys. Rev. 133, A37 (1964).
8. E. Adler, Phys. Rev. 134, A728 (1964).
9. N. Bloembergen, R. K. Chang, S. S. Jha, and C. H. Lee, Phys. Rev. 174, 813 (1968); 178, 1528(E) (1969). This paper summarizes most of the earlier work.
10. S. S. Jha, Phys. Rev. 140, A2020 (1965).
11. H. Cheng and P. B. Miller, Phys. Rev. 134, A683 (1964).
12. S. S. Jha, Phys. Rev. 145, 500 (1966).
13. J. Rudnick and E. A. Stern, Phys. Rev. B 4, 4274 (1971).
14. S. S. Jha and C. S. Warke, Phys. Rev. 153, 751 (1967).
15. K. C. Rustagi, Il Nuovo Cimento 53B, 346 (1968).
16. C. Kittel, Quantum Theory of Solids (Wiley, New York, 1963), p.105.

17. General formulas for the nonlocal response are given by J. R. Bower, Phys. Rev. B 14, 2427 (1976).
18. N. Bloembergen and Y. R. Shen, Phys. Rev. 141, 298 (1966).
19. C. C. Wang and A. N. Duminski, Phys. Rev. Lett. 20, 668 (1968).
20. C. C. Wang, Phys. Rev. 178, 1457 (1969).
21. R. W. Terhune, P. D. Maker, and C. M. Savage, Phys. Rev. Lett. 8, 404 (1962).
22. C. H. Lee, R. K. Chang, and N. Bloembergen, Phys. Rev. Lett. 18, 167 (1967).
23. F. Brown, R. E. Parks, and A. M. Sleeper, Phys. Rev. Lett. 14, 1029 (1965).
24. H. Sonnenberg and H. Heffner, J. Opt. Soc. Am. 58, 209 (1968).
25. F. Brown and M. Matsuoka, Phys. Rev. 185, 985 (1969).
26. G. V. Krivoschchenko and V. I. Stroganov, Fiz. Tverd. Tela 11, 124 (1969); 11, 2663 (1969) [translation: Sov. Phys. - Solid State 11, 89 (1969); 11, 2151 (1970)].
27. J. E. Sipe, V. C. Y. So, M. Fukui, and G. I. Stegeman, Phys. Rev. B 21, 4389 (1980).
28. C. S. Wang, J. M. Chen, and J. R. Bower, Optics Commun. 8, 275 (1973).
29. J. M. Chen, J. R. Bower, C. S. Wang, and C. H. Lee, Optics Commun. 9, 132 (1973).
30. P. B. Johnson and R. W. Christy, Phys. Rev. B 6, 4370 (1972).

## Figure Captions

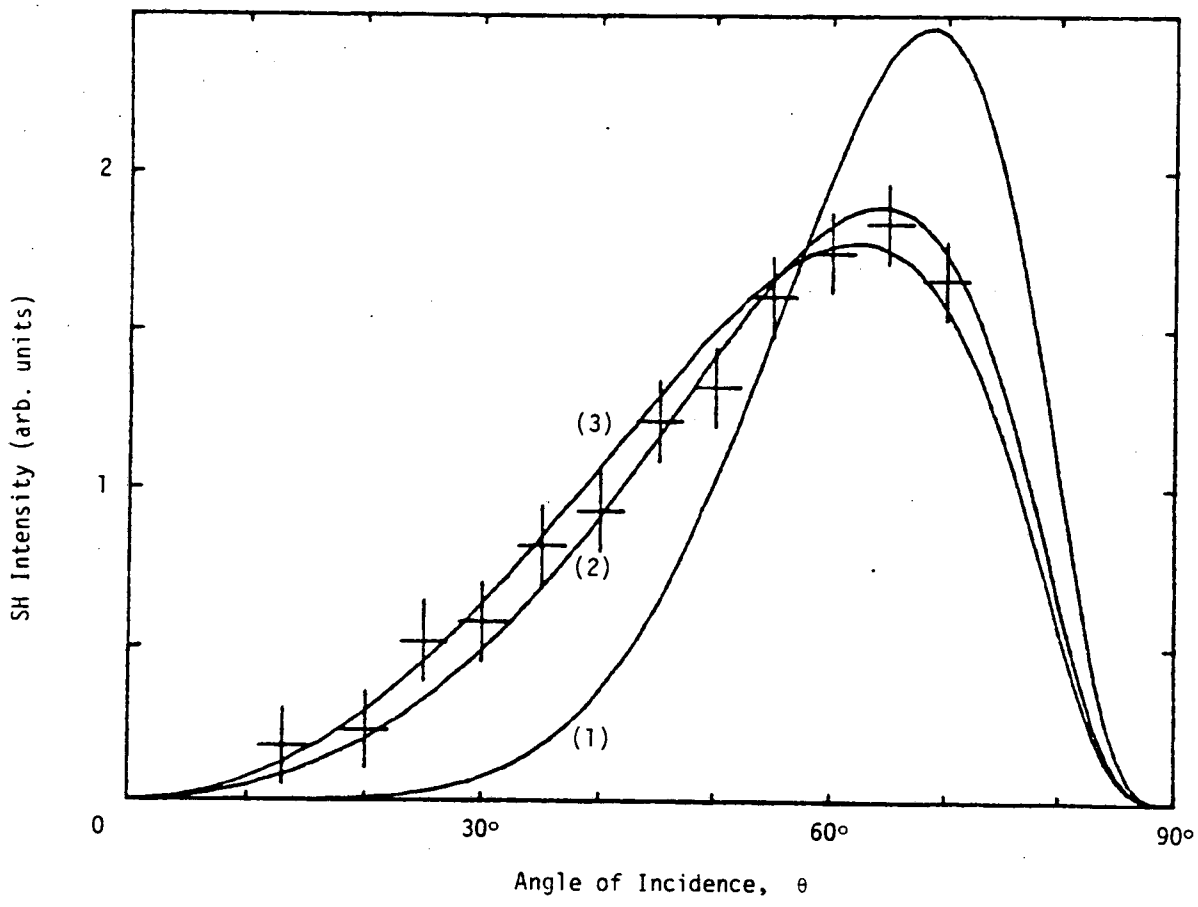
Fig. 1: Geometry for SHG by two neighboring centrosymmetric media. The pump radiation has the form  $\vec{E}(\omega)e^{ik_x(\omega)x+ik_z^{(1)}(\omega)z}$ ; the reflected SH field is given by  $\vec{E}(2\omega)e^{i2k_x(\omega)x-ik_z^{(1)}(2\omega)z}$ , with p- and s-polarized components as indicated.

Fig. 2: The data of Bloembergen et al.<sup>9</sup> for SHG by a silver surface as a function of the angle of incidence  $\theta$  of a p-polarized ruby pump laser. The solid curves represent least squares fits to the forms of the three terms of Eq. (7a). In evaluating these expressions,  $\epsilon_1 = 1$  and the values of Johnson and Christy<sup>30</sup> have been used for  $\epsilon_2$ .



XBL 8211-6793

Fig. 1



XBL 8210-2914

Fig. 2

### III. SECOND-HARMONIC GENERATION BY ADSORBATES ON METAL SURFACES

As the discussion of the previous chapter has indicated, SHG by centrosymmetric media is expected to be strongly influenced by the detailed structure of the material's surface. Here we present results of a series of experiments on SHG by a silver surface and the influence on this process of various molecular adsorbates. The special electrodynamic phenomena observed on an appropriately roughened silver surface and the accompanying enhancement found for various nonlinear scattering processes are analyzed in Appendix II.

#### A. Detection of Molecular Monolayers by Second-Harmonic Generation<sup>1</sup>

The experiments described in this section represent the first efforts to study the influence of molecular adsorbates on the SHG by metallic surfaces in a controlled environment. We have observed with a silver surface in an electrochemical cell that single molecular monolayers are easily detectable.

##### 1. Theoretical Considerations

An aligned monolayer of molecules can be characterized by a second-order nonlinear susceptibility per unit area  $S_{\chi}^{\leftrightarrow(2)}$  ( $2\omega = \omega + \omega$ ). Neglecting local-field corrections,<sup>2</sup>  $S_{\chi}^{\leftrightarrow(2)}$  can be taken simply as the sum of the corresponding nonlinear molecular polarizabilities  $\alpha^{\leftrightarrow(2)}$  ( $2\omega = \omega + \omega$ ):

$$S_{\chi}^{\leftrightarrow(2)} = N\alpha^{\leftrightarrow(2)}, \quad (1)$$

where  $N$  denotes the surface density of the molecules. Let us now con-

sider the signal generated by such a nonlinear slab lying above a metallic surface. Far below the plasma frequency of the metal, we know that  $\epsilon \ll 0$  and that only normal electric fields can exist at the surface. Consequently, only the  $\chi_{\perp\perp\perp}^{(2)}$ -component of  $\alpha^{(2)}$  is relevant, in which case we anticipate only a p-polarized output. For a nonlinear slab with a local, isotropic dielectric constant  $\epsilon'$  lying in a dispersionless dielectric medium with constant  $\epsilon_0$ , we find a radiated SH field of

$$E(\omega) = i32\pi\epsilon_0^{-1/2}c^{-1}[\epsilon_0/\epsilon'(\omega)]^2[\epsilon_0/\epsilon'(2\omega)]\tan\theta \sin^2\theta \cos^2\phi S_{\chi_{\perp\perp\perp}^{(2)}} E^2(\omega). \quad (2)$$

The angles  $\theta$ ,  $\phi$  in this expression, which has been obtained with the aid of Eq. (7) of Ch. II, refer to the polarization of the pump beam. Let us rewrite Eq. (2) in a more readily accessible form for comparison with experiment. For a pump pulse of duration  $T$ , intensity  $I(\omega)$ , and area  $A$ , the SH signal is given by<sup>3</sup>

$$S = 2^{10}\pi^3\omega\epsilon_0^{-3/2}c^{-3}h^{-1}|\epsilon_0/\epsilon'(\omega)|^4|\epsilon_0/\epsilon'(2\omega)|^2\tan^2\theta \sin^4\theta \cos^4\phi |S_{\chi_{\perp\perp\perp}^{(2)}}|^2 \times I^2(\omega)AT \text{ photons/pulse}. \quad (3)$$

In particular, a p-polarized pump incident at  $\theta = 45^\circ$  with  $I(\omega) = 1 \text{ MW/cm}^2$  at  $1.06 \mu\text{m}$ ,  $A = 1 \text{ cm}^2$  and  $T = 10 \text{ nsec}$  will generate  $\sim 75$  photons/pulse for a monolayer of density  $N = 4 \times 10^{14} \text{ cm}^{-2}$  of molecules with  $\alpha_{\perp\perp\perp}^{(2)} = 1 \times 10^{-30} \text{ esu}$ . (In this estimate,  $\epsilon_0 = \epsilon'(\omega) = \epsilon'(2\omega) = 1$  has been assumed.) Such a signal should be readily detectable and distinguishable from the comparable SH of  $\sim 100$  photons/pulse generated by a bare silver surface with the same excitation.<sup>4</sup> It should be noted that the parameters chosen to describe the pump laser in the estimate above

can be easily implemented in the laboratory. As far as the magnitude of the second-order nonlinearity is concerned, we must realize that  $\alpha^{(2)} = 0$  holds for undistorted centrosymmetric molecules. For noncentrosymmetric structures, small aliphatic molecules typically exhibit a nonresonant  $\alpha^{(2)}$  in the range of  $5 \times 10^{-32}$  esu to  $5 \times 10^{-31}$  esu, depending on the degree of asymmetry.<sup>5,6</sup> Noncentrosymmetric aromatic compounds tend to have large nonlinearities. Conjugated double bonds and the associated delocalized  $\pi$  electrons are particularly favorable. Mono- and disubstituted benzene derivatives, for example, are generally characterized by  $\alpha^{(2)} \sim 5 \times 10^{-31} - 5 \times 10^{-30}$  esu, with  $\alpha^{(2)} > 10^{-29}$  esu for some species.<sup>6,7</sup> Since our calculation indicates measurable SH signals from monolayers with  $|\chi^{(2)}| \gtrsim 5 \times 10^{-16}$  esu, we expect various adsorbed species to alter significantly the SHG by a silver surface.

## 2. Experimental Apparatus

A Q-switched  $\text{Nd}^{3+}$ :YAG laser operating at a wavelength of  $1.06 \mu\text{m}$  provided pump radiation in the form of 10 ns pulses at a repetition rate of 10 Hz. The unfocused beam of diameter  $\sim 6$  mm passed through various short-wavelength cutoff filters and a horizontal polarizer before reaching the sample. The operation of the laser was monitored continuously by recording the intensity of the reflection from an interposed glass slide. For our studies with a roughened silver sample, we collected a large solid angle of the diffusively scattered harmonic radiation with an  $f/1$  aspherical lens. The signal at  $.53 \mu\text{m}$  was detected by means of a high-gain photomultiplier (RCA 7265) and was recorded on an integrator of time constant 1s with a  $10 \mu\text{s}$  window gated on the laser pulse. The intensity of the reflected fundamental radiation exceeded that at the SH by a factor of  $\sim 10^{15}$ , so it was necessary to take care to pro-

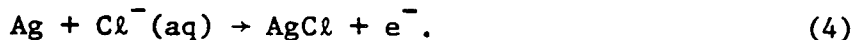


vide sufficient spectral discrimination in the detection system. The primary suppression of the light at the fundamental frequency was obtained with cascaded color filters. The radiation at the SH frequency was then selected by a narrow-bandpass interference filter or by a monochromator.

The silver sample in our electrochemical cell was probed in situ. The rectangular glass cell was oriented to allow the pump radiation to pass through the front face at normal incidence, undergo reflection by the sample at a 45° angle of incidence, and to emerge from the adjoining glass face at normal incidence (Fig. 1). We positioned the platinum counter electrode away from the path of the incident and reflected beams. A saturated calomel reference electrode (SCE) was also present, with respect to which all potentials are quoted. Doubly distilled, deionized water was used for all electrolytes and, the glass cell was thoroughly cleaned to avoid any possible contamination. We prepared the polycrystalline silver sample by mechanical polishing with alumina powders of successively finer grades down to 0.05  $\mu\text{m}$ . For comparison with an optically flat surface, we found a freshly evaporated, optically thick silver film to be convenient.

### 3. Results

Let us first consider the behavior for a pure 0.1M KCl electrolyte. Under the application of a positive bias to the silver electrode, silver is oxidized by the half-reaction



Owing to the very low solubility of AgCl in water, little of the oxida-


tion reaction leads to the formation of aqueous silver ions. This fact was verified by the essentially complete recovery of charge in the reduction half-reaction, which is given by Eq. (4) in the reverse sense. The silver surface was initialized by running two or three oxidation-reduction cycles with a charge transfer of  $\sim 65 \text{ mC/cm}^2$  in each cycle. This procedure produced a substantial roughening of the silver surface and resulted in a sample yielding  $\sim 10^5$  photons/pulse for a pump fluence  $\sim 1 \text{ mJ/cm}^2$ .

The SH signal was monitored during the course of subsequent oxidation-reduction cycles. As Fig. 2 shows, the signal rose and fell sharply at the beginning and the end of the cycle and changed relatively little during the build-up and destruction of the  $\text{AgCl}$  layer of a thickness of 500 monolayers.<sup>8</sup> In order to study these abrupt changes more closely, we reduced the electrolytic current during the initial and final portions of the cycle. Figure 3 displays the SH signal during the final phase of the reduction reaction with the current limited to  $\sim 100 \text{ }\mu\text{A/cm}^2$ . While the entire drop in SHG occurs during the reduction of 5 or so monolayers, the final, sudden decrease actually takes place for less than one monolayer of transferred charge. We can conclude that little more than a monolayer of  $\text{AgCl}$  makes an appreciable contribution to the SHG process.

Because of the roughness of the silver surface, the observed SH signal was angularly diffused and unpolarized, with or without the adsorbate. That the signal was indeed SH radiation was verified by its quasimonochromatic character at  $0.53 \text{ }\mu\text{m}$ . It was further verified that the signal arrived in time coincidence with the pump radiation. The quadratic power dependence expected for SHG was confirmed both for the

bare silver surface before cycling and for the adsorbate-covered surface of an interrupted cycle. While the exact shape of the SH signal as a function of time during the cycle was somewhat sensitive to the initial sample preparation, the measurements were reproducible with careful control of experimental parameters. We did observe a systematic change in the SHG for increased pump-laser fluences. For fluences in the range of  $\lesssim 1$  mJ, the results were all identical to those of Fig. 2. The curve of Fig. 4 is representative for fluences  $\sim 10$  mJ/cm<sup>2</sup>. At still higher fluences the SH versus time begins to assume a triangular form. We attribute these effects to laser-induced desorption and, for the higher fluences, to a gross reforming of the silver surface.<sup>9</sup>

We have also performed analogous measurements with a K<sub>2</sub>SO<sub>4</sub> electrolyte. Just as for the case of the KCl electrolyte, some deposition of the silver salt on the electrode is anticipated during the course of an oxidation-reduction cycle. Figure 5 gives the SH signal as a function of time for the indicated oxidation-reduction cycles. A similar curve for a KCl electrolyte is included for comparison. Note that the SHG by Ag<sub>2</sub>SO<sub>4</sub> is much weaker than that of AgCl.

On the basis of the results just described, we anticipated that it would be possible to measure appreciable SHG by molecules which adsorb only a single monolayer. From studies of surface-enhanced Raman scattering,<sup>10</sup> it is known that the electrically neutral pyridine molecule () will adsorb on a silver surface held near the point of zero charge,<sup>11</sup>  $V_{\text{Ag-SCE}} \sim -0.7\text{V}$ . Figure 6 illustrates the dependence of the surface-enhanced Raman signal for various vibrational modes of pyridine on the applied bias, expressed in terms of the silver-SCE voltage. In the case of SHG, the signal rose sharply after the completion of an oxi-

dation-reduction cycle when a reverse bias was applied. This result can be seen in Fig. 2 for a pyridine concentration of 0.05M in the 0.1M KCl electrolyte. The exact dependence of the SH signal on the reverse bias is shown in Fig. 7 for an electrolyte with and without dissolved pyridine. The maximal increase in SHG of  $\sim 50$  times was obtained for  $V_{\text{Ag-SCE}} \sim -1.0\text{V}$ . Clearly the SH signal from the pyridine-covered silver sample is readily distinguishable from that of the bare metal. The absolute magnitude of the SH signal exhibited a dependence on the strength of the electrochemical cycling, as one would expect from a sample with differing degrees of roughness. The ratio of the pyridine/silver to bare silver SHG, however, remained essentially unaltered. If we assume that the same ratio is maintained even for a flat surface, then we can immediately estimate the surface nonlinear susceptibility of the pyridine/silver system. Relying on the calibration of Bloembergen et al.<sup>4</sup> for the flat silver surface, we infer a value of  $|S_{\chi}^{(2)}| \sim 3 \times 10^{-15}$  esu.

We observed that when 0.05M pyridine was dissolved in the electrolytic solution a few minutes after the completion of an oxidation-reduction cycle, an increase of only a factor of  $\sim 20$  in the SH signal occurred for  $V_{\text{Ag-SCE}} = -1.0\text{V}$ . The electrochemical cycling had apparently produced a clean silver surface suitable for the adsorption of pyridine, which during the time delay had begun to be contaminated. In fact, we saw no SHG associated with pyridine for the case of a freshly evaporated silver film held under reverse bias. On the other hand, following a weak electrochemical cycle with a charge transfer of just  $2 \text{ mC/cm}^2$  (oxidation and reduction of an average of 8 atomic layers of silver), we already noted a growth by a factor of  $\sim 10$  in the angularly diffused SH

radiation for  $V_{\text{Ag-SCE}} = -1.0\text{V}$ . All of the measurements described above were taken with a pump fluence restricted to  $\sim 1 \text{ mJ/cm}^2$  in order to avoid laser-induced changes of the surface. At a fluence of  $30 \text{ mJ/cm}^2$ , for example, the SH signal from adsorbed pyridine decreased to an intermediate value with a  $\sim 15 \text{ sec}$  time constant.

Another species whose adsorption on silver has been studied by means of surface-enhanced Raman scattering is the cyanide anion,  $\text{CN}^-$ . According to the work of Benner et al.,<sup>12</sup> introduction of cyanide anions into the electrolytic solution will lead to adsorption to silver in the form of silver cyanide complexes  $[\text{Ag}(\text{CN})_3]^{2-}$  when the sample is held under reverse bias following the completion of an oxidation-reduction cycle. Figure 8 shows the experimental SH and surface-enhanced Raman scattering intensities over a range of reverse bias voltages.<sup>13</sup> Once again, we find a marked difference between the SHG with and without adsorption.

#### 4. Discussion

These studies give clear evidence for the high surface sensitivity of SHG at interfaces between two centrosymmetric media. By measuring the electrolytic current, we found that the substantial increase in SH signal upon the deposition of  $\text{AgCl}$  on the silver surface could be accounted for by the first monolayer and that subsequent layers had little effect on the SHG process, as we would expect for the bulk of a centrosymmetric medium. Only the surface layer, for which the inversion symmetry must be broken, can contribute effectively to the second-order nonlinearity. The much weaker nonlinearity associated with adsorbed  $\text{Ag}_2\text{SO}_4$  compared with  $\text{AgCl}$  (Fig. 5) can be understood on the basis of the much higher degree of symmetry present in the former than in the

latter structure.

The findings for pyridine and cyanide, known to adsorb only in monolayers, further demonstrate the strong influence of surface properties on SHG. If we assume that the surface nonlinearity derived in the discussion of pyridine adsorption arises solely from the nonlinearity of the aligned (acentric) pyridine molecules, we can then deduce a value for the molecular nonlinear polarizability. If we apply Eq. (1) with an adsorbate surface density of  $N = 4 \times 10^{14} \text{ cm}^{-2}$  [Ref. 11], this leads us to  $\alpha_{111}^{(2)}$  (pyridine)  $\sim 8 \times 10^{-30}$  esu. Performing the same calculation for the adsorbed cyanide species, we obtain  $\alpha_{111}^{(2)}$  (cyanide complex)  $\sim 2 \times 10^{-30}$  esu. These values for the molecular nonlinear polarizabilities lie in the upper end of the range expected for corresponding free species. As will be discussed in Sec. C in greater detail, interactions of the adsorbate with the silver substrate may serve to increase the nonlinear response.

It should be noted that several of the previously proposed mechanisms to explain the sensitivity of SHG by silver surfaces to airborne contaminants<sup>14</sup> are not compatible with our observations in these studies. First, the notion that a change in the linear fields (and in the concomitant surface discontinuities) resulting from the presence of adsorbates could cause the increase in SHG without any modification of the intrinsic nonlinearity certainly cannot explain a 50-fold jump in SH signal. Thus, a model of the nonlinearity as one governed strictly by the silver substrate, as suggested by Bloembergen et al.,<sup>4</sup> is inappropriate. Brown and Matsuoka<sup>15</sup> invoke the dc-induced SHG process via the third-order nonlinearity. While manifestations of this effect have been observed in electrochemical cells<sup>16</sup> where the double charge layer

of the electrolyte can induce very strong static fields, our measurements on roughened silver in pure electrolytes (see Figs. 7 and 8) show little dependence on the bias voltage. We can therefore rule out the possibility that the jump in SHG upon introduction of neutral pyridine molecules results from a modification of the dc fields at the silver surface. The influence of surface scattering of the silver conduction electrons in modifying the SH signal, as developed by Rudnick and Stern,<sup>17</sup> is also unlikely to produce a 50-fold increase in SHG.

The fact that no change in SH signal was observed for an uncycled silver sample biased in an electrolyte containing pyridine or that a reduced signal was found if pyridine was added only at a delayed time after the completion of an oxidation-reduction cycle indicates that the cycling procedure is necessary to provide a clean silver surface for pyridine adsorption. Simply producing a heightened pyridine concentration above the silver sample would not increase the SHG, since these molecules are not expected to show any net orientation.

A comparison of the bias dependence of the SH and Raman signals for the two adsorbates raises interesting questions. Neither for pyridine (Figs. 6 and 7) nor for cyanide (Fig. 8) does the SH intensity vary in the same manner as the Raman intensity. Since the surface density  $N$  of the adsorbates is expected to change with the bias voltage, the linear dependence of the incoherent Raman process on  $N$  departs from the quadratic dependence on  $N$  of the intensity from the coherent SHG process. Even taking this fact into account, the observed behavior clearly cannot be explained strictly in terms of the adsorbate surface coverage. Given the strong dependence of the SHG process on orientation (since  $\langle \alpha^{\pm 2} \rangle = 0$  for an isotropic angular average), the differing bias depen-

dences for SH and Raman scattering are suggestive of the presence of a bias-induced reorientation of the adsorbates. For the case of adsorbed pyrazine (Sec. C), the bias dependence of the SH intensity agrees relatively closely with that for Raman scattering.

## B. Application: Equilibrium and Transient Study of Pyridine Adsorption<sup>18</sup>

Here we rely on the monolayer sensitivity of the SHG process to investigate the adsorption of pyridine on a silver electrode. The surface-specific SH signals are sufficiently large so as to allow measurement of both the equilibrium and transient behavior. For this system, it was also possible to observe surface-enhanced Raman scattering<sup>10</sup> (SERS), the results of which are compared to those obtained by means of SHG.

### 1. Experimental Apparatus

The configuration for measurements of SHG has been described above. For Raman scattering, cw excitation was provided by a 30 mW beam of an argon ion laser operating on the 514 nm line. The p-polarized light was focused to  $\approx 2 \text{ mm} \times 0.25 \text{ mm}$  at the silver-electrolyte interface, where it was incident at a  $20^\circ$  angle. The resulting SERS signal from the adsorbed pyridine was collected along the surface normal, imaged on the entrance slit of a double monochromator, and detected with a cooled, low-noise photomultiplier. As in the previously mentioned experiments, the electrochemical cell consisted of a polycrystalline silver electrode, a platinum counter electrode and a reference SCE. The silver sample was initialized by running three oxidation-reduction cycles, each with a charge transfer of  $\approx 90 \text{ mC/cm}^2$ . Pyridine was added to the 0.1M KCl electrolyte under a reverse bias of  $V_{\text{Ag-SCE}} = -0.2\text{V}$ .



## 2. Results and Discussion

An adsorption isotherm for pyridine was obtained from measurement of the SH signal. SH intensities were registered under successive increases in the pyridine concentration; however, in order to verify that an equilibrium had been attained and that no irreversible changes were occurring in the system, we determined that the SH signal for a weak solution of pyridine could be recovered by the dilution of a concentrated one. We also checked that we were operating at sufficiently low pump fluences to avoid laser-induced surface effects.

The observed SH signal came from both the adsorbed molecules and the silver substrate. Neglecting local-field corrections arising from interactions between adsorbed molecules,<sup>2</sup> the nonlinear polarization associated with the adsorbed molecules should be linear in their surface density,  $N$ . According to the model developed in Appendix II for the electrostatics of the roughened silver surface, the net nonlinear polarization from both the adsorbed molecules and the silver is expected to be normal to the plane of the substrate. For our excitation at 1.06  $\mu\text{m}$ , the intrinsic nonlinearity of both the pyridine and silver has a nonresonant character and should, consequently, produce nonlinear polarizations of the same phase. Thus, the SH intensity assumes the form:

$$I(2\omega) = (A + BN)^2, \quad (5)$$

where  $A$  and  $B$  are real constants. The constant  $A$  was found by measuring  $I(2\omega)$  in the absence of pyridine. The adsorption isotherm,  $N$  versus the bulk pyridine concentration  $\rho$ , could then be obtained by plotting  $[I(2\omega)]^{1/2} - A$  against  $\rho$ . This is shown in Fig. 9 for  $V_{\text{Ag-SCE}} = -1.0\text{V}$ ,

a bias giving rise to a large SH signal from pyridine.

Adsorption isotherms can, in general, be quite complicated depending on the mechanism of adsorption involved. In many cases, however, the simple Langmuir curve applies:<sup>19</sup>

$$N = \rho (K + \rho)^{-1} N_0, \quad (6)$$

where  $K$  is a constant at a fixed temperature and  $N_0$  is the saturated value of  $N$  for a monolayer surface coverage. In terms of the adsorption free energy  $\Delta G$  in aqueous solution, we have<sup>7</sup>

$$K = 55 \exp(-\Delta G/RT) \quad (7)$$

in mole/l (M), where  $R = 1.99 \text{ cal mole}^{-1} \text{ K}^{-1}$  is the gas constant. A Langmuir isotherm predicts the behavior of a system for which the binding energy of any surface site is identical and for which interactions between adsorbed molecules may be neglected. The first assumption is a reasonable one for the silver surface; the second stipulation may be less well satisfied, particularly at high coverages. Examination of the experimental data indicates that a good fit can be obtained with the Langmuir form for  $K = 1.1 \times 10^{-2} \text{ M}$ , as is shown in Fig. 9. The corresponding adsorption free energy  $\Delta G$  is then 5.1 kcal/mole for pyridine on silver. Repeated measurements yielded some variation in the observed isotherms, with  $\Delta G$  values lying between 4.8 and 5.2 kcal/mole.

As an alternative method of finding the adsorption isotherm, we recorded the pyridine SERS signal for the integrated strength of the  $1005 \text{ cm}^{-1}$  line as a function of the bulk concentration of pyridine.

The equilibrium SERS intensity was measured<sup>20</sup> at  $V_{\text{Ag-SCE}} = -0.6\text{V}$ , for which the signal is strongest. As Fig. 10 illustrates, the variation of this SERS signal<sup>21</sup> with changing pyridine concentration has a characteristic saturation behavior resembling that of Fig. 9. The solid curve in Fig. 10 is, as before, a theoretical fit using the Langmuir model of Eq. (6) with  $K = 4 \times 10^{-3}\text{M}$  or  $\Delta G = 5.7\text{ kcal/mole}$ . In other trials, we found  $\Delta G$  ranging from 5.2 to 5.7 kcal/mole.

Our analysis of the isotherms by both SHG and SERS has presupposed that no coverage-dependent reorientation of the adsorbate occurs. The SH signal is expected to be particularly sensitive to orientational effects. In a recent study of pyridine adsorption on silver in ultrahigh vacuum,<sup>22,23</sup> analysis of the vibrational spectra obtained by electron energy loss spectroscopy has indicated that the adsorbed molecules undergo a structure phase transition. For surface densities  $\lesssim 3 \times 10^{14}\text{ cm}^{-2}$ , the pyridine molecules lie essentially flat on the silver surface; at higher surface densities, the pyridine molecules coordinate with the silver through the nitrogen lone pair and assume an upright position. If the same sort of abrupt reorientation of the adsorbate were to occur in the aqueous environment, we would not have observed such smooth variations in SH and SERS intensities as a function of the bulk pyridine concentration. The lack of an analogous phase transition can be understood if we realize that the pyridine adsorbed out of solution may be stabilized by the surrounding electrolyte and could well favor the upright orientation for all surface coverages.

A simple Langmuir model has the following dynamical equation governing the adsorption of molecules at a surface:

$$dN/dt = -\alpha N + \beta\rho(N_o - N), \quad (8)$$

where  $\alpha$  and  $\beta$  are constants related to the desorption and adsorption, respectively, with  $\alpha/\beta = K$ . The equilibrium solution of Eq. (8) takes the form of Eq. (6), which, as Figs. 9 and 10 attest, fit the experimental results fairly well. The transient solution of Eq. (8) can be written as

$$N(t) = \frac{\rho N_o}{K + \rho} + \left( N(0) - \frac{\rho N_o}{K + \rho} \right) e^{-t/\tau}, \quad (9)$$

with  $\tau = (\alpha + \beta\rho)^{-1}$ . We have taken some transient measurements to determine whether the Langmuir model is also appropriate in this regime. The SH and SERS signals were recorded as functions of time after the final  $V_{\text{Ag-SCE}}$  value was applied subsequent to the completion of an electrolytic cycle. A large transient effect was observed. In the case of SERS, with 50 mM pyridine and  $V_{\text{Ag-SCE}} = -0.8\text{V}$ , for example, the signal [Fig. 11(a)] first increased rapidly to a certain large magnitude and then decayed exponentially to the equilibrium value with a time constant  $\tau \approx 36\text{s}$ . This behavior presumably indicates that during the establishment of the double charge layer at the silver electrode, more pyridine molecules appeared in regions with large surface enhancements before relaxing to their equilibrium configuration.


The transient behavior of the SHG is even more complicated. For  $V_{\text{Ag-SCE}} < -0.7\text{V}$ , the signal also overshoot its steady state-value and then decayed [Fig. 11(b)]. The time-dependent decay of  $[I(2\omega)]^{1/2} - A = BN$  can be approximated reasonably well by the sum of two exponentials with time constants  $\tau_1$  and  $\tau_2$ . For  $-0.9\text{V} > V_{\text{Ag-SCE}} > -1.0\text{V}$  and 2.5

$\text{mM} < \rho < 70 \text{ mM}$ ,  $\tau_1$  ranged from 5 to 12s and  $\tau_2$  varied between 24 and 84s. The time constants for SHG and SERS did not depend strongly on  $\rho$  and appeared to increase rather than to decrease as  $\rho$  was augmented. This indicates that the Langmuir model of Eq. (9) is too simple to explain the dynamics of adsorption for the case under study. The actual spatial distribution of the pyridine molecules in solution must also be incorporated into a complete model. At a 50 mM pyridine concentration, as  $V_{\text{Ag-SCE}}$  was increased from - 1.1 to - 0.9V, the decay showed only slight changes, but when  $V_{\text{Ag-SCE}}$  was further increased to the - (0.75 - 0.85)V range,  $\tau_2$  grew dramatically to 360s. Then for  $V_{\text{Ag-SCE}} \gtrsim - 0.7\text{V}$ , the signal no longer overshoot its steady state, but instead approached it from below. A similar voltage dependence was also observed for  $\rho = 5 \text{ mM}$ . This more complex transient behavior of SHG as compared with SERS suggests that molecular reorientation may be important, since this is expected to affect SHG more strongly. We have, however, not been able to formulate a simple model to explain the transient response of both SERS and SHG.

In this study we have investigated a system with the aid of both SERS and SHG. While the former can give important information about vibrational transitions, it is practical only for a limited selection of substrates (roughened noble metals). As we shall see in Ch. IV, the latter technique is applicable even in the absence of any particular surface-enhancement mechanism and also has potential as a spectroscopic tool.

### C. Centrosymmetric Adsorbate: Pyrazine<sup>24</sup>

The pyridine molecule (Nc1ccncc1) has no center of inversion and should,

consequently, have a nonvanishing dipolar second-order polarizability  $\alpha^{(2)}$ . Thus, an aligned monolayer of noninteracting pyridine molecules should give rise to SHG through the surface nonlinear susceptibility  $S_X^{(2)} = N\alpha^{(2)}$ . If we consider the centrosymmetric pyridine molecule () , however, we expect  $\alpha^{(2)} = 0$  for the free molecule, and we cannot explain the nonlinear response of an adsorbed pyridine monolayer without considering symmetry-breaking interactions. We describe below the experimentally observed SHG associated with the adsorption of pyrazine on a roughened silver electrode and discuss possible mechanisms to explain our findings.

### 1. Experimental Apparatus

We have previously (Sec. A) indicated the salient features of the 1.06  $\mu\text{m}$  pump laser, the electrochemical cell, and of the detection system. As in the previously mentioned experiments, the fluence of the p-polarized laser excitation was limited to  $\sim 1 \text{ mJ/cm}^2$  in order to avoid laser-induced surface damage or desorption. The mechanically polished polycrystalline silver electrode was prepared prior to any measurements by three oxidation-reduction cycles, each with a charge transfer of  $\sim 90 \text{ mC/cm}^2$ , in the usual 0.1M KCl electrolyte. Solid pyrazine is moderately soluble in water with the aid of agitation. Consequently, when we desired to introduce pyridine into the electrolyte after the initialization procedure, we added a more concentrated solution in which pyrazine had previously been dissolved.

### 2. Results

The principal findings in this investigation are summarized in Fig. 12. The plot represents the SH intensity from generation at the silver surface as a function of the reverse bias applied between the silver

and platinum electrodes, registered by the Ag-SCE potential  $V_{\text{Ag-SCE}}$ . The SH signal in Fig. 11 does not exhibit a pronounced dependence on the voltage in the case of the pure electrolyte. Upon introduction of pyrazine, however, we observe an increase in SH signal and a characteristic voltage dependence in the SH intensity. It should be noted that we recorded the SH signal while making the silver electrode potential more negative at each step, since irreversible changes in the surface chemistry or structure seem to be induced by large reverse biases.<sup>25</sup>

In the pyrazine solution, the maximal SH intensity was found to be  $\sim 10$  times as great as that originating from the roughened silver surface in the pure electrolyte. By way of comparison, the adsorption of pyridine gave rise to a  $\sim 50$ -fold increase in SHG (Sec. A). The SH radiation was angularly diffused and unpolarized, as one would expect in view of the rough profile of the silver surface on the scale of an optical wavelength. That the signal was, in fact, SH was verified by checking its monochromaticity and its quadratic variation with the intensity of the fundamental excitation.

### 3. Discussion

The peak in the SH intensity for the electrolyte containing pyrazine around  $V_{\text{Ag-SCE}} = -0.4\text{V}$  lies in the range of potentials for vibrational spectra of the adsorbed species which have been observed by SERS.<sup>11,25,26</sup> The large increase in SHG induced by this adsorption can not be explained simply as the result of the net dipolar nonlinear susceptibility of the unperturbed, aligned adsorbates, which, of course, vanishes because of the inversion symmetry of the free pyrazine molecule. Clearly, we need to consider the interaction of the molecules with the substrate in order to account for our observations.

Generally speaking, we may break down the types of interaction into two groups, chemical and electrodynamic ones, depending on whether or not the change in the electronic states of the pyrazine/silver system in the absence of optical fields needs to be considered. By the very fact that pyrazine is adsorbed to the silver substrate, it is clear that the electronic states of both systems must be somewhat altered, thus lifting the inversion symmetry of the free pyrazine molecules. In order to evaluate the importance of such an effect in explaining the SHG associated with pyrazine adsorption, let us consider the magnitude of the observed nonlinearity. Following the procedure of Sec. A, we estimate from the  $\sim 10$ -fold increase in SHG upon adsorption of pyrazine that the surface nonlinear susceptibility of the pyrazine/silver interface is  $\chi_{111}^{(2)} \sim 1.5 \times 10^{-15}$  esu. If we assume that this nonlinearity results from the dipolar nonlinear polarizabilities of the perturbed, adsorbed pyrazine molecules, we deduce a value  $\alpha_{111}^{(2)}$  (adsorbed pyrazine)  $\sim 4 \times 10^{-30}$  esu for a surface density of  $N = 4 \times 10^{14}$   $\text{cm}^{-2}$ . By comparison, we found only twice as large a value of  $\alpha^{(2)}$  for adsorbed pyridine. One would therefore conclude that a fairly substantial change of the electronic states of pyrazine, producing an asymmetry comparable to that of the pyridine molecule, would be required for this mechanism to account for the experimental results. The small binding energy expected for adsorption of pyrazine (cf. results of Sec. B for pyridine and measurements in vacuo of Ref. 23) would then appear to rule out this explanation. Moreover, Avouris and Demuth<sup>23</sup> have measured only minimal shifts in the energies of electronic transitions in pyrazine upon adsorption to silver. They did, however, find evidence for charge-transfer states, which have no analog in the free molecules. Transitions to such charge-transfer



states involve movement of an electron centered in the pyrazine molecule to the metal or vice versa. It has been suggested by Whittle and Burstein<sup>27</sup> that these highly polar states may explain the nonlinearity associated with pyrazine adsorption. Interestingly, the pyrazine charge-transfer states appear for energies  $\geq 1.4$  eV according to the work of Avouris and Demuth and could be in resonance with the SH frequency and nearly resonant with the fundamental for our experiment with a 1.06  $\mu\text{m}$  pump.

Even in the absence of a significant change in the electronic states of the pyrazine (or of the metal) caused by adsorption, SHG is still possible through electrodynamic interactions. Let us consider a classical model of an electron attached to a spring obeying Hooke's law. For this configuration, representing an electron in a centrosymmetric pyrazine molecule, an external field cannot induce any SH response (within the dipole approximation). If we now place our electron and spring just above a dielectric slab, however, we must take the induced image charge into account. We then no longer observe a net linear restoring force on the electron and the SHG process becomes dipole-allowed. With the aid of essentially this elementary model and experimental values for the dielectric constants and image-plane spacing, Antoniewicz<sup>28</sup> obtains a correct order-of-magnitude estimate of  $\alpha_{\text{eff}}^{(2)}$  (adsorbed pyrazine). The neglect of the nonlocality of the dielectric constant of the metal in Antoniewicz's model is a questionable point, since the same procedure has led to erroneous results in the theory of SERS.<sup>29</sup> From a broader perspective, the mechanism considered here is that of quadrupole SHG, which is nonvanishing even for centrosymmetric systems. The presence of the metal surface can induce large field gradients (through the

image-dipole mechanism or otherwise), possibly making the usually insignificant quadrupole terms important.

In the studies of adsorbed pyrazine by SERS,<sup>25,26</sup> it has been found that infrared-active vibrational modes are present in Raman spectra. For the free molecules, these modes are symmetry-constrained not to contribute to the Raman scattering (within the dipole approximation). In analogy with our discussion above, both the lowering of molecular symmetry<sup>25,26</sup> and the importance of quadrupolar terms<sup>30</sup> have been suggested to explain the observations.

## References

1. C. K. Chen, T. F. Heinz, D. Ricard, and Y. R. Shen, Phys. Rev. Lett. 46, 1010 (1981).
2. Local-field effects are discussed in Appendix II.
3. With the convention adopted here of  $\vec{E}(t) = \vec{E}(\omega)e^{-i\omega t} + \text{c.c.}$ , the intensity is given by  $I(\omega) = (c\sqrt{\epsilon_0}/2\pi)|\vec{E}(\omega)|^2$ .
4. N. Bloembergen, R. K. Chang, S. S. Jha, and C. H. Lee, Phys. Rev. 174, 813 (1968).
5. J. F. Ward and I. J. Bigio, Phys. Rev. A 11, 60 (1975).
6. B. F. Levine and C. G. Bethea, J. Chem. Phys. 63, 2666 (1975).
7. J. L. Oudar and H. Le Person, Optics Commun. 15, 258 (1975); 18, 410 (E) (1976).
8. The number of monolayers was deduced from the flow of charge under the assumption that the surface density of AgCl was given by  $(N_V)^{2/3}$ , with  $N_V$  the volume density of AgCl in the crystalline solid. The values quoted should be taken as upper bounds, since no allowance has been made for the increased area of the roughened surface.
9. G. Boyd and Z. Yu have observed laser-induced reforming of the roughened silver samples directly in electron micrographs (unpublished).
10. Surface-enhanced Raman scattering is discussed in Appendix II.
11. D. L. Jeanmaire and R. P. Van Duyne, J. Electroanal. Chem. Interfacial Electrochem. 84, 1 (1977).
12. R. E. Benner, R. Dornhaus, R. K. Chang, and B. L. Laube, Surf. Sci. 101, 341 (1980).
13. C. K. Chen, T. F. Heinz, D. Ricard, and Y. R. Shen, "Surface En-

- hanced Second-Harmonic Generation and Raman Scattering," submitted to Phys. Rev. B.
14. See discussion of Chapter II.
  15. F. Brown and M. Matsuoka, Phys. Rev. 185, 985 (1969).
  16. C. H. Lee, R. K. Chang, and N. Bloembergen, Phys. Rev. Lett. 18, 167 (1967).
  17. J. Rudnick and E. A. Stern, Phys. Rev. B 4, 4274 (1971).
  18. C. K. Chen, T. F. Heinz, D. Ricard, and Y. R. Shen, Chem. Phys. Lett. 83, 455 (1981).
  19. M. J. Rosen, Surfactants and Interfacial Phenomena (Wiley, New York, 1978), Ch.2.
  20. Similar results were obtained for SHG and SHG with  $V_{\text{Ag-SCE}} = -0.8\text{V}$  for both measurements.
  21. We note that our result differs somewhat from the "S" shaped curve of Jeanmaire and Van Duyne.<sup>11</sup>
  22. J. E. Demuth, K. Christmann, and P. N. Sanda, Chem. Phys. Lett. 76, 201 (1980).
  23. Ph. Avouris and J. E. Demuth, J. Chem. Phys. 75, 4783 (1981).
  24. T. F. Heinz, C. K. Chen, D. Ricard, and Y. R. Shen, Chem. Phys. Lett. 83, 180 (1981).
  25. R. Dornhaus, B. M. Long, R. E. Benner, and R. K. Chang, Surf. Sci. 93, 240 (1980).
  26. G. R. Erdheim, R. L. Birke, and J. R. Lombardi, Chem. Phys. Lett. 69, 495 (1980).
  27. D. J. Whittle and E. Burstein, Bull. Am. Phys. Soc. 27, 377 (1982).
  28. P. R. Antoniewicz, Phys. Rev. B 26, 2285 (1982).
  29. See, for example, the discussion of the article of H. Metin in

Surface Enhanced Raman Scattering, edited by R. K. Chang and T. E. Furtak (Plenum, New York, 1982).

30. R. Dornhaus, "Spectral Properties of Molecules Adsorbed on Metal Surfaces from Surface Enhanced Raman Scattering," presented at the Third International Conference on Vibrations at Surfaces (1982).

## Figure Captions

- Fig. 1: Schematic representation of the experimental apparatus. The unfocused, p-polarized pump beam at  $1.06 \mu\text{m}$  consists of 10 ns pulses from a  $\text{Nd}^{3+}$ :YAG laser. In addition to the silver sample, the electrolytic cell contains a platinum counter electrode and a reference saturated calomel electrode (SCE).
- Fig. 2: The SH signal from a silver sample during an oxidation-reduction cycle in 0.1M  $\text{KCl}$  electrolyte. The corresponding current and Ag-SCE voltages are indicated in the lower figure. The response after the completion of the electrolytic cycle is that observed with 0.05M pyridine in the electrolyte also.
- Fig. 3: Detail of the completion of an oxidation-reduction cycle of silver in a 0.1M  $\text{KCl}$  electrolyte. The SH signal, electrolytic current and Ag-SCE voltage are given as functions of time. Note that the precipitous drop at  $t \approx 2$  minutes corresponds to a charge transfer less than that needed for the complete reduction of a monolayer of  $\text{AgCl}$ .
- Fig. 4: Same as Fig. 2, but with a pump fluence of  $\sim 10 \text{ mJ/cm}^2$  rather than  $\sim 1 \text{ mJ/cm}^2$ . The laser repetition rate is 10 Hz.
- Fig. 5: Comparison of SHG for two similar oxidation-reduction cycles of a silver electrode in 0.1M  $\text{K}_2\text{SO}_4$  solution (above) and in 0.1M  $\text{KCl}$  solution (below). The Ag-SCE voltage and electrolytic current for the cycles is also shown. These cycles were obtained by ramping the applied Ag-Pt at a constant rate.
- Fig. 6: Surface-enhanced Raman scattering intensity for pyridine adsorbed on silver following the completion of an oxidation-reduction cycle in a 0.1M  $\text{KCl}$  + 0.05M pyridine electrolyte after

the data of Jeanmaire and Van Duyne.<sup>11</sup> The curves represent the dependence on the reverse bias of the Raman signal for different Stokes shifts: (a)  $1006 \text{ cm}^{-1}$ , (b)  $1035 \text{ cm}^{-1}$ , (c)  $3056 \text{ cm}^{-1}$ , (d)  $1215 \text{ cm}^{-1}$ , (e)  $1594 \text{ cm}^{-1}$ , and (f)  $623 \text{ cm}^{-1}$ .

Fig. 7: SHG by a silver sample plotted against the reverse bias applied following the completion of an oxidation-reduction cycle in a  $0.1\text{M KCl}$  electrolyte in the presence and absence of  $0.05\text{M pyridine}$ .

Fig. 8: As in Fig. 7, but with or without  $0.01\text{M KCN}$  in the electrolyte. The adsorbed cyanide species is believed to be the  $[\text{Ag}(\text{CN})_3]^{2-}$  complex.<sup>12</sup> The integrated intensity of the surface-enhanced Raman signal for a Stokes of  $2110 \text{ cm}^{-1}$  as measured with an argon ion laser is also indicated.<sup>13</sup>

Fig. 9: Equilibrium adsorption isotherm for pyridine in a  $0.1\text{M KCl}$  solution and a silver electrode held at  $V_{\text{Ag-SCE}} = -1.0\text{V}$ . The data points are computed from the measured SH signal. The solid curve is a theoretical fit to the experiment using the Langmuir model of Eq. (8).

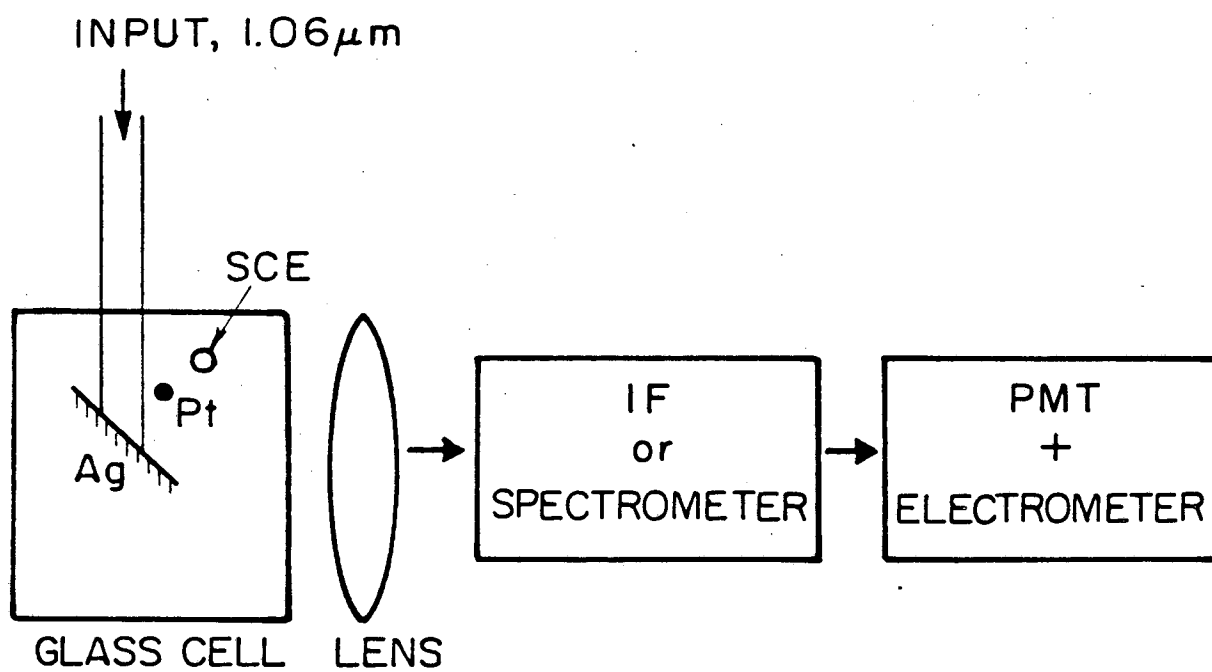
Fig. 10: Same as Fig. 9, but obtained with SERS for a  $1005 \text{ cm}^{-1}$  Stokes shift with  $V_{\text{Ag-SCE}} = -0.6\text{V}$ .

Fig. 11: Transient SERS (a) and SHG (b) at  $50 \text{ mM pyridine}$  concentration immediately following an oxidation-reduction cycle.  $V_{\text{Ag-SCE}}$  remains constant for  $t \geq 0$ .

Fig. 12: SH intensity from the cycled silver surface as a function of its potential  $V_{\text{Ag-SCE}}$  in an electrolytic solution of  $0.1\text{M KCl}$  with and without  $0.05\text{M pyrazine}$  present. The error bars are indicative of the uncertainty in the relative shape of the

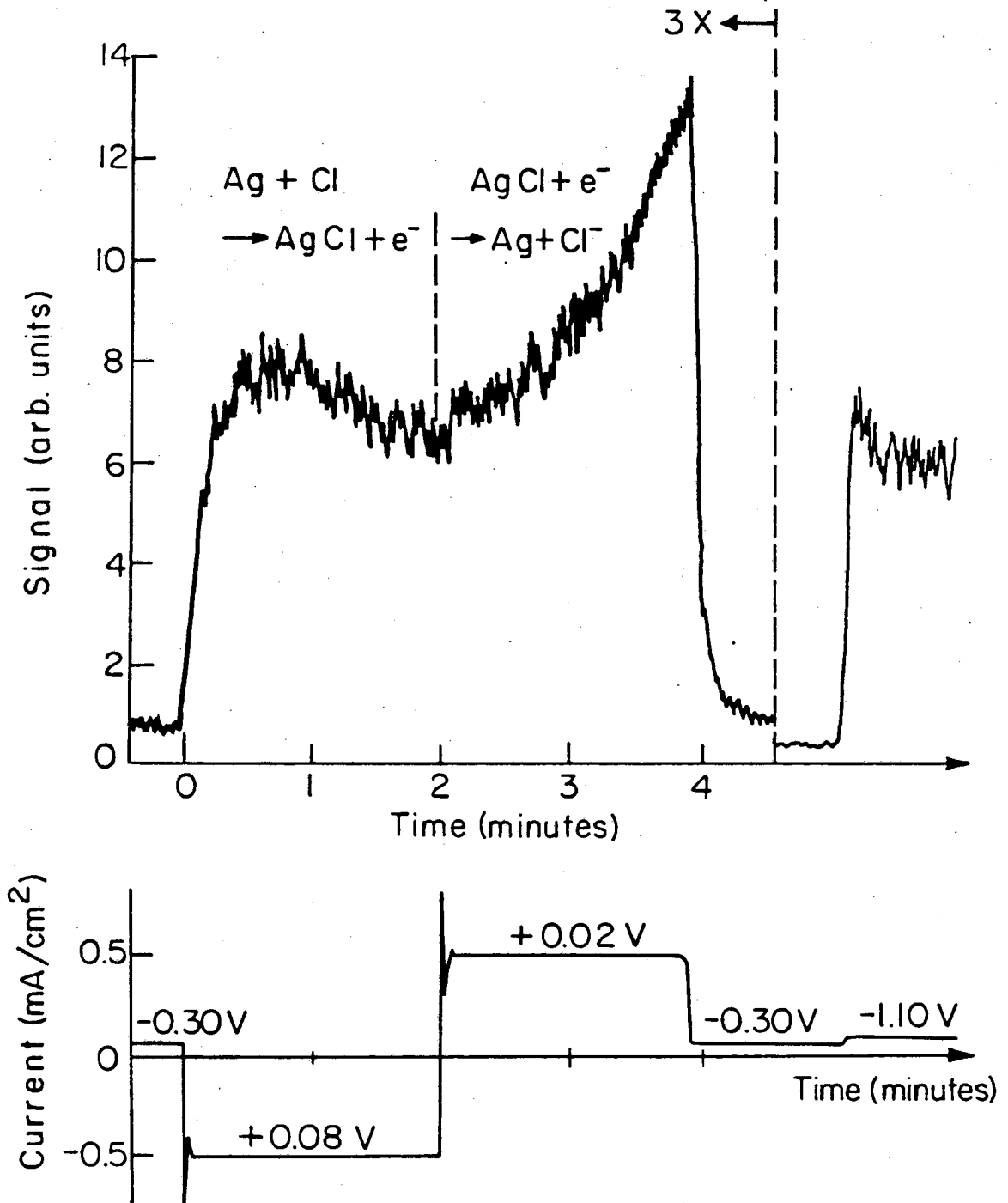
voltage dependence; the overall ratio of the signals in the two cases may be subject to a somewhat larger error.





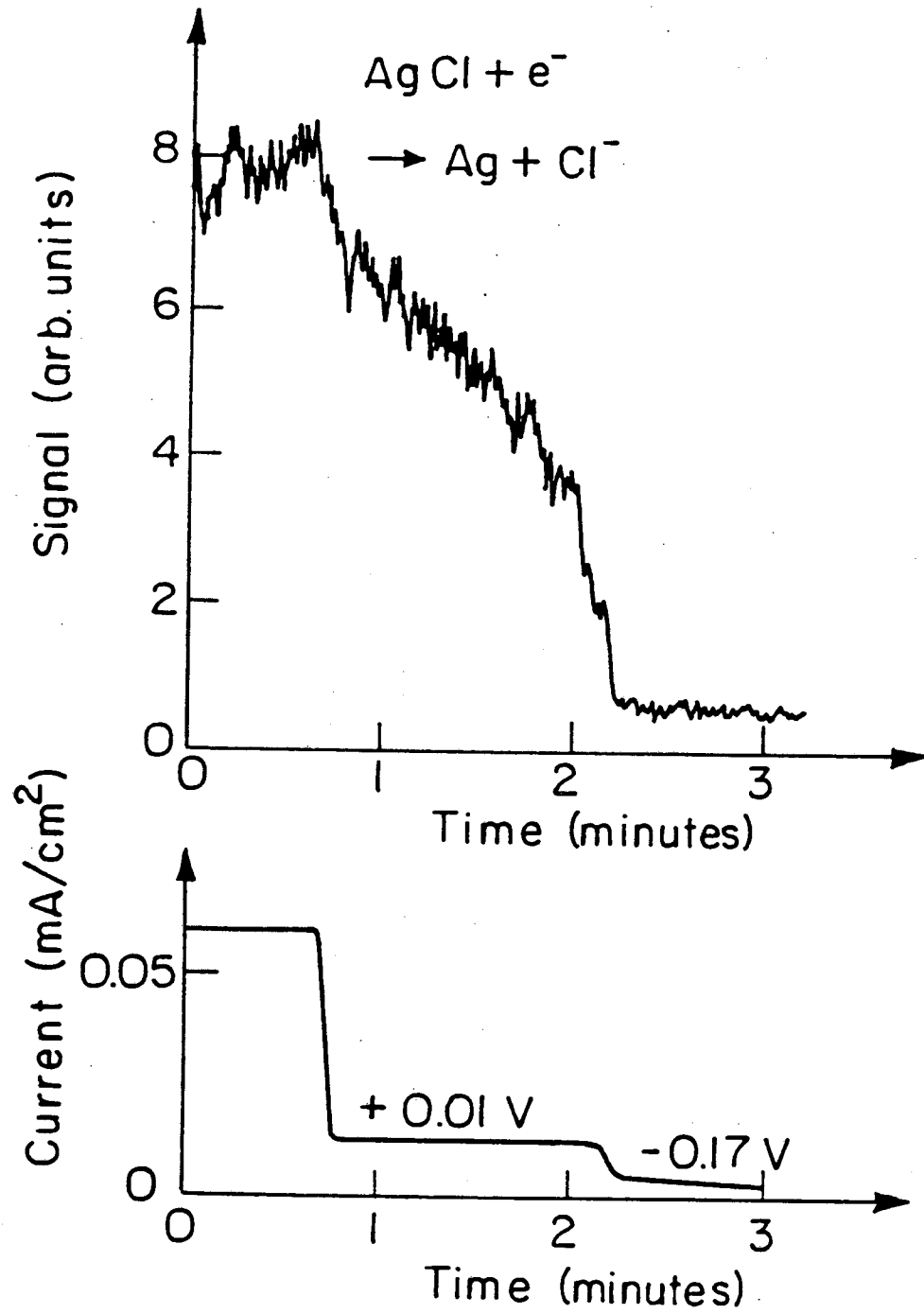
XBL 8012-13337

Fig. 1



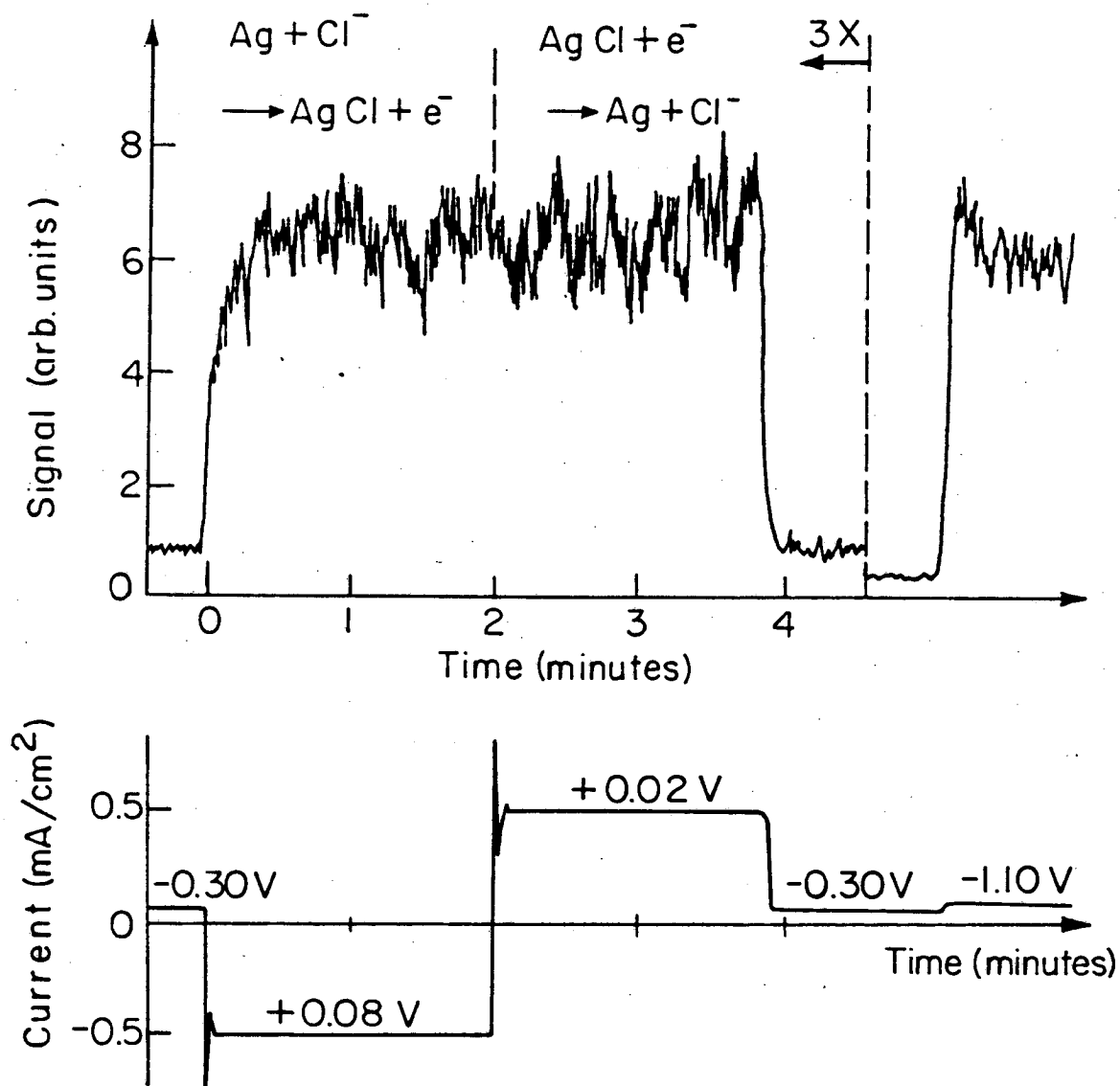
XBL 8012-13338A

Fig. 2



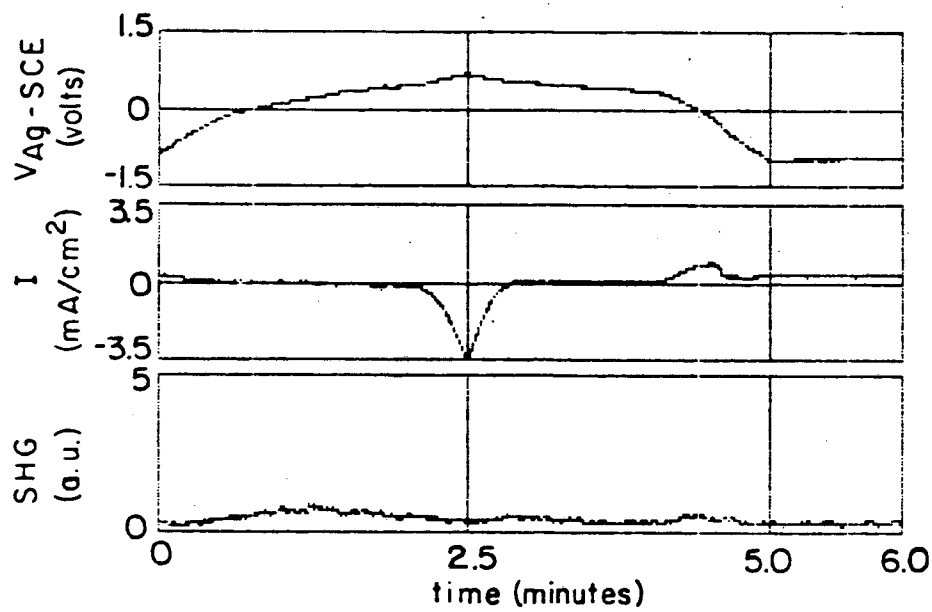
XBL 8012-13340

Fig. 3

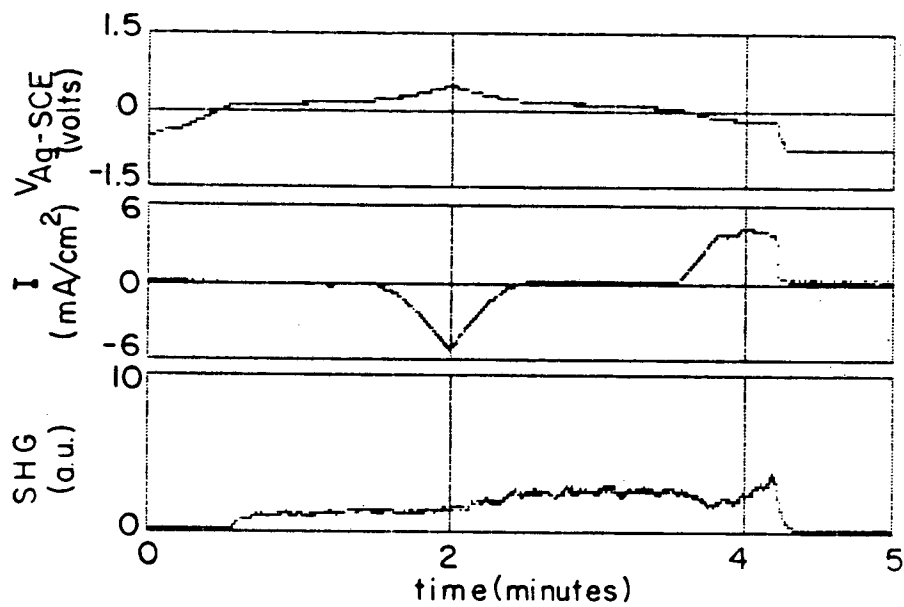


XBL 8012-13338

Fig. 4



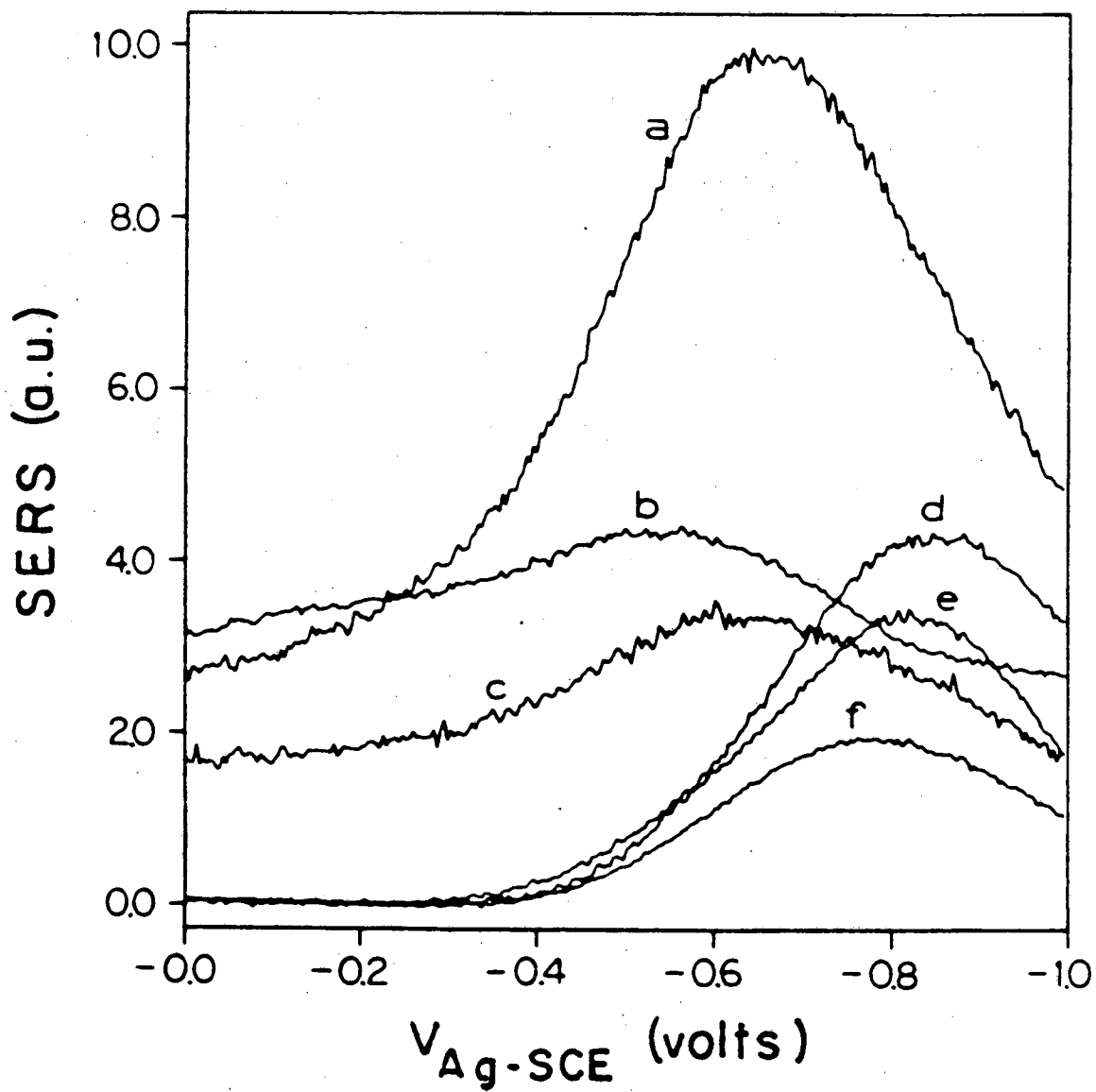
A



B

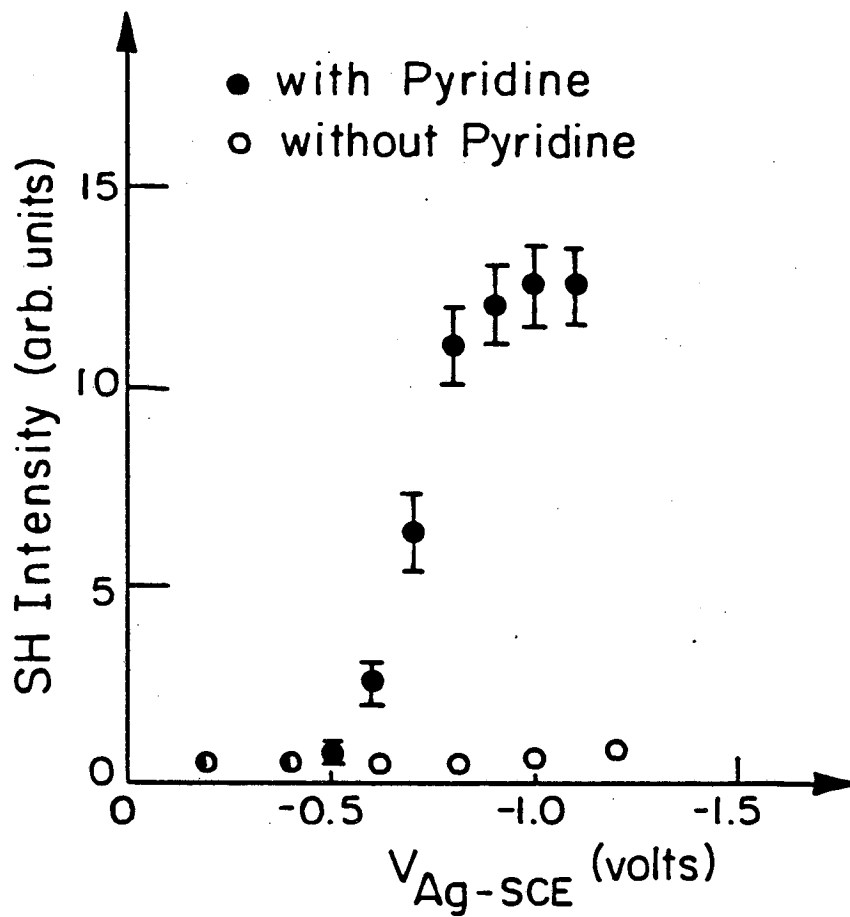
XBL 824-5586A

Fig. 5



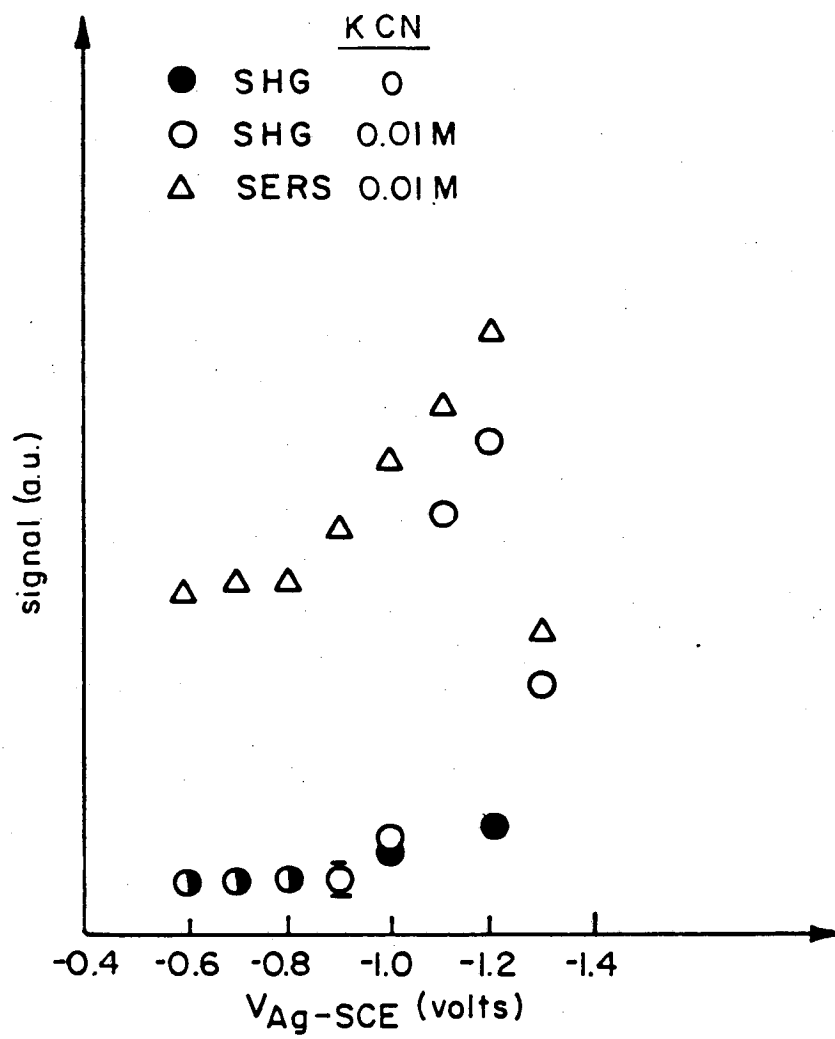
XBL 827-10756

Fig. 6



XBL 8012-13339

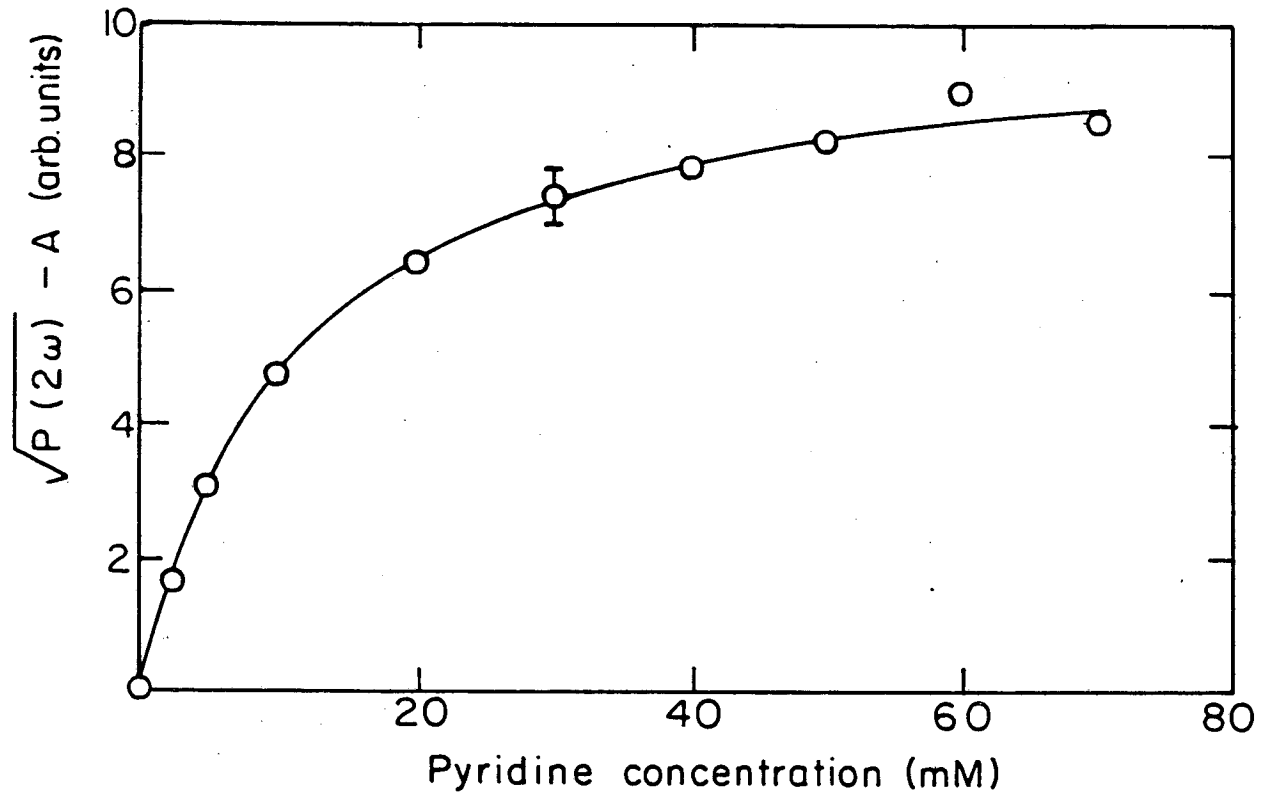
Fig. 7



XBL 824-5588

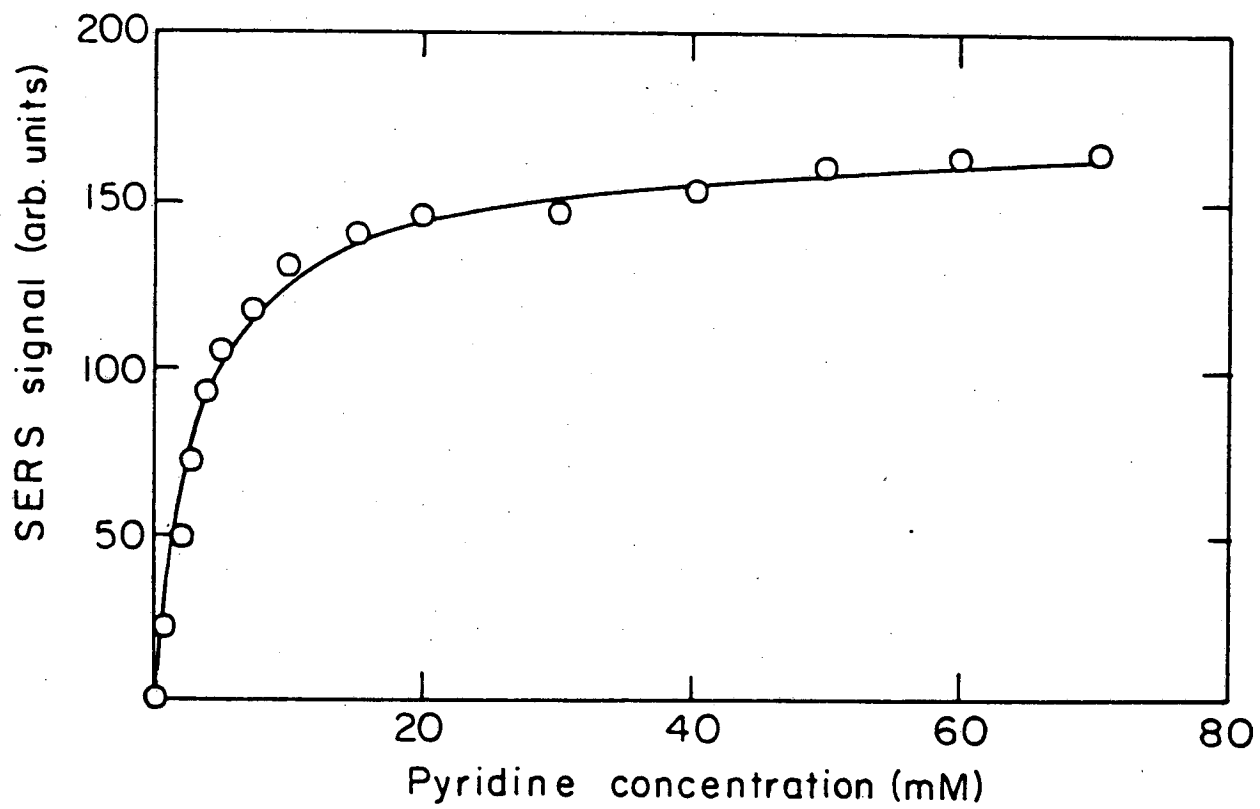
Fig. 8





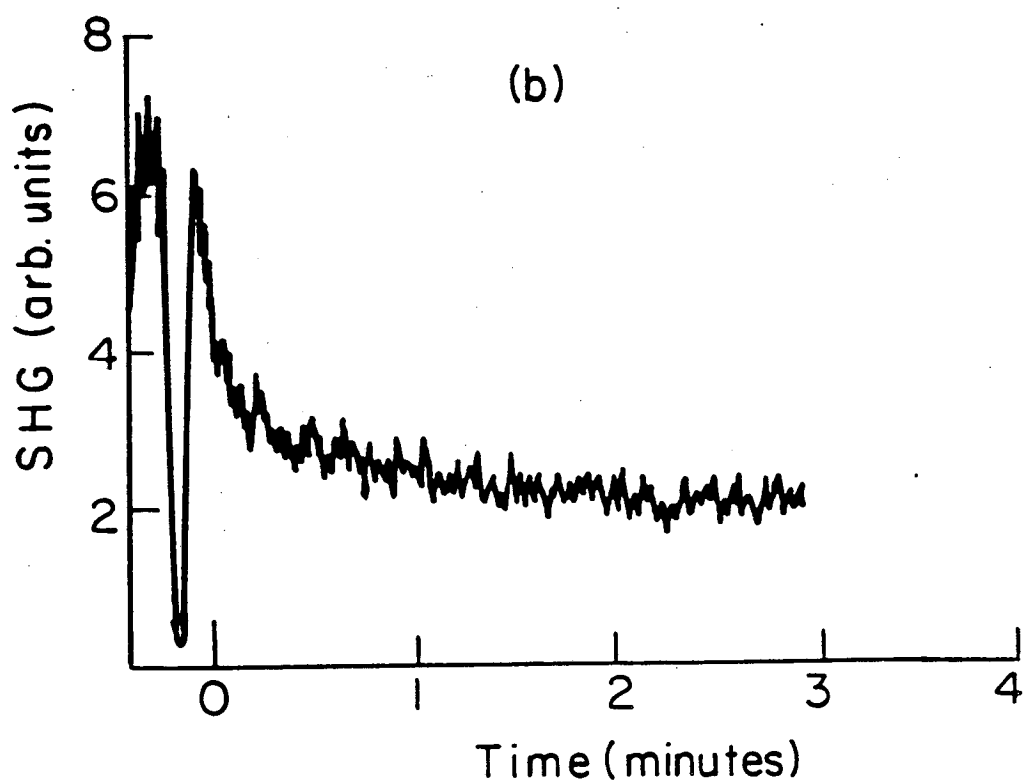
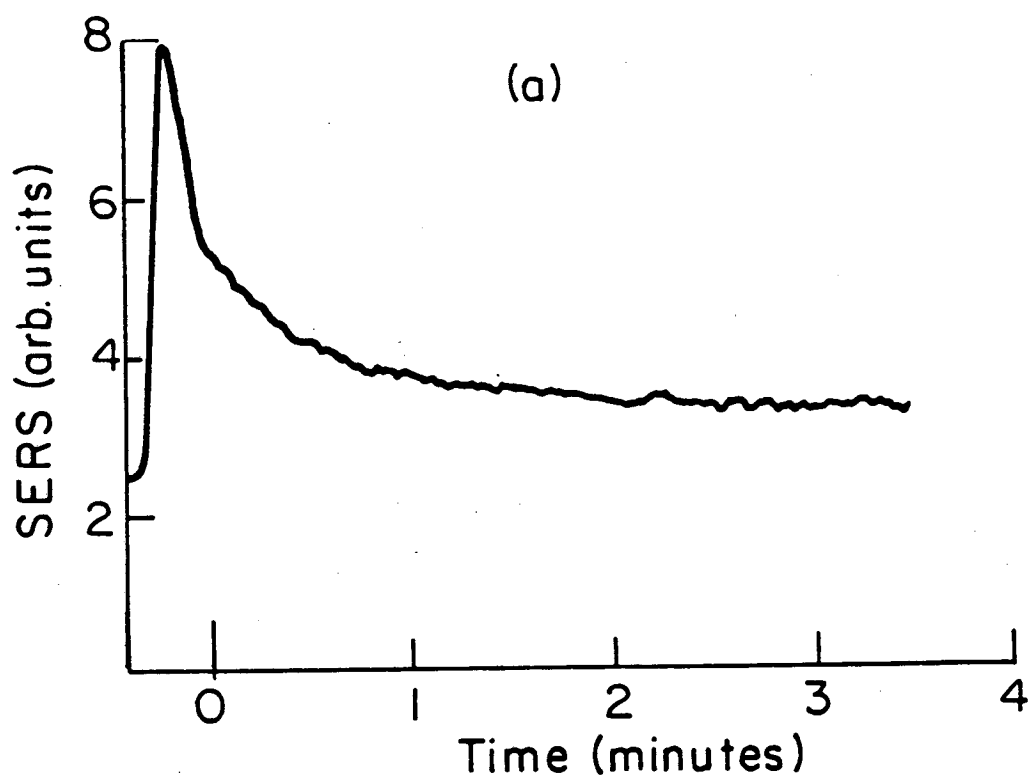
XBL 815-5824

Fig. 9



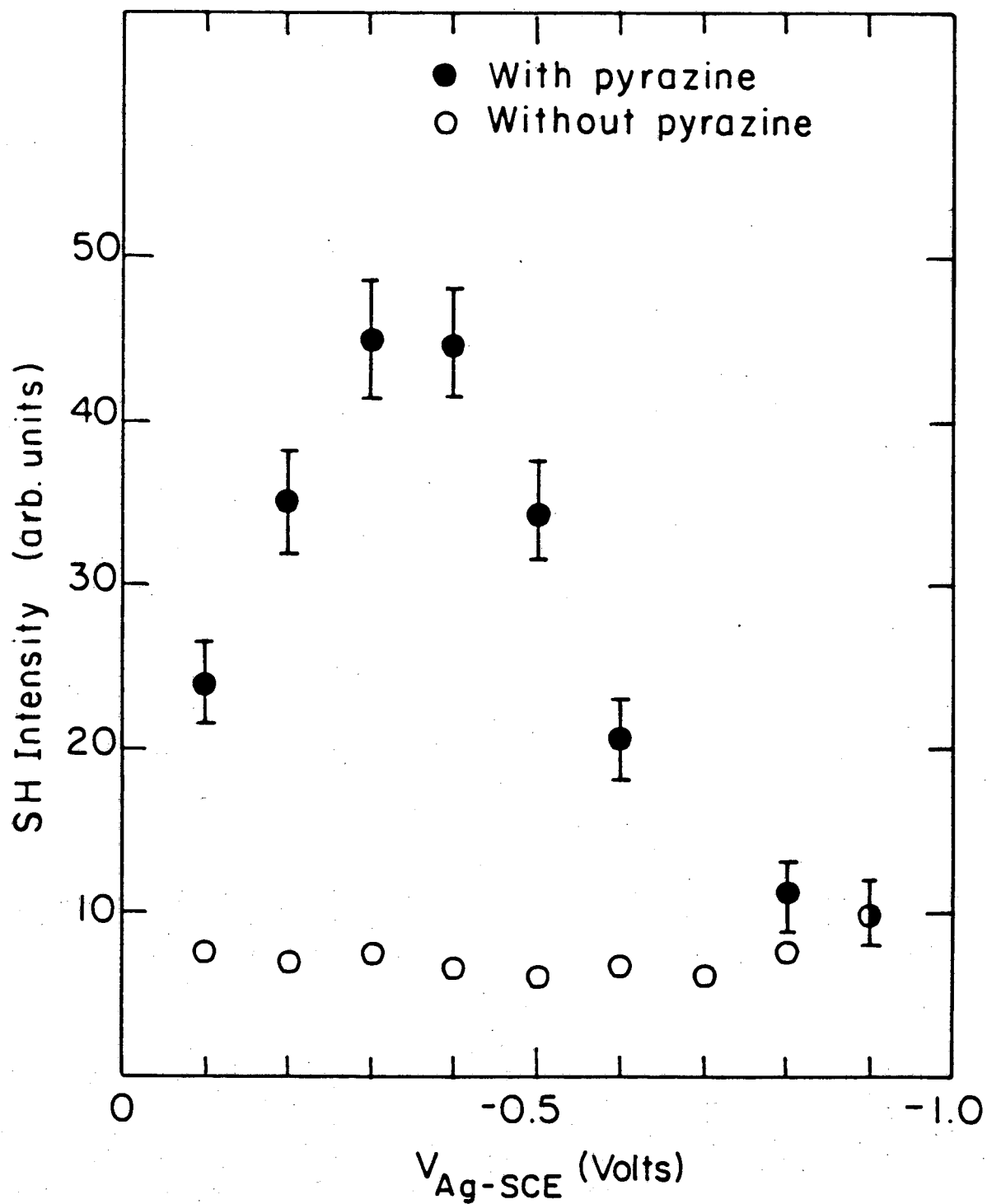
X BL 815 - 5825

Fig. 10



XBL 815-5826

Fig. 11



XBL 815-5782

Fig. 12

#### IV. SECOND-HARMONIC GENERATION BY ADSORBATES ON INSULATING SURFACES

The experiments described in the preceding chapter have demonstrated the surface sensitivity of the SHG process. While the measurements performed with silver substrates were facilitated by the enhancement in the nonlinear signal associated with the distinctive electrodynamics of the roughened surface, the results presented in this chapter indicate the general viability of SHG as a tool for surface studies. Here we probe molecular adsorbates on flat, insulating substrates. With optically smooth interfaces, we can also take advantage of the information contained in the spectral and polarization dependences of the SH signal. By bringing the fundamental or harmonic frequency into resonance with a molecular transition, not only can we increase the strength of the nonlinear signal, but we may also study the spectroscopy of the adsorbed species. The polarization properties are determined by the symmetry and orientation of the adsorbates, which are, conversely, partially specified by the observed SHG.

##### A. Theoretical Considerations

We wish to consider the second-order nonlinear response of a monolayer of noncentrosymmetric, partially ordered molecules. For the experiments to be discussed below, the effect of the substrate on the nonlinear signal is of secondary importance. The nonlinearity of the substrate is apt to be rather small, especially in comparison with that of resonantly excited adsorbates. If more precision is required, the contribution of the substrate to the SH intensity can be measured for the bare surface and the net signal can then be adjusted so as to isolate

the response of the adsorbates. Such a procedure, including an experimental determination of the relative phase of the substrate and net SH signals, has been used in the work of Sec. C below. At this point, let us consider the central problem of the monolayer alone.

### 1. Macroscopic Description

From the point of view of macroscopic electrodynamics, the monolayer can be fully characterized by its second-order surface nonlinear susceptibility  $S_{\chi}^{(2)}$ . In the interest of clarity, we shall neglect the linear susceptibility of the monolayer and of the surrounding media, corrections for which can be included in a straightforward manner.

By application of the boundary conditions of Appendix I, we can calculate the intensity of the SH radiation generated in the forward or reflected direction by excitation of a plane wave of frequency  $\omega$  and polarization  $\hat{e}(\omega)$ :

$$I(2\omega) = 32\pi^3 \omega^2 c^{-3} \sec^2 \theta |\hat{e}(2\omega) \cdot S_{\chi}^{(2)} : \hat{e}(\omega) \hat{e}(\omega)|^2 I^2(\omega). \quad (1)$$

In this equation  $\theta$  represents the angle of incidence,  $I(\omega)$  is the pump intensity, and  $\hat{e}(2\omega)$  is the detected polarization at the SH frequency. With the aid of this expression (or an analogous one for two separate pump beams), we can deduce the elements of the tensor  $S_{\chi}^{(2)}$  from experimental data. Table 1 lists the distinct nonzero elements of  $S_{\chi}^{(2)}$  when different symmetries exist. Unless the procedure of preparing the adsorbed layer lowers the symmetry, we expect the monolayer to have the same or a higher symmetry than the substrate. Thus for a substrate with an isotropic surface having inversion symmetry in the plane,  $S_{\chi}^{(2)}$  will have three distinct nonzero elements to describe SHG:  $S_{\chi_{zzz}}^{(2)}$ ,  $S_{\chi_{zii}}^{(2)}$ ,

$S_{\chi_{izi}}^{(2)} = S_{\chi_{iiz}}^{(2)}$ , with  $i = x, y$ .  $S_{\chi_{zii}}^{(2)}$  can be isolated under s-polarized excitation, while  $S_{\chi_{izi}}^{(2)}$  can be separated by detecting the s-polarized output for a pump beam of mixed polarization. One further measurement should then determine  $S_{\chi_{zzz}}^{(2)}$ .

## 2. Microscopic Description

The macroscopic susceptibility is given by a sum of the individual molecular polarizabilities, corrected for local-field effects:

$$S_{\chi}^{\leftrightarrow(2)}(2\omega = \omega + \omega) = \sum_{\substack{\text{unit} \\ \text{area}}} \alpha_n^{\leftrightarrow(2)}(2\omega = \omega + \omega) : \vec{L}_n(2\omega) \vec{L}_n(\omega) \vec{L}_n(\omega). \quad (2)$$

This formula is the two-dimensional analog of that of Armstrong et al.<sup>2</sup>  $\alpha_n^{\leftrightarrow(2)}(2\omega = \omega + \omega)$  is the second-order nonlinear polarizability of the n-th molecule and the  $\vec{L}_n$  is the corresponding local-field factor. If only one species of molecule is present and the local-field factors are unimportant (as is the case for sufficiently dilute systems), then Eq. (2) reduces to

$$S_{\chi}^{\leftrightarrow(2)} = N \langle \alpha^{\leftrightarrow(2)} \rangle, \quad (3)$$

where  $N$  is the surface density of the adsorbates and the angular brackets signify an average over molecular orientations of the adsorbed molecules. Note that the ratio of any two elements of the tensor  $S_{\chi}^{\leftrightarrow(2)}$  is given by the ratio of the angular average of  $\alpha^{\leftrightarrow(2)}$  projected in different directions. With some knowledge of the form of  $\alpha^{\leftrightarrow(2)}$ , we can then obtain values for angular averages of the molecular orientation from the experimentally determined polarization dependences, i.e., from the ratio of tensor elements of  $S_{\chi}^{\leftrightarrow(2)}$ . This type of analysis is applied in Secs. B

and C of this chapter.

The expression for the molecular polarizability for SHG can be derived from second-order time-dependent perturbation theory:<sup>3</sup>

$$\begin{aligned} \alpha_{ijk}^{(2)}(2\omega = \omega + \omega) = & \sum_{n, n' \neq g} \left\{ \frac{\langle g | p_i | n \rangle \langle n | p_j | n' \rangle \langle n' | p_k | g \rangle}{(2\omega - \omega_{ng} + i\Gamma_{ng})(\omega - \omega_{n'g} + i\Gamma_{n'g})} + \right. \\ & + \frac{\langle g | p_k | n \rangle \langle n | p_j | n' \rangle \langle n' | p_i | g \rangle}{(2\omega + \omega_{n'g} + i\Gamma_{n'g})(\omega + \omega_{ng} + i\Gamma_{ng})} - \\ & - \frac{\langle g | p_k | n \rangle \langle n | p_j | n' \rangle \langle n' | p_i | g \rangle}{(2\omega - \omega_{n'n} + i\Gamma_{n'n})} \times \left( \frac{1}{\omega + \omega_{ng} + i\Gamma_{ng}} + \right. \\ & \left. \left. + \frac{1}{\omega - \omega_{n'g} + i\Gamma_{n'g}} \right) \right\} + \left\{ \text{same with } j \leftrightarrow k \right\}. \quad (4) \end{aligned}$$

Here  $\langle n' | \vec{p} | n \rangle$ ,  $\omega_{n'n}$ , and  $\Gamma_{n'n}$  denote, respectively, the dipole moment, frequency, and linewidth of a transition from state  $|n\rangle$  to state  $|n'\rangle$ , and it has been assumed that the unperturbed system has a fully occupied, nondegenerate ground state  $|g\rangle$ . When the harmonic frequency  $2\omega$  approaches  $\omega_{ng}$  for some excited state  $|n\rangle$ , the first term in Eq. (4) contains a resonant contribution. Separating the resonant term, we can express  $\alpha_{ijk}^{(2)}$  as

$$\begin{aligned} \alpha_{ijk}^{(2)}(2\omega = \omega + \omega) = & \left[ \alpha_{ijk}^{(2)} \right]_{NR} - \pi^{-1} \hbar^{-2} \tilde{\alpha}^{(1)}(2\omega) \langle g | p_i | n \rangle \times \\ & \times \sum_{n' \neq g} \frac{\langle n | p_j | n' \rangle \langle n' | p_k | g \rangle + \langle n | p_k | n' \rangle \langle n' | p_j | g \rangle}{\omega - \omega_{n'g}}. \quad (5) \end{aligned}$$

The nonresonant terms, which should have only a mild frequency dependence, are represented by  $\left[ \alpha_{ijk}^{(2)} \right]_{NR}$ , and  $\tilde{\alpha}^{(1)}(2\omega)$  is the resonant linear molecular polarizability at the frequency  $2\omega$ , normalized so that



$\int \text{Im}[\alpha^{(1)}(2\omega)]d(2\omega) = 1$ . This formula is also valid for inhomogeneously broadened nondegenerate states. Barring the presence of additional resonances, the frequency dependence of  $\alpha_{ijk}^{(2)}(2\omega = \omega + \omega)$  near the resonance will be governed by  $\tilde{\alpha}^{(1)}(2\omega)$ . Thus we find that resonant SHG can give the same spectral information as a linear measurement. Note that in contrast to the linear absorption, the SH intensity, which is proportional to  $|\alpha_{ijk}^{(2)}|^2$ , will have resonant contributions from both the real and imaginary parts of  $\tilde{\alpha}^{(1)}(2\omega)$ . Similar resonances also occur of course whenever the fundamental frequency  $\omega \approx \omega_{ng}$ . From the experimental perspective, probing such a resonance may be more difficult, since the molecules will then absorb power from the pump beam and may be subject to laser-induced desorption.

For orientational studies, resonant SHG can be advantageous because it enhances the strength of the nonlinear signals. Furthermore, if the resonant contribution is dominant, a simpler form for the tensor  $\alpha^{(2)}$  may result, as a comparison of Eqs. (4) and (5) reveals.

## B. Study of Rhodamine Dyes Adsorbed on Fused Silica<sup>4</sup>

The resonant SHG measurements described here were performed on a submonolayer of rhodamine dye molecules adsorbed on a fused silica substrate. Spectra of the  $S_0 \rightarrow S_2$  electronic transition have been obtained. We have also studied the polarization dependence of the SH signal, which we use in the construction of a model for the orientation of the adsorbates. A value for the second-order nonlinear polarizability at resonance is deduced.

### 1. Experimental Apparatus

The basic elements of the set-up are indicated in Fig. 1. The tun-

able excitation at the fundamental frequency (over the range of 600-720 nm) was provided by a dye laser driven by the second harmonic of the 1.06  $\mu\text{m}$  output of a Q-switched  $\text{Nd}^{3+}$ :YAG laser. The dye laser consisted of an oscillator, a transversely pumped preamplifier, and a longitudinally pumped amplifier stage. The oscillator wavelength was varied by adjusting a diffraction grating mounted in the Littrow configuration.<sup>5</sup> In order to improve the dye laser linewidth and to avoid damaging the grating, a single prism beam expander<sup>6</sup> was inserted in front of the diffraction grating. The performance of the amplifying stages, particularly their preservation of the spectral quality of the beam, was improved by introducing a delay of a few nanoseconds in the arrival time of the pump radiation. Relying on a variety of different dyes, we were able to scan the desired range of wavelengths continuously. The 10 ns pulses produced by the dye laser were focused to an area of  $\sim 10^{-3} \text{ cm}^2$  on the sample, which was held at a  $45^\circ$  angle of incidence. The reflected SH signal was detected by an RCA 1P28 photomultiplier. The accompanying light at the fundamental frequency was blocked by color filters or a saturated aqueous solution of  $\text{CuSO}_4$ . A monochromator served to select precisely the SH frequency. In contrast to the situation for the roughened silver samples, here the smooth interface gave rise to a well-collimated reflected SH beam, permitting collection and imaging of the full harmonic output. Quartz optics were used at all points for the SH signal, which might have been attenuated in passing through normal glass.

In the absence of any surface enhancement SH signals were small and their detection required some care. First, it was imperative to remove any radiation at the SH frequency from the pump beam, which was accomplished with cut-off filters. Second, the background in the detec-

tion system was reduced by limiting the open window of the gates to  $\sim 1$   $\mu$ s. Electrical noise from the Q-switched  $\text{Nd}^{3+}$ :YAG laser was eliminated from the detection electronics by means of a high-speed electro-optic isolator in the trigger line. The photomultiplier output was averaged by a gated integrator. For especially weak signals, photoelectrons were counted directly and analyzed by the method of Appendix III. Background counts could be reduced to below 1 per 1000 laser shots.

Because of changes in the profile of the pump beam and in the collection efficiency of the detection system, it was necessary to normalize the SH signal to a reference with the same quadratic intensity dependence. A thin quartz plate was chosen for this purpose. When adjusted to the peak of a Maker fringe,<sup>7</sup> this source provided an essentially constant SH conversion efficiency  $[I(2\omega)/I^2(\omega)]$  over the relevant range of wavelengths. The actual normalization was accomplished by inserting the quartz plate in the beam just in front of the sample. Since the quartz SH signal completely overwhelmed the SH signal from the sample, the former could be recorded directly upon the addition of an attenuator, without otherwise altering the set-up.

Submonolayers of rhodamine 6G and rhodamine 110 dye molecules were formed on a fused silica substrate in the following manner. The substrate was carefully cleaned and mounted on a high-speed motor. A few drops of  $3 \times 10^{-4}$  M ethanolic solution of the dye was then placed on the substrate, which was immediately spun at 2000 rpm for 2 minutes. The substrate itself was optically flat to  $\lambda/10$  and had a 30' wedge, producing clearly separated front- and back-face reflections. By measuring the optical absorption of the strong  $S_0 \rightarrow S_1$  transition for several of such samples in tandem, we inferred an average surface density of dye

molecules of  $N = 5 \times 10^{13} \text{ cm}^{-2}$ .

## 2. Results

Figure 2 displays the observed SH spectra for the monolayer samples of rhodamine 110 and rhodamine 6G in the region of the  $S_0 + S_2$  electronic transition. The resonant SHG process is described in Fig. 3, which also gives the transition energies of the relevant states for the two dyes dissolved in ethanol. The spectrum was measured with a p-polarized pump, which produced a peak reflected SH signal amounting to  $\sim 10^4$  photons/pulse. The SH signal of the substrate alone was negligible, being a few orders of magnitude less strong than that of the resonant monolayer.

Measurements of the SHG by the adsorbed monolayers were taken for both p- and s-polarized excitation. In either case, only p-polarized light was observed at the SH, the s component being at least an order of magnitude less intense. We found a ratio  $R \sim 2$  for the strength of the SH signal arising from p-polarized excitation to that for s-polarized light. Since the SH radiation had the same polarization for either type of excitation, it was not necessary to compensate for a possible change in the collection efficiency in the two measurements. The SH intensity was independent of rotations of the sample about its surface normal. Figure 4 shows the constancy of the SH output for an s-polarized pump under such an excitation.

In order to determine the absolute SH conversion efficiency,  $I(2\omega)/I^2(\omega)$ , for our monolayer samples, we needed a nonlinear reference. We found it convenient simply to replace our sample by a freshly evaporated silver film, for which the SH conversion efficiency has already been established.<sup>7</sup> For s-polarized excitation of our rhodamine 110

sample, we then obtained  $I(2\omega)/I^2(\omega) \sim 7 \times 10^{-29}$  esu on resonance.

Throughout the experiment, the energy of the pump pulses was limited to  $\sim 1$  mJ, spread over the spot area of  $\sim 10^{-3}$  cm<sup>2</sup>. Under these conditions, we verified by continuously monitoring the SH signal as a function of time that no laser-induced desorption occurred.<sup>9</sup>

### 3. Analysis and Discussion

The SH spectra of Fig. 2 show the dominance of the resonant terms. A detailed study of the line shape and a careful determination of its center could provide insight into the structure of the adsorbed molecules and their interactions with the substrate. In this case, the position of the peak in the SHG is sufficiently similar to that of the molecules in solution so as to make such spectra useful in identifying the adsorbed species. The much greater magnitude of the nonlinear signals of the dye molecules compared to that of the fused silica substrate can be understood as resulting from the large dipole moments of the molecular transitions and the near-resonance of the fundamental frequency with the  $S_0 \rightarrow S_1$  transition (Fig. 3). In fact, the somewhat skewed appearance of the spectrum for rhodamine 6G on the short-wavelength side probably results from approaching this secondary resonance.

The absence of s-polarized SH output for either s- or p-polarized pump radiation is in agreement with the predictions of Table 1 when inversion symmetry in the plane is assumed to exist. Under this symmetry, only an input of mixed polarization can generate an output with an s-polarized component (through  $\chi_{xyzy}^{(2)} = \chi_{yyz}^{(2)}$ ). The rotational invariance of Fig. 4 is consistent with the expected isotropy of the adsorbed layer in the plane. The presence of a strong SH signal then implies that the interface must not have reflection symmetry with respect to the x-y

plane, either because there is a net average orientation of the molecules along the surface normal or because the electronic states of the adsorbate and of the substrate are distorted through their mutual interaction. In view of the substantial strength of the SHG, the former seems more reasonable. Given the small shifts in the energy levels of dye molecules, the nonlinear polarizability of the free molecules should approximate closely that of the adsorbed species.

The optical properties of the rhodamine dyes have been widely studied, both by linear<sup>5</sup> and (third-order) nonlinear techniques.<sup>10</sup> The delocalized  $\pi$  electrons in the system of three adjoining phenyl groups are responsible for the low-lying electronic transitions. It follows that the molecules can be treated as being planar and exhibiting mirror symmetry about the plane perpendicular to the molecule passing through the oxygen atom and the opposite carbon atom of the central phenyl group. Hence, the relevant transition dipole moments must always lie in the plane of the molecule, either along the line of symmetry (say, the  $z'$  direction) or perpendicular to it ( $x'$  direction). It has been deduced from both experiment and theory<sup>10,11</sup> that the  $S_0$  and the  $S_2$  states are even under the reflection operation, while the  $S_1$  state is odd. The  $S_0 \rightarrow S_1$  and  $S_1 \rightarrow S_2$  transition dipole moments must then be directed along the  $x'$  axis, while the  $S_0 \rightarrow S_2$  moment must be parallel to the  $z'$  axis. With these results in hand, Eq. (5) indicates that the resonant contribution to  $\alpha^{(2)}$  with intermediate state  $|n'\rangle = S_1$  gives rise to a nonzero value only for the  $z'x'x'$  element of the tensor. Because of its large transition dipole moment and its near-resonant character, the  $S_1$  state should in fact be the sole significant intermediate state. Furthermore, the shape of the SH spectra shows that the fully nonresonant

term of Eq. (5) is negligible. Thus for resonant SHG the single coefficient  $\alpha_{z'x'x'}^{(2)}$  determines the surface nonlinear susceptibility  $S_{\chi}^{*(2)}$  through Eq. (3). Consequently, the ratio of various tensor elements and, through Eq. (1), the polarization dependences must depend only on the geometrical factors associated with the adsorbate orientation.

We now evaluate models of the adsorbate orientation in light of the polarization dependences. The simplest model of flat adsorption is not consistent with the strong SHG observed, since such a layer of unperturbed molecules would exhibit inversion symmetry. If we take the rhodamine molecules to be coordinated with the surface through the two amino groups, while allowing the plane of the molecules to be canted relative to the surface, then we should consider a model in which the  $x'$  axes of the molecules lie in the plane in a randomly distributed fashion. With a well-defined model, we can make a theoretical prediction of the polarization ratio  $R$ . From Eq. (1), we can write

$$R = \left| \frac{2^{-3/2} (S_{\chi_{zxx}}^{(2)} + S_{\chi_{zzz}}^{(2)} - S_{\chi_{xzx}}^{(2)})}{2^{-1/2} (S_{\chi_{zxx}}^{(2)})} \right|^2. \quad (6)$$

The symmetry relation  $S_{\chi_{zyy}}^{(2)} = S_{\chi_{zxx}}^{(2)}$  has been applied in obtaining this expression. The value of a given tensor element of  $S_{\chi}^{*(2)}$  is computed in accordance with Eq. (3) as

$$S_{\chi_{ijk}}^{(2)} = N \alpha_{z'x'x'}^{(2)} \langle (\hat{i} \cdot \hat{z}') (\hat{j} \cdot \hat{x}') (\hat{k} \cdot \hat{x}') \rangle, \quad (7)$$

with the average extended over adsorbate orientation, i.e. over orientations of the primed coordinate system with respect to the fixed unprimed system. Clearly, in the model with  $\hat{x}'$  always lying in the  $x$ - $y$

plane of the surface, only  $S_{\chi_{zxx}}^{(2)}$  can be nonzero; whence  $R = \frac{1}{2}$  by Eq. (6), regardless of the tilt angle or distribution of angles of the adsorbate with respect to the surface.

An alternate possibility for adsorption would result from bonding by one of the amino groups and the acid group. Let us model this by assuming the molecular  $y'$  axes (the directions normal to the plane of each molecule) to be randomly oriented in the plane of the surface. Then we deduce from Eq. (6) that

$$\begin{aligned}
 S_{\chi_{zxx}}^{(2)} &= \frac{1}{2} N \alpha_{z'x'x'}^{(2)} \langle \cos^3 \theta' \rangle \\
 S_{\chi_{xzx}}^{(2)} &= - \frac{1}{2} N \alpha_{z'x'x'}^{(2)} \langle \cos \theta' \sin^2 \theta' \rangle \\
 S_{\chi_{zzz}}^{(2)} &= N \alpha_{z'x'x'}^{(2)} \langle \cos \theta' \sin^2 \theta' \rangle, \tag{8}
 \end{aligned}$$

which implies

$$R = (2 \langle \cos \theta' \rangle / \langle \cos^3 \theta' \rangle - 3/2)^2. \tag{9}$$

Here  $\theta'$  is the angle between the  $z'$  axis of an adsorbed molecule and the surface normal, and the averages are to be extended over the distribution of all such angles for the adsorbates. This model<sup>12</sup> agrees with the experimental value of  $R = 2$  provided that  $\langle \cos^3 \theta' \rangle / \langle \cos \theta' \rangle = 0.69$  or, for a narrow distribution of angles,  $\theta' \approx 34^\circ$ .

Within the framework of the last model, we can estimate the value of the nonlinear polarizability of the adsorbates. For s-polarized excitation, the only relevant component of the surface susceptibility



tensor is  $S_{\chi_{zyy}}^{(2)} = \frac{1}{2}N\langle \cos^3\theta' \rangle \alpha_{z'x'x'}^{(2)}$ . With  $\langle \cos^3\theta' \rangle \sim \cos^3 34^\circ$  and  $I(2\omega)/I^2(\omega) = 7 \times 10^{-29}$  esu, we deduce from Eq. (1) that  $|\alpha_{z'x'x'}^{(2)}| \sim 3 \times 10^{-29}$  esu.

We can compare the value of  $|\alpha_{z'x'x'}^{(2)}|$  obtained by experiment and the model adsorption geometry with that predicted by a direct evaluation of the quantum-mechanical expression of Eq. (5), which for our problem reduces to

$$\alpha_{z'x'x'}^{(2)} = \frac{-2\pi^{-1}\hbar^{-2}\tilde{\alpha}^{(1)}(2\omega)}{\omega - \omega_{S_1S_0}} \langle S_0 | p_{z'} | S_2 \rangle \langle S_2 | p_{x'} | S_1 \rangle \langle S_1 | p_{x'} | S_0 \rangle. \quad (10)$$

The matrix elements from the ground state can be easily determined by a direct measurement of the optical density of a dilute solution of the dyes:<sup>10</sup>

$$\begin{aligned} \langle S_1 | p_{x'} | S_0 \rangle &= 7.7D \\ \langle S_2 | p_{z'} | S_0 \rangle &= 2.7D. \end{aligned} \quad (11)$$

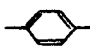
The matrix element between the two excited states has been calculated using a free-electron model of the response of the  $\pi$  electrons. Hermann<sup>10</sup> calculates following the method of Kuhn<sup>13</sup> a value of

$$\langle S_2 | p_{x'} | S_1 \rangle = 11D. \quad (12)$$

Treating the linear lineshape factor  $|\tilde{\alpha}^{(1)}(2\omega)|$  as having a triangular profile of width 40 nm, we infer from Eq. (10) a theoretical estimate  $|\alpha_{z'x'x'}^{(2)}| \sim 2 \times 10^{-28}$  esu, in rough agreement with the figure found

above.

### C. Study of p-Nitrobenzoic Acid Adsorbed on Fused Silica

In this section a more highly developed procedure for determining the orientation of molecular adsorbates by means of the polarization dependences of the SHG process is presented. This technique is applied to the problem of p-nitrobenzoic acid ( $\text{NO}_2$    $\text{COOH}$ ) adsorbed onto a fused silica substrate out of an ethanolic solution. An adsorption isotherm for this system has been obtained as well. SHG is a particularly appropriate probe for the liquid/solid interface. Other optical measurements fail to provide the intrinsic discrimination of SHG against signals arising from the randomly oriented molecules in the solution. The first two parts of our discussion treat the question of the measurement of the nonlinearity of an adsorbate layer and the inference of molecular orientation in a somewhat general manner. The subsequent paragraphs describe the experimental aspects, the results obtained, and their interpretation.

#### 1. Measurement of the Surface Nonlinear Susceptibility $S_{\chi}^{+(2)}$

The orientation of the molecular adsorbates is reflected in the values of the tensor elements of the second-order surface nonlinear susceptibility  $S_{\chi}^{+(2)}$ . From an experimental point of view, the goal is then to make an accurate measurement of this quantity. Let us consider the problem of a thin plane of a medium with linear dielectric constant  $\epsilon'$  and a surface nonlinearity described by  $S_{\chi}^{+(2)}$  surrounded by media with linear dielectric constants  $\epsilon_1$  and  $\epsilon_2$ . While a bulk magnetic-dipole contribution to the nonlinearity is permitted in centrosymmetric media, we shall not treat it separately since it can be incorporated into  $S_{\chi}^{+(2)}$ , as was discussed in Chap. II. The intensity of the reflected SH signal

of polarization  $\hat{e}(2\omega)$  for a pump beam of intensity  $I(\omega)$  and polarization  $\hat{e}(\omega)$  propagating through medium 1 can be written as

$$I(2\omega) = \frac{32\pi^3 \omega^2 \sec^2 \theta}{c^3 \epsilon_1(\omega) \epsilon_1'(2\omega)} |\vec{e}'(2\omega) \cdot \overset{\leftrightarrow}{S}_\chi^{(2)} : \vec{e}'(\omega) \vec{e}'(\omega)|^2 I^2(\omega). \quad (13)$$

In this generalized version of Eq. (1), the angle  $\theta$  represents that of the radiated SH signal with respect to the surface normal. If medium 1 shows dispersion, this angle will differ from that of the incoming pump radiation. The vectors  $\vec{e}'(\Omega)$  are related to the polarization vectors in medium 1 by the Fresnel coefficients:

$$\vec{e}'(\Omega) = \overset{\leftrightarrow}{L}(\Omega) \vec{e}(\Omega). \quad (14)$$

$\overset{\leftrightarrow}{L}$  assumes a diagonal form when expressed in the basis of the surface normal (z-direction), the normal to the plane of incidence (y-direction) and intersection of the surface and the plane of incidence (x-direction). Denoting the wavevectors as in Chap. II, we have

$$L_{xx}(\Omega) = 2[\epsilon_1(\Omega) k_z^{(2)}(\Omega)] [\epsilon_2(\Omega) k_z^{(1)}(\Omega) + \epsilon_1(\Omega) k_z^{(2)}(\Omega)]^{-1} \quad (15a)$$

$$L_{yy}(\Omega) = 2[k_z^{(1)}(\Omega)] [k_z^{(1)}(\Omega) + k_z^{(2)}(\Omega)]^{-1} \quad (15b)$$

$$L_{zz}(\Omega) = 2\epsilon_2(\Omega)/\epsilon'(\Omega) [\epsilon_1(\Omega) k_z^{(1)}(\Omega)] [\epsilon_2(\Omega) k_z^{(1)}(\Omega) + \epsilon_1(\Omega) k_z^{(2)}(\Omega)]^{-1}. \quad (15c)$$

In principle, we can determine  $\overset{\leftrightarrow}{S}_\chi^{(2)}$  for the system under study from Eqs. (13)-(15) by measuring  $I(2\omega)/I^2(\omega)$  for a variety of input and output polarizations. From a practical standpoint, it may be difficult

to obtain accurate values in this manner because of the need for frequent realignment and recalibration of the experimental apparatus. Such measurements require the use of a nonlinear reference, as we have seen in the previous section of this chapter. A more convenient approach consists in taking advantage of a nulling scheme. If we adjust the output polarizer so that it blocks the SH signal generated by a given input polarization, then we know from Eq. (13) that

$$\vec{e}'(2\omega) \cdot S_{\chi}^{\leftrightarrow(2)} : \vec{e}'(\omega) \vec{e}'(\omega) = 0. \quad (16)$$

Of course,  $\vec{e}'(\omega)$  is related to the input polarization  $\hat{e}(\omega)$ , and  $\vec{e}'(2\omega)$  in this equation is associated with the polarization passed by the analyzer. Eq. (16) defines some linear combination of tensor elements of  $S_{\chi}^{\leftrightarrow(2)}$  that vanishes, thus yielding the value for a ratio of different elements of  $S_{\chi}^{\leftrightarrow(2)}$ . By repeating this procedure for several input polarizations, we should be able to deduce all of the ratios of the tensor elements of  $S_{\chi}^{\leftrightarrow(2)}$ . Only a single measurement of SH intensity  $I(2\omega)/I^2(\omega)$  is required to define the overall scale of  $S_{\chi}^{\leftrightarrow(2)}$ .

Let us treat the problem of a layer with inversion symmetry and isotropy (or cubic symmetry) in the plane. In this case, there are just three independent elements of  $S_{\chi}^{\leftrightarrow(2)}$ :  $S_{\chi_{\perp\perp\perp}}(2)$ ,  $S_{\chi_{\perp\parallel\parallel}}(2)$ , and  $S_{\chi_{\parallel\perp\parallel}}(2) = S_{\chi_{\parallel\parallel\perp}}(2)$ . The relation holding for a null in the SH signal [Eq. (16)] can then be cast in the form:

$$e'_{\perp}(2\omega) [e'_{\perp}(\omega)]^2 \left\{ S_{\chi_{\perp\perp\perp}}(2) + [\vec{e}'_{\parallel}(\omega)/e'_{\perp}(\omega)]^2 S_{\chi_{\perp\parallel\parallel}}(2) + 2[\vec{e}'_{\parallel}(\omega) \cdot \vec{e}'_{\parallel}(2\omega)] \times \right. \\ \left. \times [e'_{\perp}(\omega)e'_{\perp}(2\omega)]^{-1} S_{\chi_{\parallel\perp\parallel}}(2) \right\} = 0. \quad (17)$$

Assuming  $e_{\perp}'(\omega)$ ,  $e_{\perp}'(2\omega) \neq 0$ , this relation leads to the following expression for a ratio of tensor elements:

$$\frac{S_{\chi_{\perp\perp\perp}}^{(2)} + [\vec{e}_{\parallel}'(\omega)/e_{\perp}'(\omega)]^2 S_{\chi_{\perp\parallel\parallel}}^{(2)}}{S_{\chi_{\parallel\perp\perp}}^{(2)}} = -2 \frac{\vec{e}_{\parallel}'(\omega) \cdot \vec{e}_{\parallel}'(2\omega)}{e_{\perp}'(\omega)e_{\perp}'(2\omega)}. \quad (18)$$

Note that the coefficient  $[\vec{e}_{\parallel}'(\omega)/e_{\perp}'(\omega)]^2$  defining the combination of tensor elements depends only on the input polarization and is independent of the null polarization, i.e., of  $\vec{e}'(2\omega)$ . Consequently, we can determine the two independent ratios of the elements of  $S_{\chi}^{*(2)}$  in a direct manner by finding the SH null of two appropriately chosen pump polarizations. The two measurements could be made either at a fixed angle of incidence with two different selections for the pump polarization or at two different angles of incidence with, say, the same p-polarized pump beam. This analysis has been couched in terms of linearly polarized signals. If the dielectric media are lossless at the fundamental frequency and  $S_{\chi}^{*(2)}$  has the same (not necessarily real) phase for all its elements, then a linearly polarized pump will generate a linearly polarized harmonic output. For other circumstances, a linearly polarized pump can give rise to an elliptically polarized beam at the SH. The procedure described above is still applicable, only in this case both a polarizer and a compensator are needed to block the SH signal.

The given method will fully specify the nonlinear susceptibility tensor  $S_{\chi}^{*(2)}$  up to an overall phase factor. Theoretical considerations may sometimes be used to determine this phase. With entirely off-resonant response, for example, the tensor  $S_{\chi}^{*(2)}$  should be real throughout. At other times, the absolute phase can be found only experimentally. Interference techniques have already been exploited for resolving the

analogous problem for bulk nonlinear effects.<sup>13</sup> The basic notation is to produce a SH output from the pump beam by a source with a known phase and to combine this beam with the SH output of the system under study. Typically an off-resonant, noncentrosymmetric crystal serves as the reference material. Using the dispersion of air between the fundamental and harmonic frequencies, we can generate interference fringes by varying the distance between the reference and the sample. This method will be illustrated below in the determination of the phase associated with the nonlinearity of the interface in the presence and absence of adsorbed p-nitrobenzoic acid. Once this phase difference has been found, the nonlinearity arising just from the adsorbate layer can be deduced.

## 2. Inference of the Molecular Orientation

We shall now discuss the question of obtaining the orientation of adsorbed molecules from a knowledge of the corresponding macroscopic surface nonlinear susceptibility tensor  $S_{\chi}^{(2)}$ . The case of adsorbed molecules oriented randomly with respect to direction in the plane of the interface will be treated in detail. We shall assume that local-field corrections can be neglected. Although the algebraic complexity of the problem will grow, the general framework outlined below should still be applicable under the inclusion of any given local-field factors. The want of accurate and general expressions for the local fields constitutes a more fundamental problem, but not one unique to measurements of SHG. Under the stated conditions, the molecular orientation can be specified by the two Euler angles  $\theta'$  and  $\psi'$  of the molecular coordinate system  $x'y'z'$  shown in Fig. 5. It follows from Eq. (3) that the two independent ratios of the components of  $S_{\chi}^{(2)}$  (which has three independent components) can be related to ratios of averages over molecular orienta-

tions of expressions in  $\theta'$  and  $\psi'$ . The molecular orientation for narrow distributions of  $\theta'$  and  $\psi'$  can consequently be deduced. These conclusions are, of course, predicated on a knowledge of the ratios of the relevant elements of  $\alpha^{(2)}$ , the nonlinear polarizability of the adsorbed species. Note, however, that the surface coverage  $N$  falls out of all of these ratios.

As a first example, suppose the adsorbed molecule has a second-order polarizability  $\alpha^{(2)}$  in which only  $\alpha_{z'z'z'}^{(2)}$  is significant. In this instance, Eq. (3) yields

$$S_{\chi_{||\perp||}}^{(2)} = \frac{1}{2}N \langle \cos\theta' \sin^2\theta' \rangle \alpha_{z'z'z'}^{(2)} \quad (19a)$$

$$S_{\chi_{\perp||\perp||}}^{(2)} = \frac{1}{2}N \langle \cos\theta' \sin^2\theta' \rangle \alpha_{z'z'z'}^{(2)} \quad (19b)$$

$$S_{\chi_{\perp\perp\perp}}^{(2)} = N \langle \cos^3\theta' \rangle \alpha_{z'z'z'}^{(2)} \quad (19c)$$

Since the molecular nonlinearity defines only the  $z'$  axis, the angle  $\psi'$  does not appear in these formulas. The factors of  $\frac{1}{2}$  in Eqs. (19a) and (19b) arise from an isotropic average over the azimuthal angle  $\phi'$ . In light of the discussion above, it should prove convenient to measure quantities of the form  $[S_{\chi_{\perp\perp\perp}}^{(2)} + b\chi_{\perp||\perp||}^{(2)}] [S_{\chi_{||\perp||}}^{(2)}]^{-1}$ . We can arrange the input polarization so that  $b = [\vec{e}'(\omega)/e'_\perp(\omega)]^2 = 2$ , in which case we find from Eq. (19) that

$$R \equiv \frac{S_{\chi_{\perp\perp\perp}}^{(2)} + 2\chi_{\perp||\perp||}^{(2)}}{S_{\chi_{||\perp||}}^{(2)}} = \frac{2\langle \cos\theta' \rangle}{\langle \cos\theta' \sin^2\theta' \rangle} \quad (20a)$$

Experimentally, the ratio  $R$  follows directly from the null angle of the

SH signal, as specified by Eq. (18):

$$R = \frac{-2\vec{e}_{\parallel}'(\omega) \cdot \vec{e}_{\parallel}'(2\omega)}{e_{\perp}'(\omega)e_{\perp}'(2\omega)}. \quad (20b)$$

Thus with an appropriately polarized pump beam, we obtain a weighted average of the tilt angles  $\theta'$  of the principal axes of the adsorbed molecules simply by a nulling of the SH output.

A more elaborate example is provided by the treatment of a planar molecular structure with  $C_{2v}$  symmetry, such as p-nitrobenzoic acid. Call the principal axis  $z'$ , the perpendicular direction in the plane of the molecule  $x'$ , and the normal to the molecular plane  $y'$ . The symmetry-allowed components of  $\alpha^{(2)}$  are as follows:  $\alpha_{z'z'z'}^{(2)}$ ,  $\alpha_{z'x'x'}^{(2)}$ ,  $\alpha_{x'z'x'}^{(2)}$  =  $\alpha_{x'x'z'}^{(2)}$ ,  $\alpha_{z'y'y'}^{(2)}$ , and  $\alpha_{y'x'y'}^{(2)}$  =  $\alpha_{y'y'z'}^{(2)}$ . We shall neglect the last two components in the list. They involve transition dipole moments perpendicular to the molecular plane, which are usually small compared with the in-plane moments for molecules like p-nitrobenzoic acid having delocalized electrons. From Eq. (3), we find that

$$S_{X_{\parallel\parallel\parallel}}^{(2)} = \frac{1}{2}N \langle \cos\theta' \sin^2\theta' \alpha_{z'z'z'}^{(2)} - \cos\theta' \sin^2\theta' \sin^2\psi' (\alpha_{z'x'x'}^{(2)} + 2\alpha_{x'z'x'}^{(2)}) + \cos\theta' \alpha_{x'z'x'}^{(2)} \rangle \quad (21a)$$

$$S_{X_{\perp\parallel\parallel}}^{(2)} = \frac{1}{2}N \langle \cos\theta' \sin^2\theta' \alpha_{z'z'z'}^{(2)} - \cos\theta' \sin^2\theta' \sin^2\psi' (\alpha_{z'x'x'}^{(2)} + 2\alpha_{x'z'x'}^{(2)}) + \cos\theta' \alpha_{z'x'x'}^{(2)} \rangle \quad (21b)$$

$$S_{X_{\perp\perp\perp}}^{(2)} = N \langle \cos^3\theta' \alpha_{z'z'z'}^{(2)} + \cos\theta' \sin^2\theta' \sin^2\psi' (\alpha_{z'x'x'}^{(2)} + 2\alpha_{x'z'x'}^{(2)}) \rangle. \quad (21c)$$



For a narrow distribution of orientations, two independent ratios of the expressions appearing on the left-hand side of Eq. (21) should lead to a specification of the angles  $\theta'$  and  $\psi'$  in terms of ratios of components of  $S_X^{(2)}$ . The quantity  $R = [S_{X_{\perp\perp\perp}}^{(2)} + 2S_{X_{\perp\parallel\parallel}}^{(2)}][S_{X_{\parallel\parallel\parallel}}^{(2)}]^{-1}$  defined above is now given by

$$R = \frac{2\langle \cos\theta' (\alpha_{z'z'z'}^{(2)} + \alpha_{z'x'x'}^{(2)}) \rangle}{\langle \cos\theta' \sin^2\theta' \alpha_{z'z'z'}^{(2)} - \cos\theta' \sin^2\theta' \sin^2\psi' (\alpha_{z'x'x'}^{(2)} + 2\alpha_{x'z'x'}^{(2)}) + \cos\theta' \alpha_{x'z'x'}^{(2)} \rangle} \quad (22)$$

Under the assumption that averages over  $\theta'$  and  $\psi'$  can be carried out independently, Eq. (22) can be rewritten as

$$\frac{\langle \cos\theta' \rangle}{\langle \cos\theta' \sin^2\theta' \rangle} = \frac{R}{2} \cdot \frac{\alpha_{z'z'z'}^{(2)} - (\alpha_{z'x'x'}^{(2)} + 2\alpha_{x'z'x'}^{(2)}) \langle \sin^2\psi' \rangle}{\alpha_{z'z'z'}^{(2)} + \alpha_{z'x'x'}^{(2)} - (R/2)\alpha_{x'z'x'}^{(2)}} \quad (23)$$

This equation provides a relationship between  $\langle \cos\theta' \rangle / \langle \cos\theta' \sin^2\theta' \rangle$  and  $\langle \sin^2\psi' \rangle$ , i.e., between the angle of a molecule's principal axis with respect to the surface normal and the angle of rotation of the plane of the molecule about its principal axis. In this case of p-nitrobenzoic acid,  $\alpha_{z'z'z'}^{(2)}$  dominates the nonlinear response. Consequently, Eq. (20) will be applied to deduce  $\langle \cos\theta' \rangle / \langle \cos\theta' \sin^2\theta' \rangle$ . The importance of the corrections induced by the presence of finite values for  $\alpha_{z'x'x'}^{(2)}$  and  $\alpha_{x'z'x'}^{(2)}$  can be gauged from the more complete expression of Eq. (23).

### 3. Properties of p-Nitrobenzoic Acid

Before turning to the experiment itself, it seems appropriate to present some of the pertinent chemical and optical properties of p-nitrobenzoic acid (PNBA).

In the past few years, several studies have been conducted on the adsorption of monocarboxylic acids on oxidized metal surfaces. Inelas-

tic electron tunneling spectroscopy has been the most widely applied technique in these investigations. Vibrational spectra for a broad class of carboxylic acids adsorbed on alumina (formed as the native oxide of aluminum) have been obtained in this manner.<sup>14</sup> Monolayers of the adsorbate of interest were deposited on the alumina surface by spinning a sample covered with a dilute solution of the acid at high speed. The principal findings for systems prepared in the indicated fashion were that a saturated monolayer of the acid could chemisorb at room temperature and that the adsorbed species was a symmetrically positioned, bidentate carboxylate ion ( $\text{RCO}_2^-$ ). Hall and Hasma<sup>14</sup> speculated that the adsorbates were not strictly normal to the plane of the surface by making a comparison with results for adsorbed sulfonic acids.<sup>15</sup> Recently infrared spectra for a monolayer of adsorbed PNBA have been obtained by observation of the electromagnetic radiation emitted by the surface.<sup>16</sup> The vibrations characteristic of an adsorbed carboxylate structure were noted in these experiments on an oxidized copper surface. Adsorbed PNBA monolayers have also been used in studies of surface-enhanced Raman scattering<sup>17</sup> and Raman-gain spectroscopy.<sup>18</sup>

As far as the optical response of PNBA is concerned, we have, as discussed below, probed both resonant and off-resonant SHG. Figure 6 shows the measured molar extinction coefficient of PNBA dissolved in ethanol as a function of wavelength. The peak in the (linear) adsorption at  $\sim 260$  nm corresponds to the lowest-lying transition of any substantial strength. The excited state is expected to have  $A_1$  symmetry<sup>19</sup> and the transition dipole moment from the ground state should be directed along the principal ( $z'$ ) axis of the molecule. The presence of delocalized  $\pi$  electrons in the noncentrosymmetric mono- and disubstituted

benzene derivatives can give rise to a quite strong nonlinear response, as the experimental work of Levine and Bethea<sup>20</sup> and of Oudar and coworkers<sup>21</sup> has demonstrated. For a mono- or p-disubstituted compound (with  $C_{2v}$  symmetry) the symmetry-allowed elements of  $\alpha^{(2)}$  are  $\alpha_{z'z'z'}^{(2)}$ ,  $\alpha_{z'x'x'}^{(2)}$ ,  $\alpha_{x'z'x'}^{(2)} = \alpha_{x'x'z'}^{(2)}$ ,  $\alpha_{z'y'y'}^{(2)}$ , and  $\alpha_{y'z'y'}^{(2)} = \alpha_{y'y'z'}^{(2)}$ , for SHG. It was suggested earlier that  $\alpha_{z'y'y'}^{(2)}$  and  $\alpha_{y'z'y'}^{(2)}$  should be much smaller than the other nonvanishing components. This contention has been verified by the detailed theoretical studies of aniline, nitrobenzene, and p-nitroaniline performed by Lalama and Garito.<sup>22</sup> In fact, for excitation in the near-infrared and visible  $\alpha_{z'y'y'}^{(2)}$  and  $\alpha_{y'z'y'}^{(2)}$  were found to be some two orders of magnitude weaker than the other symmetry-allowed elements of  $\alpha^{(2)}$ . The calculations further revealed the dominance of  $\alpha_{z'z'z'}^{(2)}$  over  $\alpha_{z'x'x'}^{(2)}$  and  $\alpha_{x'z'x'}^{(2)}$  by roughly one order of magnitude. The origin of this behavior lies in the large (static) dipole moments of some of the excited states. In the case of a resonance of the harmonic frequency with that of the low-lying  $A_1 \rightarrow A_1$  transition, the  $\alpha_{x'z'x'}^{(2)}$  element should be further suppressed relative to  $\alpha_{z'z'z'}^{(2)}$  (and to  $\alpha_{z'x'x'}^{(2)}$ ), since the resonant transition dipole moment lies parallel to  $\hat{z}'$ .

#### 4. Experimental Apparatus

The basic scheme of the experimental set-up has been discussed in Sec. B of this chapter, and only the salient differences will be mentioned here. In place of a dye laser, the SH output of the Q-switched  $Nd^{3+}$ :YAG laser at 532 nm was used directly as the pump for resonant measurements. The off-resonant response of the PNBA monolayer was probed with the radiation at 683 nm produced by stimulated Raman scattering in  $H_2$  gas of the 532 nm beam. Measurements were also taken with the unmodulated pulses from the  $Nd^{3+}$ :YAG laser at the 1.06  $\mu m$  fundamental wave-

length.

The sample cell for our studies of adsorption at a liquid/solid interface was filled with an ethanolic solution of PNBA of millimolar concentration. The pump light passed through the fused silica substrate with faces flat to  $\lambda/10$ . The reflected SH radiation generated at the interface with the solution was detected after it emerged from the window. By means of spatial filtering, we were able to block the SH signal from the front face. Such spatial filtering is, of course, particularly easy for a slightly wedged window. Typical pump intensities of the 10 ns pulses were  $\sim 100 \text{ MW/cm}^2$  over an area of a fraction of a  $\text{cm}^2$ . After passing through various dispersive elements, the SH radiation would produce on the order of 1-100 photoelectrons per pulse in the photomultiplier, corresponding to  $\sim 30$ -3000 SH photons emitted by the sample.

Data for the isotherm were collected under s-polarized excitation. In order to determine the ratio  $R = [S_{\chi_{\perp\perp\perp}}^{(2)} + 2S_{\chi_{\perp\parallel\parallel}}^{(2)}][S_{\chi_{\parallel\perp\parallel}}^{(2)}]^{-1}$ , we must adjust the input polarization so that  $\vec{e}_{\parallel}^i(\omega) \cdot \vec{e}_{\parallel}^i(\omega)/e_{\perp}^i(\omega)e_{\perp}^i(\omega) = 2$ . Taking the relevant Fresnel coefficients into account (including one for the air/glass interface), we find that this condition can be satisfied for a pump beam incident on the window at  $65^\circ$  which is linearly polarized at approximately  $32^\circ$  from the horizontal. The SH radiation null was found with the aid of a Rochon polarizer made of quartz.

Phase measurements of the SH radiation were accomplished by interference between the signal of interest and that of a thin quartz plate. The quartz reference was placed in the path of the reflected beam before the component at the fundamental frequency was blocked. The quartz plate was cut as a plane of constant  $y$ . In this case, only the projection of a normally incident electric field on the  $x$ -axis can contribute

to SHG, as for quartz<sup>23</sup>  $\chi_{xzx}^{(2)} = \chi_{xzz}^{(2)} = \chi_{zxx}^{(2)} = \chi_{zxx}^{(2)} = \chi_{zzz}^{(2)} = 0$ . The magnitude of this reference could consequently be adjusted to the desired value simply by a rotation. Interference fringes between the sample and reference SH output were observed upon translation of the reference. For a fundamental wavelength of 532 nm, the dispersion in the refractive index of air introduces a  $2\pi$  phase shift between  $E^2(\omega)$  and  $E(2\omega)$  over a distance of 1.48 cm. Because of this dispersion in the air and in the fused silica substrate, it is necessary to exercise some care to obtain well-defined fringe patterns. It proved essential to avoid the use of a wedged window, since the material dispersion would have led to an angular separation of the reflected fundamental and harmonic beams. For a flat with parallel faces this problem does not arise. With a window of 3 mm thickness, we were able to obtain fringe patterns with contrast ratios of 10-15, permitting an accurate determination of the phase. These measurements required a laser beam with a smooth profile, which was obtained by allowing the pump laser output (initially having the characteristic annular pattern of an unstable resonator) to propagate into the far-field zone.<sup>24</sup>

## 5. Results and Discussion

We shall first present our results on the adsorption isotherm of PNBA. The question of the orientation of this adsorbate will be treated subsequently.

For low surface coverages of adsorbed PNBA, we can assume that the change in the reflected electric field at the SH is proportional to the adsorbate surface density  $N$ :

$$E(2\omega) = E_0(2\omega) + AN. \quad (24)$$

Here  $E(2\omega)$  is the radiated harmonic field of a given polarization arising from the interface, and  $E_0(2\omega)$  represents the corresponding quantity in the absence of any adsorbate.  $A$  is a (complex) constant for any given excitation at the fundamental frequency. Such a simple linear relation will no longer hold if coverage-dependent reorientation of the adsorbed species or if local-field effects are significant. The readily measurable quantities are not electric fields, but the intensities, in terms of which we have

$$I(2\omega) = I_0(2\omega) |1 + AE_0^{-1}(2\omega)N|^2. \quad (25)$$

Let  $\phi$  denote the phase of the contribution of the adsorbed molecules to the harmonic field relative to that of the unperturbed interface, i.e.,  $AE_0^{-1}(2\omega) = e^{i\phi} |AE_0^{-1}(2\omega)|$ . We can then rewrite Eq. (25) in the form appropriate for obtaining an isotherm, namely,

$$N \propto [I(2\omega)/I_0(2\omega) - 1 + \cos^2 \phi]^{1/2} - \cos \phi. \quad (26)$$

Our measurements have been performed with an s-polarized pump, for which only a p-polarized output is generated. The wavelength of the excitation was chosen to be 532 nm so as to take advantage of the enhancement of the nonlinearity of PNBA arising from the resonance in the SH frequency. The relative phase of the harmonic electric fields for the interface in the presence and absence of adsorbed PNBA has been established by means of the interference technique outlined above. Data for the position of the signal null for the two cases are displayed in Fig. 6. The phase angle  $\phi$  of Eq. (26) can be inferred from the observed

phase difference and the accompanying ratio of intensities. From measurements with a  $3 \times 10^{-3}$  M PNBA solution, we find that  $\phi = 75^\circ \pm 5^\circ$ . The positive sign of  $\phi$  indicates that the nonlinearity of the adsorbed molecules is advanced with respect to that of the substrate. The absolute phase of the nonresonant nonlinearity of the substrate is expected to be real. The phase shift of  $75^\circ$  for the PNBA molecules is appropriate for resonant excitation displaced somewhat from line center (see Fig. 6).

An adsorption isotherm analyzed according to Eq. (26) with  $\phi = 75^\circ$  is depicted in Fig. 8. The glass cell and fused silica window were initially cleaned with a sequence of organic solvents, before the addition of reagent-grade ethanol. After each infusion of PNBA, we waited for  $\sim 1$  hour to allow for equilibration of the adsorption process. Certain features of the isotherm merit comment. First note the characteristic saturation behavior indicative of chemisorption of a monolayer. This leveling-off of the SH signal further shows that the contribution to the nonlinearity from PNBA in the bulk of the solution must be small. Such a contribution would manifest itself by an approximately linear growth in the value inferred for  $N$  as a function of the bulk concentration of PNBA. The nonlinear signal from the interface with a saturated coverage of PNBA was typically a factor of 10 greater than that of the interface in the absence of this adsorbate. The exact value of this ratio was not strictly reproducible from trial to trial, perhaps reflecting the existence of some surface contamination. The change in free energy of PNBA upon adsorption can be estimated from the shape of the isotherm with the aid of Eqs. (6) and (7) of Chap. III. We obtain  $\Delta G \sim 8$  kcal/mole in this manner.

The approach for deducing the adsorbate orientation has already been elaborated; but in order to apply our formalism, we must compensate for the contribution to the nonlinear signal from the ethanol/glass interface in the absence of any adsorbed PNBA. Under excitation by a pump beam of the desired polarization, we have measured the magnitude and polarization of the SH radiation from the interface when the cell contained pure ethanol and ethanol with 3 mM PNBA. We can subtract the SH fields analytically to obtain the field associated with the adsorbed layer of PNBA alone. In performing this calculation, we have assumed the off-resonant signals of the interface and the adsorbate to have the same phase for excitation at 1.06  $\mu\text{m}$  and 683 nm. For excitation at 532 nm, we have taken their phase difference to be  $\phi = 75^\circ$ . This value was previously deduced for a differently polarized excitation. It should still apply here because  $S_{\chi}^{\leftrightarrow(2)}(\text{PNBA}) \propto \langle \hat{\alpha}^{\leftrightarrow(2)}(\text{PNBA}) \rangle \approx \alpha_{z'z'z'}^{(2)}(\text{PNBA}) \cdot \langle \hat{z}'\hat{z}'\hat{z}' \rangle$ , implying that all of the elements of the nonlinear susceptibility tensor have approximately the same phase. The relative phase shift between the linearly polarized components of the SH field of the adsorbate-covered interface leads to a somewhat elliptically polarized signal.<sup>25</sup> The polarization of the signal from the adsorbed PNBA follows from a measurement of the linearly polarized field of the bare interface and of the magnitude and orientation of the principal axis of the elliptically polarized net signal. For this particular experiment, the polarization of the SH waves from the adsorbate-covered and clean interfaces did not differ greatly ( $\lesssim 15^\circ$ ). Hence, a moderately accurate measurement of the magnitudes of these SH signals was sufficient for a quite accurate determination of the polarization of the SH radiation originating in the adsorbed layer alone.



Table 2a summarizes the results for the magnitude and polarization of the SH field arising from the layer of adsorbed PNBA. Note the  $\sim 8$ -fold increase in the (relative) SH field strength for resonant excitation at 532 nm compared with that of off-resonant excitation at 1.06  $\mu\text{m}$ . The listed null angles can be immediately transformed by Eqs. (15) and (20b) into values for the ratio  $R$ . Under the neglect of all components of  $\alpha^{(2)}$  excluding  $\alpha_{z'z'z'}^{(2)}$ , we can apply Eq. (20a) to give  $\langle \cos\theta' \rangle / \langle \cos\theta' \sin^2\theta' \rangle$  as  $R/2$ . These data are displayed in Table 2b for the three pump wavelengths. We can estimate the effect of the finite values of  $\alpha_{z'x'x'}^{(2)}$  and  $\alpha_{x'z'x'}^{(2)}$  by evaluating Eq. (23). We have chosen  $\alpha_{z'x'x'}^{(2)} / \alpha_{z'z'z'}^{(2)} = -.15$  and  $\alpha_{x'z'x'}^{(2)} / \alpha_{z'z'z'}^{(2)} = -.10$ , in accordance with the results of Lalama and Garito<sup>22</sup> for p-nitroaniline under 1.06 $\mu\text{m}$  excitation. The entries in columns (ii) and (iii) correspond to the cases of  $\langle \sin^2\psi' \rangle = 0$  and  $\langle \sin^2\psi' \rangle = 1$ , respectively. For a narrow distribution of orientations,  $\langle \cos\theta' \rangle / \langle \cos\theta' \sin^2\theta' \rangle$  determines the tilt angle  $\theta'_0$ . Inspection of Table 2b reveals that  $\theta'_0 = 38^\circ \pm 6^\circ$  is compatible with all of the indicated methods of analysis of the data obtained for each of the three choices of the wavelength of the pump beam. The  $6^\circ$  uncertainty in  $\theta'_0$  is limited by the lack of knowledge of  $\langle \sin^2\psi' \rangle$  and of accurate values for the smaller components of  $\alpha^{(2)}$ . For a specified mode of analysis, the experimental data themselves are sufficient for a determination of  $\theta'_0$  to  $\sim \pm 3^\circ$ . The relatively good agreement of our results for the cases of off-, near- and resonant excitation suggests that local-field effects are not very significant for the system under study: it appears unlikely that their influence could otherwise be so similar for the three different cases.

## References

1. An improved measurement technique for these independent components of  $S_{\chi}^{(2)}$  is presented in Sec. C of this chapter.
2. See appendix of J. A. Armstrong, N. Bloembergen, J. Ducuing, and P. S. Pershan, Phys. Rev. 127, 1918 (1962).
3. N. Bloembergen and Y. R. Shen, Phys. Rev. 133, A37 (1964).
4. T. F. Heinz, C. K. Chen, D. Ricard, and Y. R. Shen, Phys. Rev. Lett. 48, 478 (1982).
5. F. P. Schäfer, "Principles of Dye Laser Operation" in Topics in Applied Physics: Dye Lasers, edited by F. P. Schäfer (Springer-Verlag, Berlin, 1978), p.1.
6. S. A. Myers, Optics Commun. 4, 187 (1971).
7. P. D. Maker, R. W. Terhune, M. Nisenoff, and C. M. Savage, Phys. Rev. Lett. 8, 23 (1962).
8. N. Bloembergen, R. K. Chang, S. S. Jha, and C. H. Lee, Phys. Rev. 174, 813 (1968).
9. Laser-induced desorption of rhodamine dyes adsorbed on glass has been studied by V. S. Letokhov, V. G. Movshev, S. V. Chekalin, Zh. Eksp. Teor. Fiz. 81, 480 (1981)[translation: Sov. Phys. JETP 54, 257 (1981)].
10. J. P. Hermann, Ph.D. thesis, Université de Paris Sud, Paris, 1974 (unpublished).
11. J. P. Hermann and J. Ducuing, Optics Commun. 6, 101 (1972).
12. S. Garoff, R. B. Stephens, C. D. Hanson, and G. K. Sorenson [J. Luminescence 24/25, 773 (1981)] have made measurements of the linear absorption and luminescence, which they believe support a flat adsorption geometry. Since their procedure for preparing the ad-

sorbed rhodamine dyes differed from ours, it is difficult to compare results.

13. E. Zernike and J. E. Midwinter, Applied Nonlinear Optics (Wiley, New York, 1973) and references therein.
14. J. T. Hall and P. K. Hansma, Surf. Sci. 76, 61 (1978) and references therein.
15. J. T. Hall and P. K. Hansma, Surf. Sci. 71, 1 (1978).
16. D. L. Allara, D. Teicher, and J. F. Durana, Chem. Phys. Lett. 84, 20 (1981).
17. C. A. Murray, D. L. Allara, and M. Rhinewhine, Phys. Rev. Lett. 46, 57 (1981).
18. J. P. Heritage and D. L. Allara, Chem. Phys. Lett. 74, 507 (1980).
19. W. Liptay, "Dipole Moments and Polarizabilities of Molecules in Excited Electronic States" in Excited States, vol. 2, edited by E. C. Lin (Academic Press, New York, 1975), p.129.
20. B. F. Levine and C. G. Bethea, J. Chem. Phys. 63, 2666 (1975).
21. J. L. Oudar and H. LePerson, Optics Commun. 15, 258 (1975); 18, 410 (1976).
22. S. J. Lalama and A. F. Garito, Phys. Rev. A 20, 1179 (1979).
23. A. Yariv, Quantum Electronics, 2nd Ed. (Wiley, New York, 1975), p. 411.
24. This scheme of propagation into the far field is discussed by A. E. Siegman, Appl. Optics 13, 353 (1974).
25. Because of a weak birefringence in the fused silica substrate, all SH signals showed some minor degree of elliptical polarization.

TABLE 1

Symmetry	SFG	SHG	Low-Freq. Limit
None	ijk	ijk = ikj	ijk = kij = jki = ikj = jik = kji
Inversion symmetry in plane	zzz zxx, zyy xxz, xxz yzy, yyz	zzz zxx, zyy xzx = xxz yzx = yyz	zzz zxx = xzx = xxz zyy = yzy = yyz
Inversion in plane and $C_4$ or higher rotational symmetry	zzz zxx = zyy xzx = yzy xxz = yyz	zzz zxx = zyy xzx = yzy = xxz = yyz	zzz zxx = zyy = xzx = yzy = xxz = yyz

Distinct nonzero elements of the second-order surface nonlinear susceptibility tensor for the general case of sum-frequency generation, for second-harmonic generation, and for the low-frequency limit of either process are given when different symmetries exist. The surface lies in a plane of constant  $z$ .

TABLE 2a

$\lambda_{\text{pump}}$	$\frac{E(2\omega)}{E_o(2\omega)}$	Null Angle
1.06 $\mu\text{m}$	.19	$40^\circ \pm 5^\circ$
683 nm	.32	$51^\circ \pm 5^\circ$
532 nm	1.6	$37^\circ \pm 5^\circ$

SH field from the adsorbed layer of PNBA for pump excitation at the three given wavelengths. The strength of this electric field relative to that of the bare interface and the angle of the orthogonal polarization are indicated.

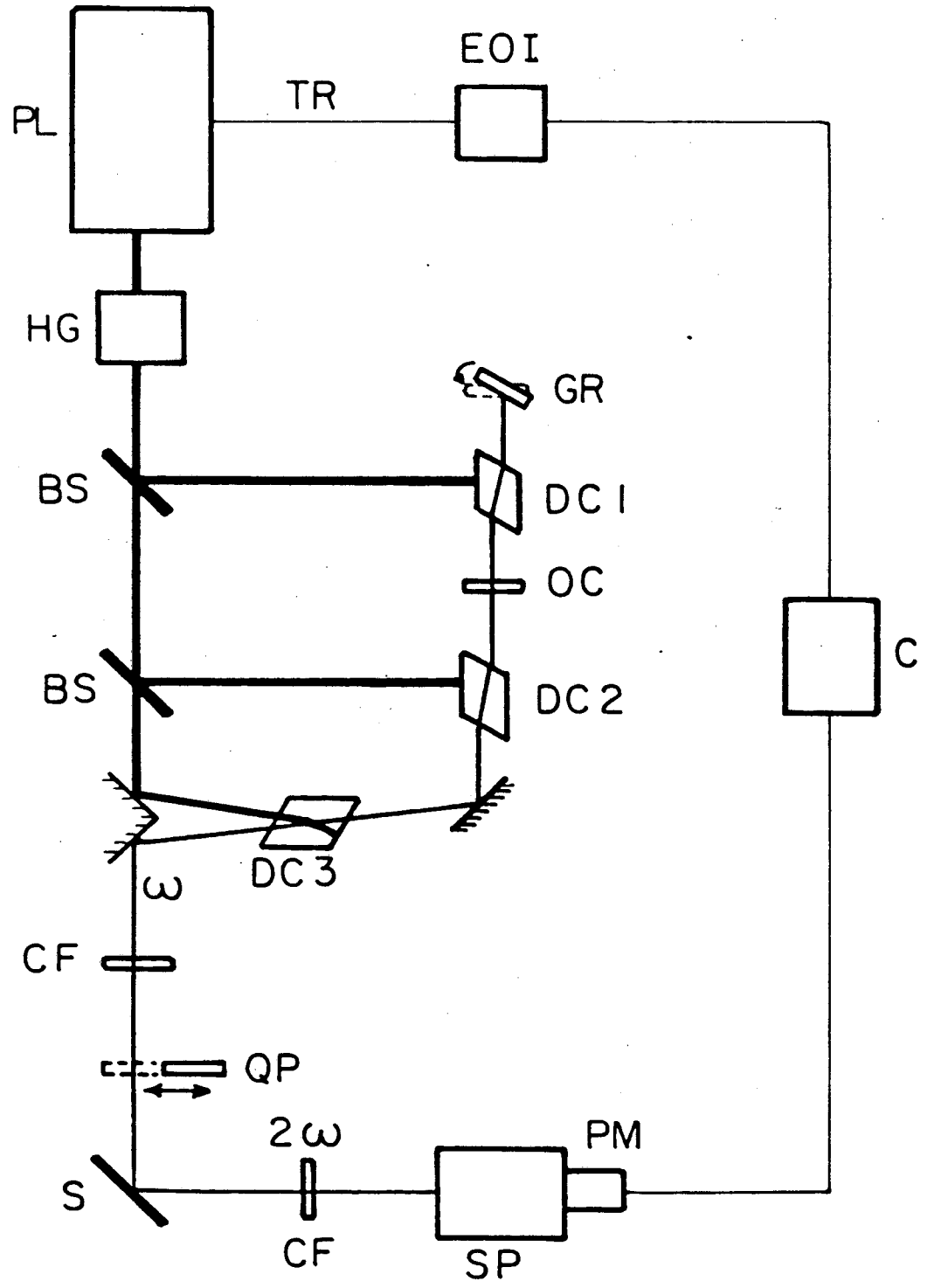
TABLE 2b

$\lambda_{\text{pump}}$	R	$\langle \cos\theta' \rangle / \langle \cos\theta' \sin^2\theta' \rangle, \theta'_o$		
		(i)	(ii)	(iii)
1.06 $\mu\text{m}$	5.3	2.6, $38^\circ$	2.3, $41^\circ$	3.2, $34^\circ$
683 nm	4.4	2.2, $42^\circ$	2.1, $44^\circ$	2.8, $37^\circ$
532 nm	5.5	2.8, $37^\circ$	2.5, $39^\circ$	3.4, $33^\circ$

The ratio  $R = \left[ \frac{S_{x_{\perp\perp\perp}}(2)}{S_{x_{\parallel\parallel\parallel}}(2)} + 2 \frac{S_{x_{\perp\parallel\parallel}}(2)}{S_{x_{\parallel\perp\perp}}(2)} \right] \left[ \frac{S_{x_{\parallel\perp\perp}}(2)}{S_{x_{\perp\perp\perp}}(2)} \right]^{-1}$  is given for the three indicated pump wavelengths. The last three columns record  $\langle \cos\theta' \rangle / \langle \cos\theta' \sin^2\theta' \rangle$  and the corresponding angle  $\theta'_o$  for a narrow distribution. Column (i) is computed for  $\alpha_{z'x'x'}^{(2)}, \alpha_{x'z'x'}^{(2)} \approx 0$ ; columns (ii) and (iii) assume  $\alpha_{z'x'x'}^{(2)} / \alpha_{z'z'z'}^{(2)} = -.15$  and  $\alpha_{x'z'x'}^{(2)} / \alpha_{z'z'z'}^{(2)} = -.10$  with  $\langle \sin^2\psi' \rangle = 0$  and  $\langle \sin^2\psi' \rangle = 1$ , respectively. In the calculation of R, we have taken  $\epsilon' = \epsilon_2 = 1.36$ .

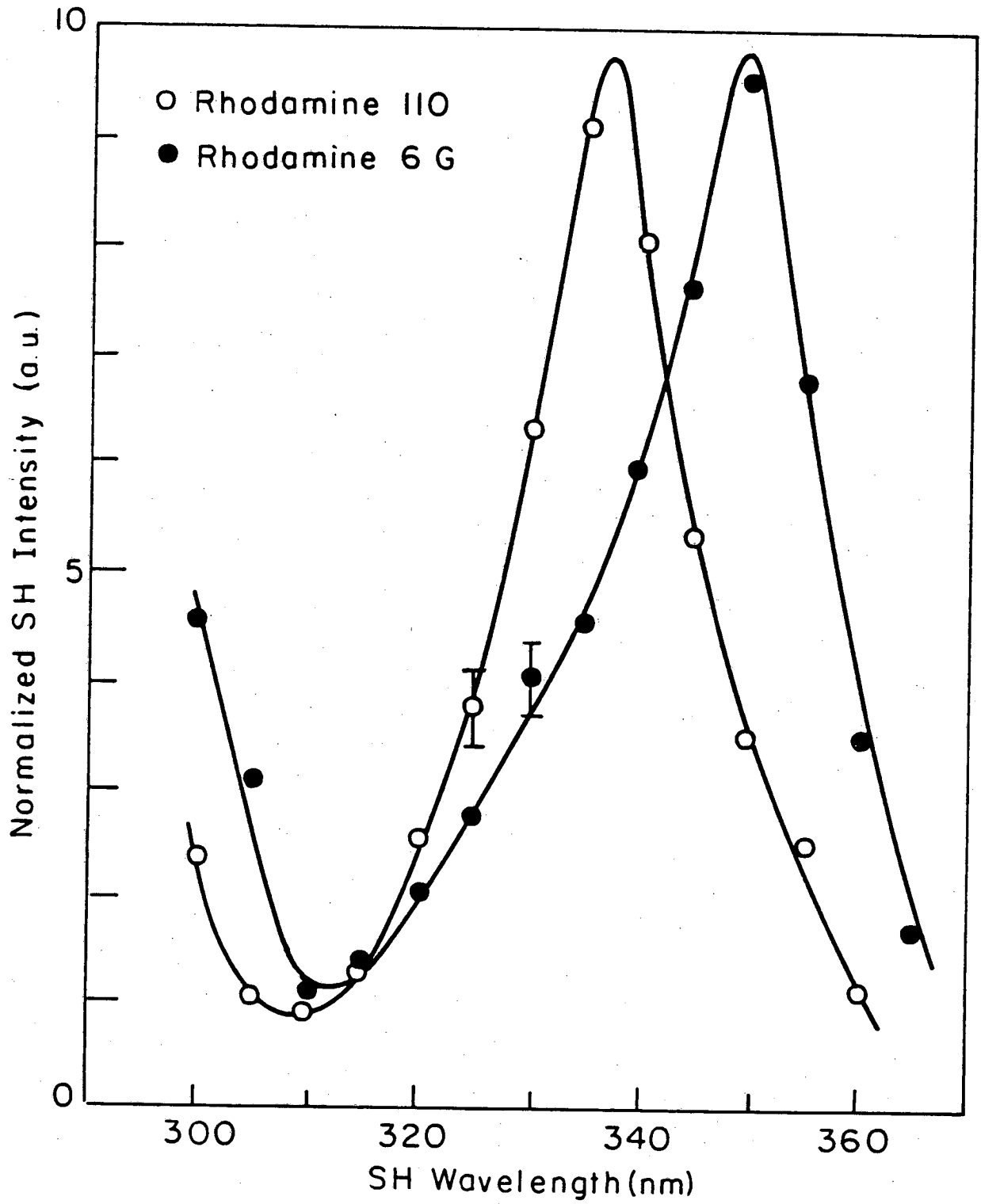
## Figure Captions

- Fig. 1: Schematic representation of experimental set-up.
- Fig. 2: Normalized SH intensity for p-polarized excitation of monolayer samples of rhodamine 110 and rhodamine 6G adsorbed on a fused silica substrate as a function of the SH wavelength in the region of the  $S_0 \rightarrow S_2$  transition.
- Fig. 3: Energy-level diagram for rhodamine 110 and rhodamine 6G with line centers for the linear absorption of the dyes dissolved in ethanol. The structures of the dyes and the molecular axes referred to in the text are shown.
- Fig. 4: SH signal for s-polarized pump radiation as the sample is rotated about its surface normal.
- Fig. 5: Diagram of the Euler angles  $\phi'$ ,  $\psi'$ , and  $\theta'$  describing the molecular axes  $x'y'z'$  in relation to the  $xyz$  coordinate system fixed to the surface.
- Fig. 6: Linear absorption of an ethanolic solution of p-nitrobenzoic acid. The molar extinction coefficient is plotted as a function of wavelength over the region of the lowest-lying strong electronic transition. The wavelengths of the second harmonics of the 683 and 532 nm pumps are noted.
- Fig. 7: Measurement of the phase of the nonlinear signal from the clean and PNBA-covered interface under s-polarized excitation at 532 nm. The total observed SH signal is shown as a function of the position of the quartz reference, indicated in degrees of phase shift induced by the dispersion of air.
- Fig. 8: Adsorption isotherm for PNBA on fused silica obtained from SHG by an s-polarized pump at 532 nm.



XBL 8210-6711

Fig. 1



XBL 8110-6773

Fig. 2



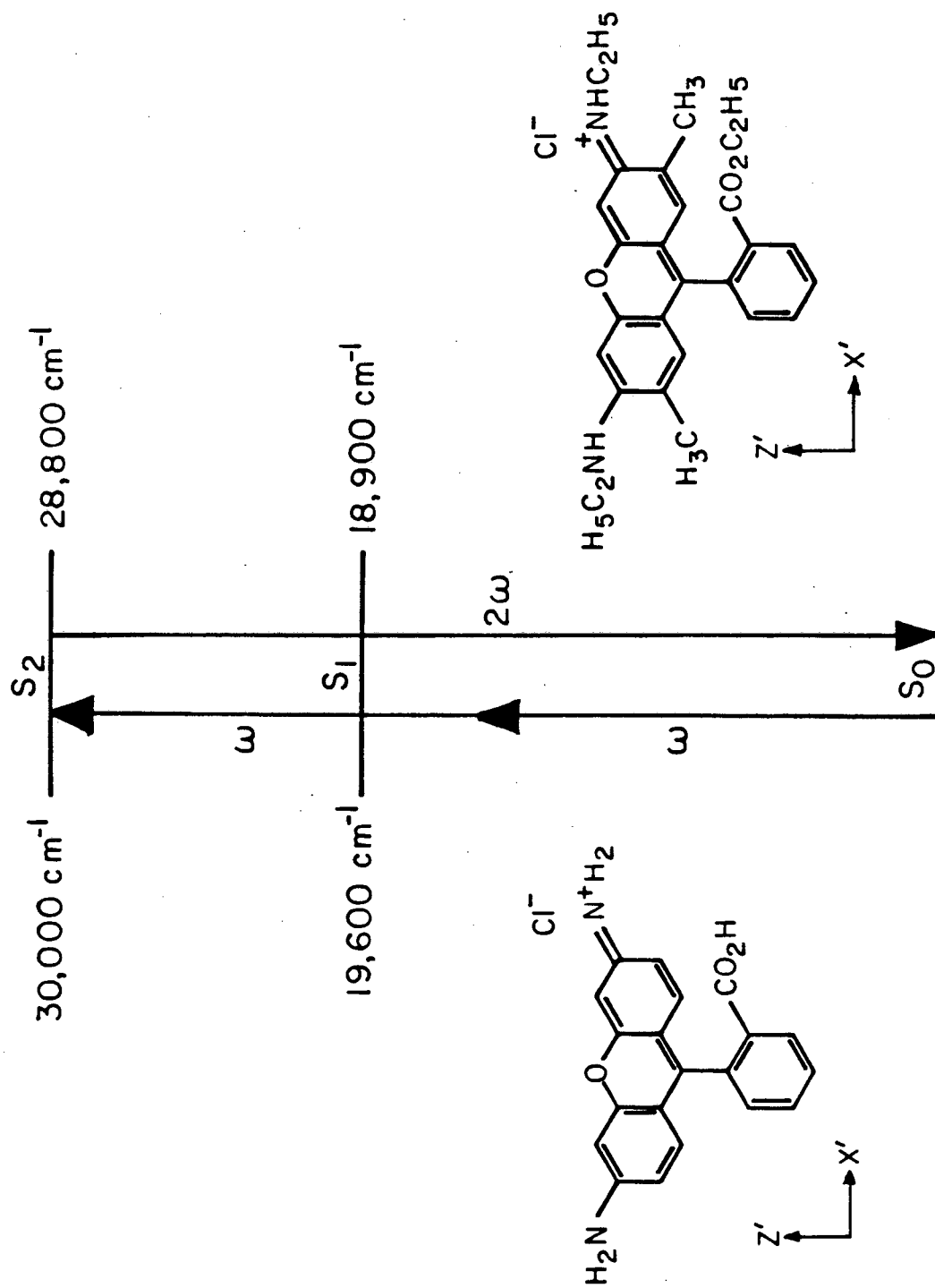


Fig. 3

XBL8111-12843

Rhodamine 110

Rhodamine 6G

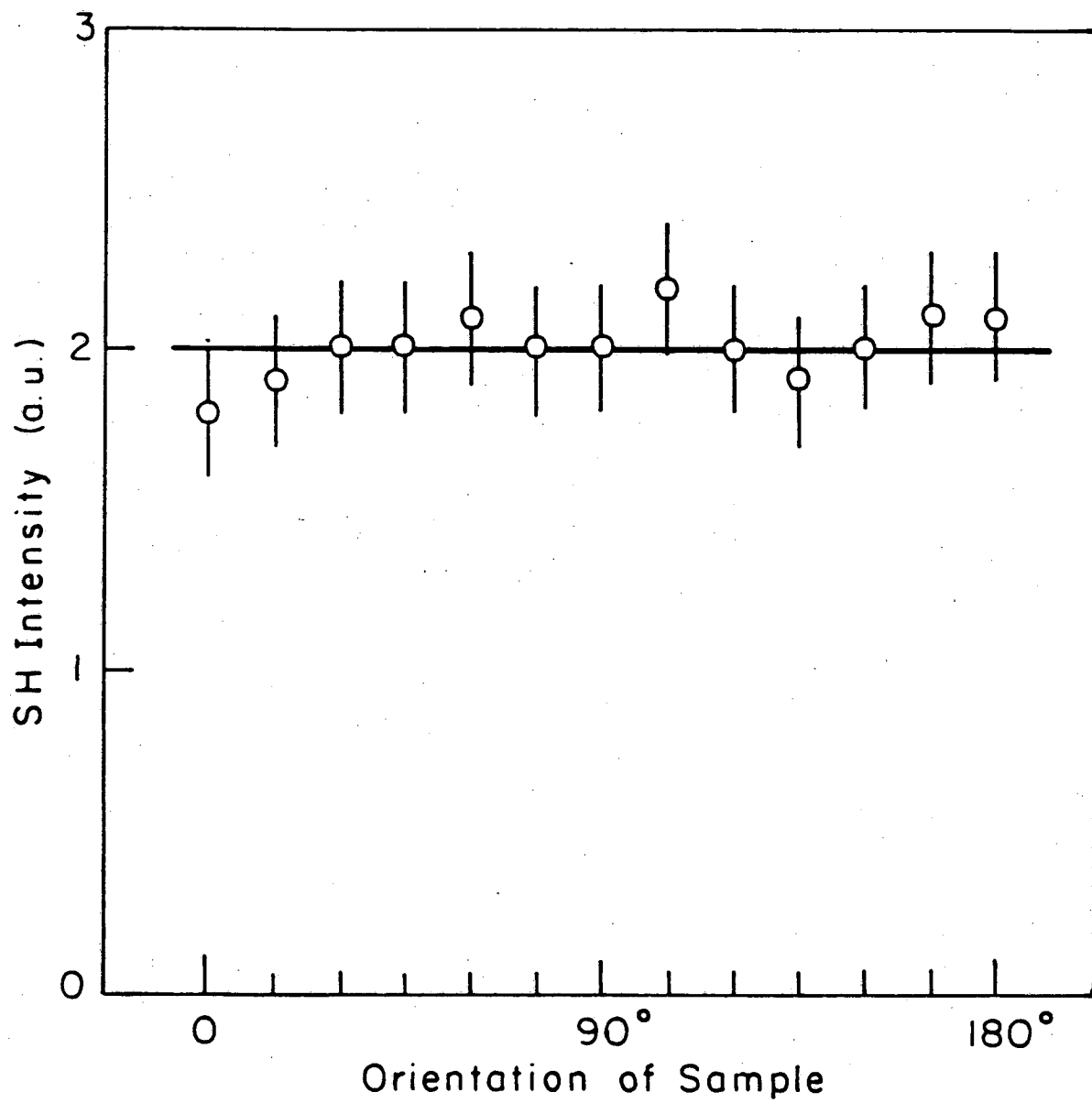
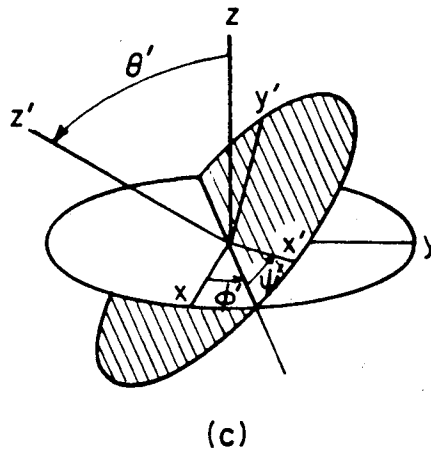
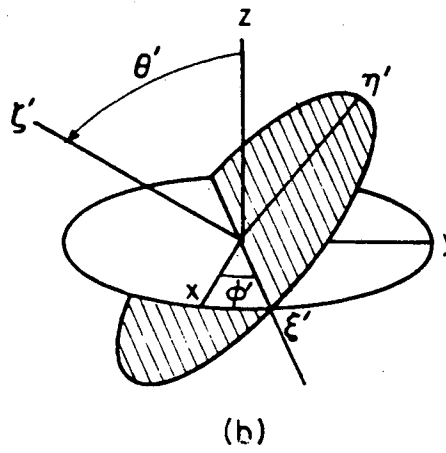
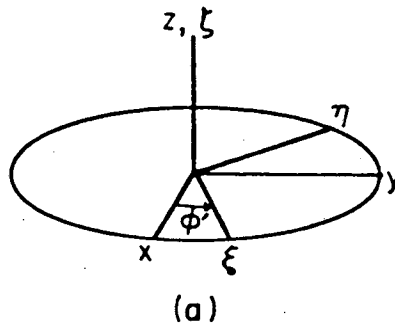


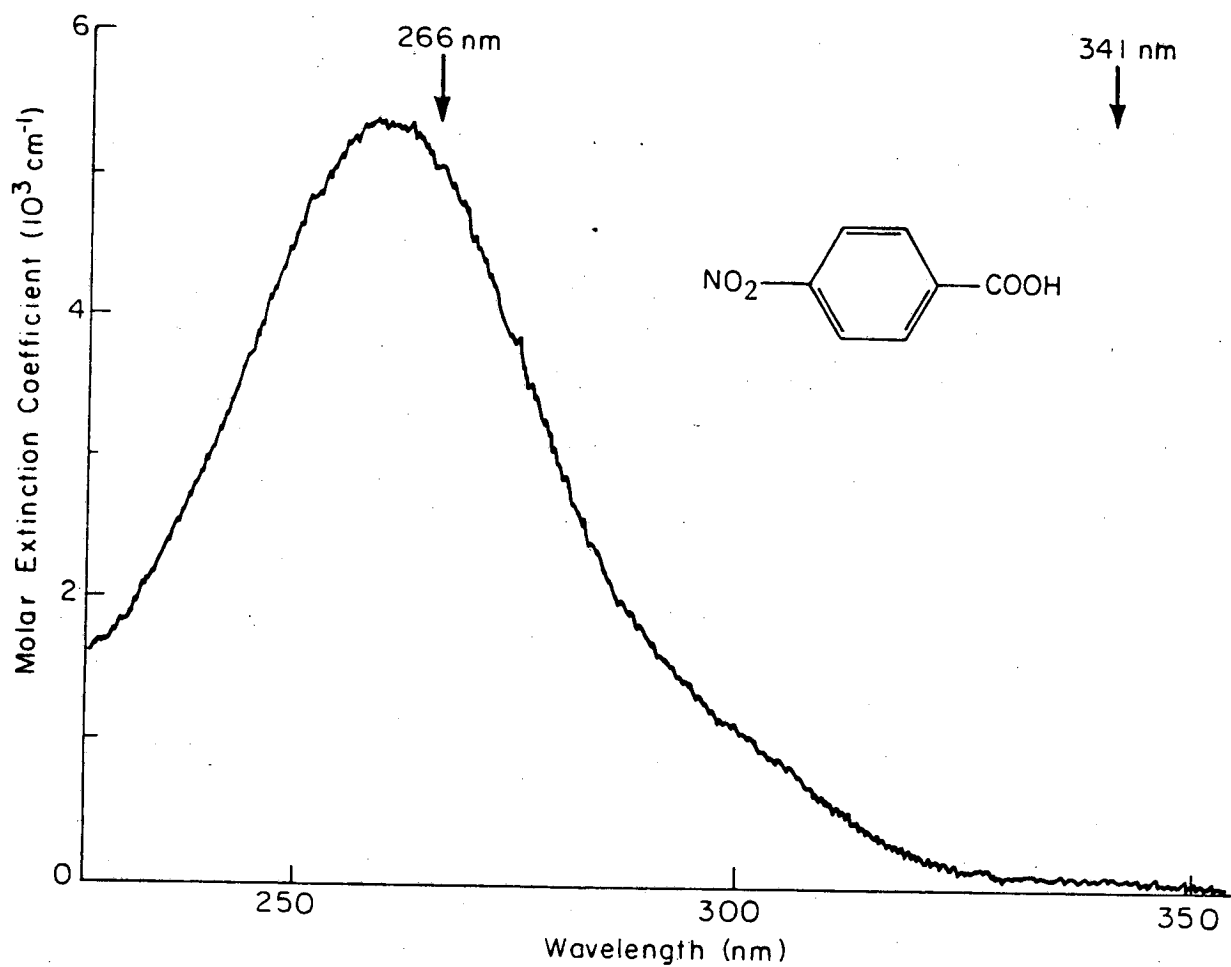
Fig. 4

XBL 8110-6770



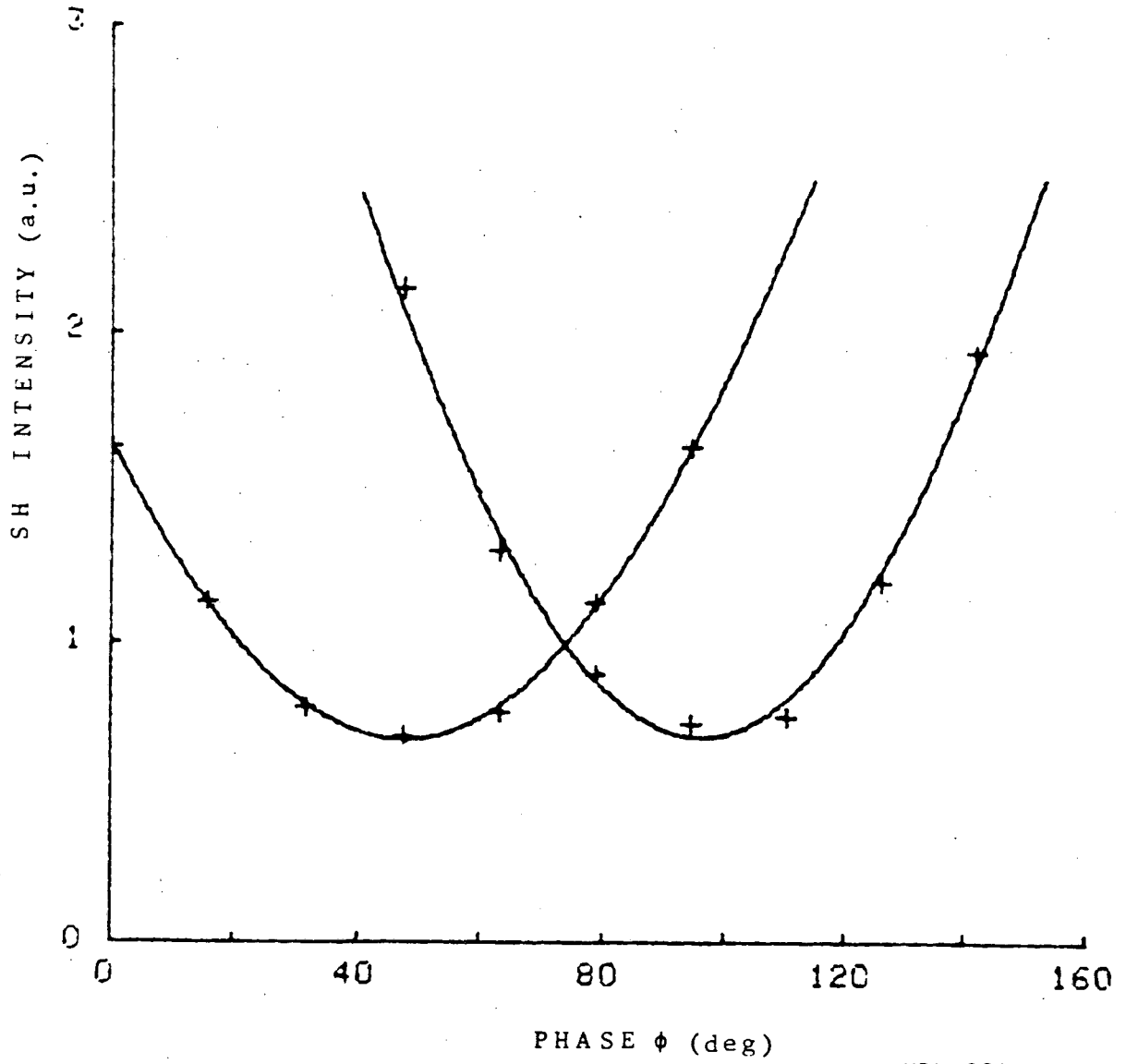
XBL 8211-6829

Fig. 5



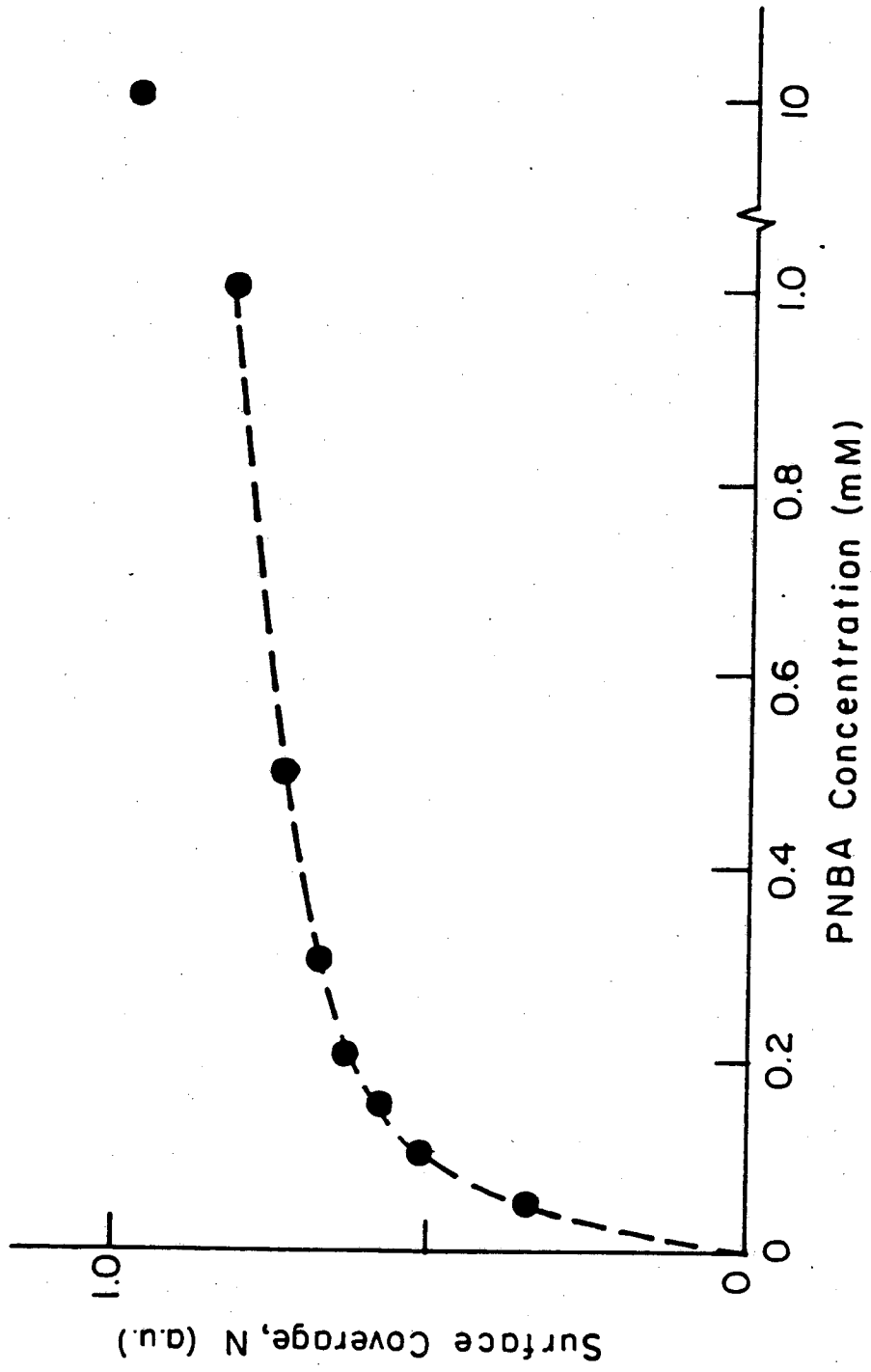
XBL 8211-6828

Fig. 6



XBL 8211-3469

Fig. 7



XBL 8211-6827

Fig. 8

## V. CONCLUSIONS AND EXTENSIONS

The work in this thesis comprises a set of experiments designed to clarify the physics of second-order nonlinear optical effects at interfaces between centrosymmetric media. The strong influence on SHG by a variety of adsorbates at monolayer coverages has been observed and can be understood in terms of the weakness of the nonlinear signals from the bulk media. In some of the cases considered, the change in the nonlinearity of the interface upon adsorption could be attributed directly to the net effect of the nonlinear polarizability of the adsorbed molecules. In strongly interacting systems, such as pyrazine adsorbed on silver, the total nonlinear response could not be accounted for as the sum of the two independent subsystems of the adsorbate layer and surrounding media. The results of such studies raise interesting questions about the basic interactions and electrostatics in the interfacial region. SHG, as a process with a high surface sensitivity, also proved useful in probing the electromagnetic resonances and enhanced local fields characteristic of a properly textured silver surface.

With our increased understanding of second-order nonlinearities at interfaces, we have also explored the potential of this intrinsically surface-specific optical probe. Since the pronounced influence of the interfacial region in this nonlinear technique stems from basic symmetry constraints, a broad range of applications may be possible. We have found the method to be useful for interfaces with both conducting and insulating substrates. While the conducting surfaces were roughened and the insulating surfaces were optically smooth, this difference does not appear to be of crucial importance. A study of adsorption in an

electrochemical cell was effected by a straightforward measurement of the reflected SH intensity. In the experiments involving optically flat surfaces we were able to garner information about the symmetry and orientation of the adsorbates from the polarization dependences of the nonlinear signals. Furthermore, we have seen that resonant SHG can serve as a probe of the surface spectroscopy, while at the same time enhancing the nonlinear signals. For more precise measurements, we have suggested a way to compensate for the nonlinearity of the bulk materials.

The principal practical limitation of such nonlinear optical techniques for the study of interfaces lies in the weakness of the signals. With current optical technology, it is not difficult to find tunable sources capable of providing a sufficient nonlinear output from any surface provided we are not constrained in the admissible intensity of the pump beams. For absorptive systems, which are susceptible to optical surface damage, this assumption may not be valid. In probing low-temperature or marginally stable interfaces, these problems would, of course, be accentuated. In addition to the key feature of their surface specificity, second-order nonlinear optical effects can provide similar, but richer information than linear optical measurements. One can determine higher moments of the orientational distribution of adsorbates, and excitation by two pulsed pump beams opens up possibilities for high-precision time-resolved work. On balance, the interpretation of nonlinear measurements is as a rule less direct than that for linear probes. Studies relying on both types of techniques may be desirable.

The current investigations present a number of immediate extensions. First in the realm of material systems, more attention might be devoted to the study of the interface between two phases of the same



substance. For example, SHG from liquid/vapor interfaces, which is known to be easily observable, might provide insight into the structure of the surface of a liquid. The range of application of our techniques could also be extended by considering the second-order nonlinear processes with excitation at two different pump frequencies, namely, sum- and difference frequency generation. Sum-frequency generation would permit the probing of vibrational transitions, with infrared and visible pump lasers giving rise to a convenient nonlinear signal in the visible region. An alternative scheme would bring the difference frequency of two visible lasers into resonance with vibrational transitions. This technique would have the advantage of alleviating potential desorption problems, although it would entail more difficulties in detecting the nonlinear signal. With two independently tunable pump beams, it should be possible to probe doubly resonant second-order nonlinearities. From a different vantage point, we might consider second-order nonlinear optical processes on well-characterized samples as a means to study electro-dynamics and local-field effects in two-dimensional systems.

## APPENDIX I: ELECTRODYNAMICS OF A POLARIZED SHEET

The nonlinear source polarization for SHG may contain a contribution localized essentially to one atomic or molecular layer at an interface. Such terms can be modeled as a sheet of polarization of vanishing thickness. While simple boundary conditions for matching the electric and magnetic fields across this layer apply, the singular nature of the current and charge density introduces certain subtleties, which have not always been treated correctly in the literature. Here the correct boundary conditions are derived and used to obtain the formula for the radiated fields.

## A. Boundary Conditions

Let us consider a source polarization  $\vec{S}_P(x,y)\delta(z)$  within a thin slab of material with a (local) dielectric constant  $\epsilon'$ . The half-spaces surrounding the sheet of polarization can have arbitrary dielectric response, and a time dependence of  $e^{-i\omega t}$  is implicitly assumed for all sources and fields. In order to apply the usual boundary conditions, imagine spreading out the sheet of polarization slightly in the  $z$ -direction, while still maintaining the same net dipole moment per unit area. For this nonsingular system, we know that the fields inside the polarized sheet will vary smoothly. The continuity of  $\vec{E}_{\parallel}$  and  $\vec{B}$  at the two separated faces of the slab then implies that  $\vec{E}_{\parallel}$  and  $\vec{B}$  must remain finite as the layer is compressed. Thus, integrating over this layer, we obtain:

$$\int_{0^-}^{0^+} \vec{E}_{\parallel}(x,y) dz = \int_{0^-}^{0^+} \vec{B}(x,y) dz = 0. \quad (1)$$

Reasoning analogously from the continuity of  $D_{\perp}$  (which includes both the induced and the source polarization), we arrive at the relation:

$$\int_{0^+}^{0^-} E_z(x,y)dz = - (4\pi/\epsilon') S_{P_z}(x,y). \quad (2)$$

Note that this expression implies that  $E_z$  becomes infinite (for  $S_{P_z} \neq 0$ ) as the slab thickness approaches zero.

With this knowledge of the electric and magnetic fields within the polarized slab, we can now apply the standard procedure for integrating Maxwell's equations over appropriately chosen surfaces and volumes to determine the relationship between the fields on opposite sides of the sheet. The magnetic fields can be handled easily. The net magnetic flux through any closed surface must vanish since  $\nabla \cdot \vec{B} = 0$ . If we then apply this result to the pillbox of Fig. 1(a) and recall that  $\vec{B}$  remains finite within the slab, we deduce directly the relation

$$\Delta B_z = B_z(z = 0^+) - B_z(z = 0^-) = 0. \quad (3)$$

Now consider the integral  $\oint \vec{B} \cdot d\vec{\ell}$  around a narrow rectangular path in the x-z plane passing through the sheet of polarization [Fig. 1(b)].

From the boundedness of  $\vec{B}$  within the slab, we obtain for such a circuit with sides of length  $l$ :

$$\Delta B_x = \oint \vec{B} \cdot d\vec{\ell}. \quad (4)$$

The right member of the equation can be evaluated by inserting the expression for  $\nabla \times \vec{B}$  from Maxwell's equations after transforming the line

integral into a surface integral. Recalling that  $\int_{0^-}^{0^+} \vec{E}_{\parallel} dz = 0$ , we then deduce that

$$\Delta B_x = -4\pi i(\omega/c) S_{P_y}, \quad (5a)$$

and, analogously,

$$\Delta B_y = +4\pi i(\omega/c) S_{P_x}. \quad (5b)$$

For the boundary conditions on the electric field, let us first integrate the Maxwell equation  $\nabla \cdot \vec{D} = 0$  over the volume of a thin pillbox bisected by the sheet of polarization [Fig. 1(a)]. Since  $\vec{E}_{\parallel}$  remains finite within the sheet, we infer by an application of the divergence theorem for a pillbox with faces of area 1 that

$$\Delta D_z = -4\pi \int \nabla \cdot [S_{P_z}(x,y)\delta(z)] d^3x. \quad (6)$$

Whence,

$$\Delta D_z = -4\pi \left( \frac{\partial S_{P_x}}{\partial x} + \frac{\partial S_{P_y}}{\partial y} \right). \quad (7)$$

Note that outside the slab the source polarization vanishes, and, hence,  $\vec{D} = \epsilon \vec{E}$  holds. For the boundary condition on  $\vec{E}_{\parallel}$ , we construct the line integral of  $\vec{E}$  about the path of Fig. 1(b). Because  $\vec{B}$  remains finite within the polarized slab, we infer from Faraday's law that  $\oint \vec{E} \cdot d\vec{\ell} = 0$ . In contrast to the situation for less singular problems, this relation does not imply the continuity of  $\vec{E}_{\parallel}$  across the boundary. In fact, re-

ferring to Eq. (2) for the contribution to the line integral from within the polarized sheet, we find a discontinuity of

$$\Delta E_x = - (4\pi/\epsilon') \frac{\partial S_P z}{\partial x} . \quad (8a)$$

Similarly,

$$\Delta E_y = - (4\pi/\epsilon') \frac{\partial S_P z}{\partial y} . \quad (8b)$$

### B. Radiated Fields

Let us now apply these boundary conditions to deduce the fields radiated by a slab of polarization oscillating at frequency  $\omega$  and exhibiting a sinusoidal spatial variation  $\vec{S}_P(x,y) = \vec{S}_P e^{ik_x x}$ . As above, the linear dielectric constant of the polarized sheet will be denoted by  $\epsilon'(\omega)$ , while the surrounding media will be characterized by constants  $\epsilon_1(\omega)$  and  $\epsilon_2(\omega)$ . Plane waves will propagate away from the layer of polarization into media 1 and 2. The direction of the outgoing waves is determined by matching the component of each wavevector parallel to the interface with that of source terms, i.e.,  $\vec{k}_{\parallel} = k_x \hat{x}$ . The magnitude of the normal component of each wavevector is then specified by the dispersion relation:

$$[\vec{k}^{(i)}]^2 = [k_x]^2 + [k_z^{(i)}]^2 = \epsilon_i(\omega)(\omega/c) . \quad (9)$$

Here and below notation  $i = 1$  or  $2$  refers to the corresponding medium. With the sign convention indicated in Fig. 1(c), we find for the amplitude of the electric field present in medium 1:

$$E_p = 14\pi k^{(1)} \frac{k_z^{(2)} S_{P_x} + (\epsilon_2/\epsilon') k_x S_{P_z}}{\epsilon_2 k_z^{(1)} + \epsilon_1 k_z^{(2)}} \quad (10a)$$

$$E_s = 14\pi k^{(1)} \frac{\epsilon_1^{-1} k^{(1)} S_{P_y}}{k_z^{(1)} + k_z^{(2)}} \quad (10b)$$

p and s signify the components of the field lying in the x-z plane and normal to this plane, respectively.

As far as the radiated fields in medium 1 are concerned, a bulk source polarization of the form  $\vec{P} = i\gamma \vec{k} e^{i\vec{k}\cdot\vec{x}}$  can be replaced by a surface layer of polarization. The equivalent polarized sheet is given by  $S_{\vec{P}}(x,y) = S_{Pe}^{i\kappa_x x + i\kappa_y y}$  with

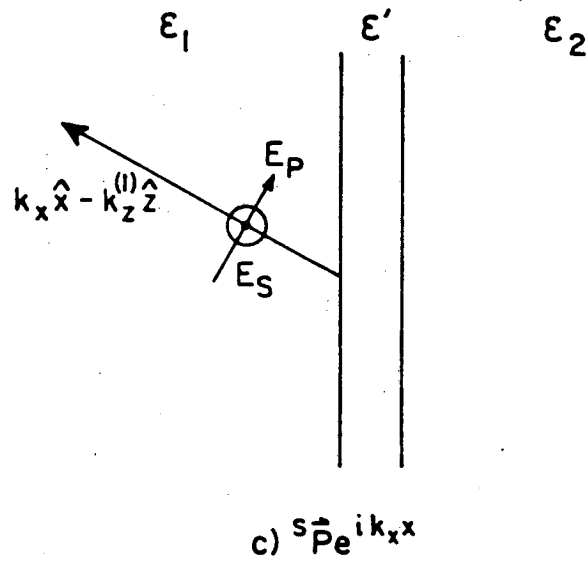
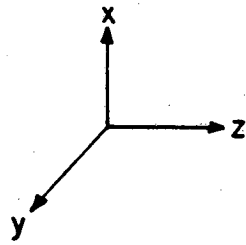
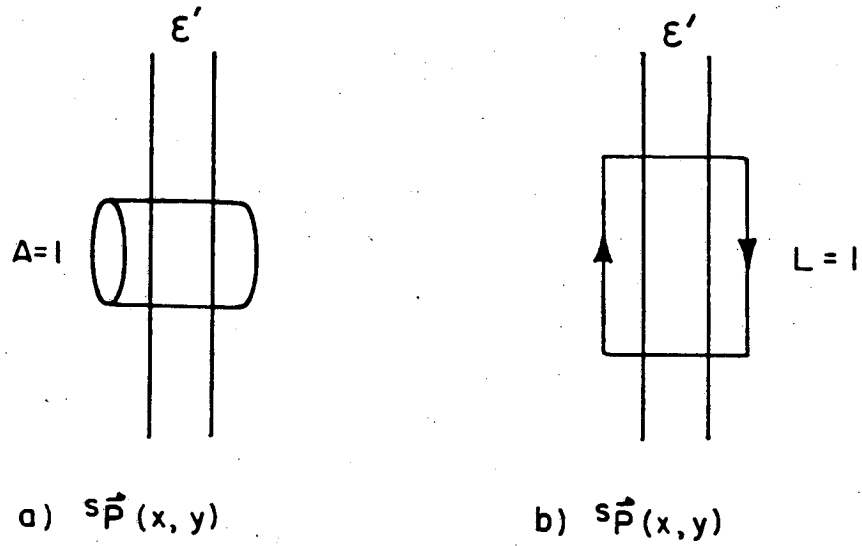
$$S_{P_x} = S_{P_y} = 0 \quad (11a)$$

$$S_{P_z} = (\epsilon'/\epsilon_1)\gamma_1 - (\epsilon'/\epsilon_2)\gamma_2 \quad (11b)$$

In this relation,  $\gamma_1$  and  $\gamma_2$  represent the strengths of the source polarization terms in media 1 and 2; it has been assumed that the spatial variation of the source polarization in the two media is identical, namely,  $\vec{\kappa}_{\parallel}^{(1)} = \vec{\kappa}_{\parallel}^{(2)} = \kappa_x \hat{x} + \kappa_y \hat{y}$ . The given result follows from a direct solution of the boundary-value problem and comparison with Eq. (10).

## Figure Caption

Fig. 1: Slab geometry. (a) and (b) show the pillbox and loop used in the derivation of the boundary conditions. The orientation of the field radiated by a sinusoidally varying polarized sheet are indicated in (c).



XBL 8211-6792

Fig. 1



## APPENDIX II: SURFACE ENHANCEMENT AND LOCAL-FIELD EFFECTS

## A. Introduction

In the SHG experiments on roughened silver surfaces described in Ch. III, an increase in SH intensity of several orders of magnitude above that for a flat silver surface was observed. Such a dramatic enhancement in the strength of optical effects on roughened silver surfaces was first observed for the Raman scattering process a few years ago.<sup>1</sup> This phenomenon of surface-enhanced Raman scattering (SERS) has attracted and continues to attract considerable attention.<sup>2</sup> An enhancement in the effective Raman cross-section by as much as a factor of  $10^6$  has been manifested by a wide range of molecular adsorbates on surfaces of various metals at solid/liquid,<sup>1,2</sup> solid/vacuum,<sup>3-6</sup> and even at solid/solid<sup>7,8</sup> interfaces. As researchers have recognized the common features of surface roughness<sup>3-17</sup> and small optical absorption of substrates exhibiting prominent enhancements, it has come to be accepted that the macroscopic electrodynamics of the surface plays a significant role in SERS: the presence of the roughened metal can produce a local field strength at the interface which greatly exceeds that of the applied field.<sup>19-25</sup> This same mechanism of local-field enhancement can account for our observations of surface enhancement of the SHG process.<sup>26-29</sup> In fact, significant surface enhancements have been reported for hyper-Raman scattering<sup>30</sup> and for one- and two-photon absorption and luminescence<sup>31-33</sup> as well.

The theory of local-field enhancements has been developed by a number of authors to treat the specific optical process under consideration.<sup>14-32</sup> Here we elaborate the theory in a more general fashion. By

extending the notion of a correction to the molecular polarizability from microscopic local fields to macroscopic ones, we can describe directly the amplification of the incident and radiated fields induced by the presence of the surface. The surface enhancement of any particular process can then be readily calculated. We present this formalism and some model calculations in Sec. B. Experimental determinations of the surface enhancement for SHG and Raman scattering with an electrochemically reformed silver surface are reported in Sec. C. The previously developed model of the roughened surface as small hemispheroids protruding from a conducting plane serves to predict the macroscopic local-field enhancements for the two optical processes and comparison is made with experiment. In the closing section, we draw some conclusions and, as a further example of the local-field theory, calculate the surface enhancement for coherent anti-Stokes Raman scattering by an adsorbate.

## B. Theory of Local-Field Enhancement

### 1. General Formalism

The mechanisms leading to the enhancement of various optical processes at surfaces can be broken down into two broad categories: those involving a change in the nature of the adsorbate by means of a direct interaction with the substrate and those involving only a modification of the local electric and magnetic fields caused by the presence of the substrate. The former group of chemical effects has been invoked in various explanations of SERS<sup>2</sup> and notably in understanding SERS by normally Raman-inactive modes of adsorbates<sup>34,35</sup> and SHG by centrosymmetric adsorbates.<sup>29</sup> The electromagnetic effects of local-field enhancements are now believed to be the main contribution to SERS of Raman-active

modes of adsorbates, and they are the only contributor to the enhancement of SHG from bare metal surfaces.<sup>26,27</sup> We shall present here a general formalism for treating this local-field enhancement.

Let us first consider an isolated molecule in space surrounded by radiation fields  $E(\omega_1)$ ,  $E(\omega_2)$ , ...,  $E(\omega_n)$  with angular frequencies  $\omega_1$ ,  $\omega_2$ , ...,  $\omega_n$ . An  $n$ -th order nonlinear dipole  $p^{(n)}(\omega = \omega_1 + \omega_2 + \dots + \omega_n)$  can then be induced in the molecule through the nonlinear polarizability  $\alpha^{(n)}(\omega = \omega_1 + \omega_2 + \dots + \omega_n)$ :

$$\vec{p}^{(n)}(\omega) = \alpha^{(n)} : \vec{E}(\omega_1) \dots \vec{E}(\omega_n). \quad (1)$$

If, however, the molecule is sitting near a surface and if it is also surrounded by other molecules, it will experience a local field  $\vec{E}_{loc}(\omega_i)$  different from the incoming field  $\vec{E}(\omega_i)$  of Eq. (1). In this case, the induced dipole will be given by

$$\vec{p}^{(n)}(\omega) = \alpha^{(n)} : \vec{E}_{loc}(\omega_1) \dots \vec{E}_{loc}(\omega_n). \quad (2)$$

These local fields can be attributed to two distinct effects: the change in the microscopic fields and the change in the average of macroscopic fields. The local variation in the microscopic fields arising from the induced dipole-dipole interaction is the usual Lorentz correction discussed in the literature.<sup>36</sup> In a homogeneous liquid, for example, it yields the familiar Lorentz-Lorentz relation of  $\ell(\omega_i) = [\epsilon(\omega_i) + 2]/3$ . The microscopic local-field correction for molecules adsorbed on a surface has recently been discussed by Bagchi et al.<sup>37</sup> and also in connection with image-dipole models for SERS.<sup>2,38-40</sup> The change in the macro-

scopic field at the surface compared with the applied field is just what we expect from reflection and refraction of the incident field. We can call this a macroscopic local field, which, in principle, is obtained from the solution of the wave equation with the appropriate boundary conditions at the surface. The macroscopic local-field correction factor  $\vec{L}(\omega)$  is then the ratio of the macroscopic local field to the incident field. As we shall see, this factor can be substantial for metals with resonant structures on the surface. Taking account of both the macroscopic and microscopic corrections, we can write for the local electric field

$$\vec{E}_{loc}(\omega_i) = \vec{\ell}(\omega_i) \vec{L}(\omega_i) : \vec{E}(\omega_i). \quad (3)$$

The nonlinear dipole  $\vec{p}^{(n)}(\omega)$  induced by the local fields now radiates. Since the neighboring dipoles also respond to this excitation at frequency  $\omega$ , the radiation appears as if  $\vec{p}^{(n)}(\omega)$  were enhanced by an additional local-field correction factor  $\vec{\ell}(\omega)$  (Ref. 41). Similarly, through the interaction of  $\vec{p}^{(n)}(\omega)$  with the surface, the macroscopic field at  $\omega$  is also enhanced by a further factor of  $\vec{L}(\omega)$ . Thus, the radiated field from the nonlinear dipole at the surface in an ambient dielectric with constant  $\epsilon$  is<sup>42</sup>

$$\vec{E}_{out}^{dip}(\omega) = e^{ikr} (k^2/\epsilon r) [(\hat{n} \times \vec{p}_{eff}(\omega)) \times \hat{n}], \quad (4a)$$

where

$$\vec{p}_{eff}^{(n)}(\omega) = \vec{\alpha}^{(n)} : \vec{\ell}(\omega) \vec{L}(\omega) \vec{\ell}(\omega_1) \vec{L}(\omega_1) \dots \vec{\ell}(\omega_n) \vec{L}(\omega_n) \vec{E}(\omega_1) \dots \vec{E}(\omega_n). \quad (4b)$$

Here  $k = \sqrt{\epsilon} (\omega/c)$  and  $\hat{n}$  is the direction of propagation of the outgoing field. The total radiated field from a collection of dipoles is, of course, obtained by summing over the individual contributions. If the process is coherent, as for SHG, the resulting radiated field can be expressed as

$$\vec{E}_{\text{out}}(\omega) = \int_S d^2x_s N(\vec{x}_s) e^{ikr} (k^2/\epsilon r) [(\hat{n} \times \vec{p}_{\text{eff}}^{(2)}(\omega, \vec{x}_s)) \times \hat{n}], \quad (5a)$$

with the integration extended over the surface covered by the nonlinear dipoles of density  $N(\vec{x}_s)$ . The total output power in a solid angle from the radiating dipoles is found in the usual manner from

$$\mathcal{P}_{\text{coh}}(\omega) = (c\sqrt{\epsilon}/2\pi) \int_{\Omega} r^2 d\Omega |\vec{E}_{\text{out}}(\omega)|^2. \quad (5b)$$

If, however, the nonlinear dipoles radiate incoherently, as in the case of Raman scattering, then the output is given by

$$\mathcal{P}_{\text{inc}}(\omega) = (c\sqrt{\epsilon}/2\pi) \int_{\Omega} r^2 d\Omega \int_S d^2x_s N(\vec{x}_s) |\vec{E}_{\text{out}}^{\text{dip}}(\omega, \vec{x}_s)|^2. \quad (6)$$

Thus, for a specified surface with known local-field correction factors, we should be able to calculate the output power. The local-field enhancement is defined as the ratio of the radiated power in the case of interest to that of a reference. For example, for SERS, the reference can be chosen as the molecules in the gas or liquid phase; for surface-enhanced SHG by a metal, the bare, flat surface can be taken as standard. As discussed below, the electrolytically roughened silver surface used in the current set of experiments exhibited an enhancement

of the Raman scattering of  $\sim 10^6$  for visible radiation, with a corresponding second-harmonic enhancement of  $\sim 10^2$  for a visible pump and  $\sim 10^4$  for near-infrared excitation.

In the following, we shall discuss a few special geometries of the metal-dielectric interface. Microscopic local-field corrections will not be taken into account. As a rough estimate of this effect, we can apply the theory of Bagchi et al.<sup>37</sup> for isotropic molecules in a square lattice of spacing 5 Å located 2.5 Å above a conducting plane. In this case, with a linear polarizability of  $\alpha^{(1)} = 10 \text{ Å}^3$ , the microscopic local-field correction factors for electric fields parallel and perpendicular to the surface are found to be  $\ell_{\parallel} = 1.6$  and  $\ell_{\perp} = 0.6$ . On the other hand, according to the Lorenz-Lorentz formula for a homogeneous liquid, the local-field correction factor for water ( $\epsilon = 1.77$ ) is  $\ell = 1.3$ .

## 2. Special Cases

We consider here three different geometries for the interface between a metal substrate, characterized by a (local) dielectric constant  $\epsilon_m(\omega)$ , and the ambient dielectric medium with a real, dispersionless dielectric constant  $\epsilon$ . A thin intermediate region of dielectric constant  $\epsilon'(\omega)$  is included to describe an adsorbed molecular layer. We first treat the simple planar boundary. Then, as an approximation of a roughened surface, we analyze the case of a small metal hemisphere lying on an infinite plane, which, for simplicity, is taken to be a perfect conductor. These hemispherical protrusions exhibit resonant response to an applied field when  $\text{Re}(\epsilon_m(\omega) + 2\epsilon) = 0$ . Finally, as a more refined model of an electrochemically roughened metal surface, we extend

our calculations to the case of a hemispheroidal boss on a conducting plane.

(a) Planar Interface

In this instance, the Fresnel coefficients for the reflection and refraction waves at a planar boundary give the relation between the incoming macroscopic fields and the macroscopic fields present at the interface, i.e., the macroscopic local-field factors. The local-field tensor  $\vec{\vec{L}}$  becomes diagonal when expressed with respect to the surface normal and directions parallel to the surface lying in and normal to the plane of incidence of the wave:

$$L_{\perp} = (\epsilon/\epsilon') 2\sqrt{\epsilon_m} \cos\theta / (\sqrt{\epsilon_m} \cos\theta + \sqrt{\epsilon} \cos\theta_m)$$

$$L_{\parallel}^P = 2\sqrt{\epsilon} \cos\theta_m / (\sqrt{\epsilon_m} \cos\theta + \sqrt{\epsilon} \cos\theta_m)$$

$$L_{\parallel}^S = 2\sqrt{\epsilon} \cos\theta / (\sqrt{\epsilon} \cos\theta + \sqrt{\epsilon_m} \cos\theta_m). \quad (7)$$

The superscripts p and s refer, respectively, to the components parallel and perpendicular to the plane of incidence.  $\theta$  denotes the angle of incidence of the light and  $\theta_m$  is the angle of refraction. The expressions above apply to the fields in the dielectric layer of constant  $\epsilon'$  just above the metal, but they are also valid for the fields just inside the metal if  $\epsilon' = \epsilon_m$ .

With the given local-field factor  $\vec{\vec{L}}$ , we can calculate the radiated power by means of Eq. (4), in conjunction with Eq. (5) for a coherent process and with Eq. (6) for an incoherent one. For Raman scattering by a layer of aligned molecules with surface density N and Raman polar-

izability  $\overset{\leftrightarrow}{\alpha}^R$ , we find a total power

$$\mathcal{P}_R(\omega_s) = (c\sqrt{\epsilon}/2\pi)(\omega_s/c)^4 N \mathcal{A} \int_{\Omega} d\Omega |\hat{n} \times \overset{\leftrightarrow}{\alpha}^R : \overset{\leftrightarrow}{L}(\omega_s) \overset{\leftrightarrow}{L}(\omega) \vec{E}(\omega)|^2. \quad (8)$$

Here the pump beam of frequency  $\omega$  illuminates an area  $\mathcal{A}$  of the interface;  $\hat{n}$  gives the direction of the outgoing radiation at the Stokes-shifted frequency  $\omega_s$ ; and the tensor  $\overset{\leftrightarrow}{L}$  is specified by Eq. (7). In the limit of  $|\epsilon_m| \gg \epsilon = \epsilon'$ , the macroscopic local-field factors simplify to  $L_{\parallel}^P = L_{\perp}^S = 0$  and  $L_{\perp} = 2$ . In this case, the total radiated power under pumping by a p-polarized beam with field strength  $E(\omega)$  incident at angle  $\theta$  is

$$\mathcal{P}_R(\omega_s) = (32c\sqrt{\epsilon}/3)(\omega_s/c)^4 N \mathcal{A} |\alpha_{\perp\perp}^R|^2 E^2(\omega) \sin^2\theta. \quad (9)$$

With excitation at grazing incidence, this radiated power exceeds by a factor of 8 that emitted by an equal number of isolated isotropically polarizable Raman scatterers in the bulk dielectric medium.

In the case of SHG, we are dealing with a coherent process, and, consequently, a uniform adsorbed layer with a nonlinear response will give rise to a collimated beam of second-harmonic radiation in the reflected direction. Equations (5) and (6) yield for the power in this beam at the harmonic frequency

$$\mathcal{P}_{SH}(2\omega) = (2\pi c/\sqrt{\epsilon})(2\omega/c)^2 N^2 \mathcal{A} |\hat{n} \times \overset{\leftrightarrow}{\alpha}^{(2)} : \overset{\leftrightarrow}{L}(2\omega) \overset{\leftrightarrow}{L}(\omega) \overset{\leftrightarrow}{L}(\omega) \vec{E}(\omega) \vec{E}(\omega)|^2 \sec\theta. \quad (10)$$

$\overset{\leftrightarrow}{\alpha}^{(2)}$  represents the second-order nonlinear polarizability of the adsorbed species, of which an area  $\mathcal{A} (\gg k^{-2})$  is exposed to radiation at



the fundamental frequency  $\omega$ . The same result (with the proper  $L_{\perp}$ ) applies for SHG by the surface layer of the metal itself. More specifically, let us write for later use the expression in the case of p-polarized excitation of a nonlinearity having only a significant  $\parallel\perp\parallel$ -component:

$$\mathcal{P}_{\text{SH}}(2\omega) = (8\pi c/\sqrt{\epsilon})(2\omega/c)^2 N^2 \mathcal{A} |\alpha_{\parallel\perp\parallel}^{(2)} L_{\parallel}^{\text{p}}(2\omega) L_{\perp}(\omega) L_{\parallel}^{\text{p}}(\omega)|^2 E^4(\omega) \cos^3 \theta \sin^2 \theta. \quad (11)$$

(b) Hemispherical Boss

In the interest of simplicity, the base plane on which the metal hemisphere rests is presumed to be perfectly conducting; the hemisphere itself is taken to be much smaller than the wavelength of light so that retardation effects need not be considered, and the macroscopic local fields can be determined by electrostatics. The presence of the conducting plane causes the component of the incident electric field normal to the surface to be doubled, while cancelling the tangential part. Then by solving the elementary boundary-value problem, we can find the relation between the macroscopic local field at a point on the hemisphere and the field present above the conducting plane, namely,

$$L_{\perp} = (\epsilon_{\text{m}}/\epsilon') 3\epsilon/(\epsilon_{\text{m}} + 2\epsilon)$$

$$L_{\parallel} = 3\epsilon/(\epsilon_{\text{m}} + 2\epsilon). \quad (12)$$

The tensor  $\vec{\vec{L}}$  assumes this diagonal form for any given point on the hemisphere when resolved into components perpendicular to and lying in the local tangent plane at the hemispherical surface. With the aid of these

local-field factors, we can now immediately compute the scattered power for the Raman and SHG processes.

The total power of Raman scattered light is specified by Eqs. (4) and (6). For a p-polarized pump beam of frequency  $\omega$  making an angle  $\theta$  with the conducting plane, an adsorbate-covered hemispherical boss of radius  $a$  produces a total output at the Raman-shifted frequency  $\omega_s$  of

$$\mathcal{P}_R(\omega_s) = (64\pi c\sqrt{\epsilon}/15)(\omega_s/c)^4 N a^2 |\alpha_{\perp\perp}^R L_{\perp}(\omega_s) L_{\perp}(\omega)|^2 E^2(\omega) \sin^2 \theta. \quad (13)$$

This expression was derived assuming that only the  $\perp\perp$ -component of the Raman polarizability was important, as is the case if  $|L_{\perp}| = |\epsilon_m/\epsilon'| |L_{\parallel}| \gg |L_{\parallel}|$ , i.e., whenever  $|\epsilon_m/\epsilon'| \gg 1$ . Comparing this result to that for Raman scattering from isolated, isotropically polarizable molecules in the bulk dielectric medium, we obtain the surface enhancement attributable to macroscopic local-field effects. Forming the ratio of total scattered power per molecule, we deduce for this quantity

$$\eta_R = (8/5) |L_{\perp}(\omega_s) L_{\perp}(\omega)|^2 \sin^2 \theta. \quad (14)$$

Second-harmonic radiation emitted by the adsorbate-covered hemisphere is angularly diffuse. If only the  $\parallel\parallel$ -component of the quadratic polarizability is appreciable, the total second-harmonic power radiated in all directions for excitation by a p-polarized pump is given by Eqs. (4) and (5) as

$$\mathcal{P}_{SH}(2\omega) = (128\pi^2 c\sqrt{\epsilon}/3)(2\omega/c)^4 N^2 a^4 |\alpha_{\parallel\parallel}^{(2)} L_{\parallel}(2\omega) L_{\perp}(\omega) L_{\parallel}(\omega)|^2 E^4(\omega) \sin^4 \theta. \quad (15)$$

Dividing this radiated power by that for an equal area of an equivalent flat surface also excited by a p-polarized pump incident at angle  $\theta$ , we arrive at the surface-enhancement factor

$$\eta_{SH} = (32/3)(ka)^2 \sin^2 \theta \sec^3 \theta \frac{|L_{\parallel}(2\omega)L_{\perp}(\omega)L_{\parallel}(\omega)|^2_{\text{sphere}}}{|L_{\parallel}^P(2\omega)L_{\perp}(\omega)L_{\parallel}^P(\omega)|^2_{\text{plane}}}. \quad (16)$$

Here  $k = \sqrt{\epsilon} \omega/c$  and the local-field factors in the numerator and denominator are those of Eq. (12) and of Eq. (7), respectively.

Neglecting the geometric factors resulting from averaging and normalization, we find from Eq. (14) that the surface enhancement for Raman scattering has the form  $\eta_R \sim |L(\omega_s)L(\omega)|^2$ ; for SHG, Eq. (16) implies that  $\eta_{SH} \sim (ka)^2 |L(2\omega)L^2(\omega)|^2$ . The former expression is just what we expect for incoherent scattering by the Raman process, the enhancement being proportional to the cross-section  $\sigma_R$ , which, in turn, varies as  $|\alpha^R|^2$ . In the case of SHG, we must compare the signal from the hemispherical surface to that from a plane. In the plane, an area  $\sim \lambda^2 = (2\pi/k)^2$  can radiate in phase for this coherent process, but for the hemisphere of radius  $a$ , only its surface area  $2\pi a^2$  can do so. For this reason, in addition to the obvious terms for a signal proportional to  $|\alpha^{(2)}(2\omega = \omega + \omega)|^2$ , an extra factor of  $(ka)^2$  is introduced into the formula for  $\eta_{SH}$ . Now inspection of Eq. (12) reveals that when the denominator  $\epsilon_m + 2\epsilon$  approaches zero, we obtain a large value for the local-field factors, and, hence, for the Raman and second-harmonic surface enhancements as well. Since this denominator must always have a positive imaginary part, the optimal enhancement should occur for  $\text{Re}(\epsilon_m + 2\epsilon) = 0$ , corresponding to the excitation of a local surface plasmon. Noble metals, which typically have dielectric constants with

negative real and small imaginary parts for infrared and visible light, can exhibit considerable surface enhancements through this mechanism.<sup>43</sup>

(c) Hemispheroidal Boss

Here we take up the generalization of the previous geometry to the case of a hemispheroidal boss with a semimajor axis of length  $a$  normal to the conducting plane and a semiminor axis of length  $b$ . The assumption of  $ka \ll 1$  is maintained to allow an electrostatic analysis. The macroscopic local fields on the protrusion are related to the field above the conducting plane in the same way as the fields on a full spheroid are related to a constant applied field directed along the principal axis. The solution to this classic problem<sup>44</sup> can be expressed succinctly with respect to the local surface normal and tangential directions. The resulting local-field factors are

$$L_{\perp} = (\epsilon_m / \epsilon') \epsilon / [\epsilon + (\epsilon_m - \epsilon)A]$$

$$L_{\parallel} = \epsilon / [\epsilon + (\epsilon_m - \epsilon)A]. \quad (17)$$

The depolarization factor  $A$  takes on the value of  $1/3$  for a sphere and approaches  $0$  for a very slender prolate spheroid.<sup>45</sup> For the geometry under consideration, the local surface plasmon resonance now occurs for  $\text{Re}[\epsilon + (\epsilon_m - \epsilon)A] = 0$ . The local-field enhancement can be particularly large for highly elongated spheroids, since in the limit of  $A \rightarrow 0$ ,  $\text{Im}[\epsilon + (\epsilon_m - \epsilon)A]$  will decrease, causing the resonant enhancement to grow. This behavior can be termed a lightning-rod effect.<sup>23,24</sup>

From Eqs. (4) and (6), we can obtain the Raman-scattered power from the hemispheroidal protrusion covered uniformly by an adsorbate.

For a p-polarized pump,

$$\mathcal{P}_R(\omega_s) = (64\pi c\sqrt{\epsilon}/3)(\omega_s/c)^4 (b/a)^4 N a^2 |\alpha_{\perp\perp}^R L_{\perp}(\omega_s) L_{\perp}(\omega)|^2 E^2(\omega) \sin^2\theta. \quad (18)$$

As before, this formula is valid if only the  $\perp\perp$ -component of the Raman polarizability is important, which holds whenever  $|\epsilon_m/\epsilon'| \gg 1$ . This and subsequent expressions are also simplified by taking the protrusion to be highly elongated ( $a/b \gg 1$ ). The macroscopic local-field enhancement in the radiated power is given by the ratio of Eq. (18) to the power radiated by an equal number  $N_{\mathcal{A}} \approx N\pi^2 ab/2$  of isolated molecules in the bulk dielectric medium:

$$\eta_R = (32/\pi)(b/a)^3 |L_{\perp}(\omega_s) L_{\perp}(\omega)|^2 \sin^2\theta. \quad (19)$$

For SHG by a uniform layer of an adsorbate with only a  $\perp\perp\perp$ -component of the nonlinearity, we deduce, according to Eqs. (4) and (5), a radiated harmonic power under p-polarized excitation of

$$\mathcal{P}_{SH}(2\omega) = (2^9 \pi^2 c\sqrt{\epsilon}/3)(2\omega/c)^4 (b/a)^4 N^2 a^4 |\alpha_{\parallel\perp\parallel}^{(2)} L_{\parallel}(2\omega) L_{\perp}(\omega) L_{\parallel}(\omega)|^2 E^4(\omega) \sin^4\theta. \quad (20)$$

The enhancement with respect to SHG by an equal area of the adsorbate-covered metal plane is then found to be

$$\eta_{SH} = (2^9/3\pi)(b/a)^3 (ka)^2 \sin^2\theta \sec^3\theta \frac{|L_{\parallel}(2\omega) L_{\perp}(\omega) L_{\parallel}(\omega)|^2_{\text{spheroid}}}{|L_{\parallel}^P(2\omega) L_{\perp}(\omega) L_{\parallel}^P(\omega)|^2_{\text{plane}}}. \quad (21)$$

The local-field factors in this expression are those of Eqs. (7) and (17); the factor of  $(ka)^2$  arises from the coherence of the SHG process,

as discussed above for the hemispherical boss. In Sec. C, we shall see how the large observed enhancements of SHG and Raman scattering are predicted by resonant excitation of these features.

### C. Surface Enhancement of Raman Scattering and SHG

As a test of our theory of local-field enhancements, we have determined experimentally the enhancements shown by Raman and second-harmonic signals from an electrochemically reformed silver surface. The Raman enhancement was found for the  $1005\text{ cm}^{-1}$  vibrational mode of adsorbed pyridine. Pyridine was chosen as the adsorbate for the relative simplicity of its surface chemistry and for the ease in making reference measurements from the neat liquid. The enhancement of the second-harmonic radiation was that of the silver substrate itself. Both measurements were performed on the same sample under the same excitation. Pulses of 10 ns duration at a wavelength of  $0.683\text{ }\mu\text{m}$  were provided by stimulated Raman scattering in hydrogen gas of a frequency-doubled Q-switched Nd:YAG laser. In other respects, the experimental arrangement was similar to that described in Ch. III.

The silver electrode was prepared by several of the conventional electrochemical cyclings in a pure 0.1M KCl electrolyte prior to the addition of pyridine (0.05M) and a final cycling. The p-polarized pump beam fell on the silver sample in solution at a  $45^\circ$  angle. The Raman signal from the adsorbed pyridine as recorded for  $V_{\text{Ag-SCE}}$  between  $-0.4\text{V}$  and  $-0.7\text{V}$ . In this range of potentials, it is believed that approximately a monolayer of pyridine is adsorbed to the silver surface.<sup>1</sup> A comparison of the signal from the adsorbed species (assumed to have a

surface density of  $4 \times 10^{14} \text{ cm}^{-2}$ ) can be made with that from an equal number of molecules in solution. This was accomplished by measuring the Raman scattering from neat pyridine with the same apparatus. After carefully accounting for the collection volume, we found the surface enhancement to be  $\eta_R \sim 1.4 \times 10^6$ . The surface-enhanced second-harmonic signal was also measured under the same conditions. Because of the large intrinsic nonlinearity of silver at  $0.683 \mu\text{m}$ , the adsorbed pyridine did not materially change the SHG. The surface enhancement for SHG was determined by comparing the integrated strength of the angularly diffused signal from the roughened surface with that of the highly collimated harmonic output from a smooth, freshly evaporated silver film in pure water. The observed enhancement was  $\eta_{SH} \sim 1 \times 10^2$ ; an enhancement of  $\sim 1 \times 10^4$  was found for  $1.06 \mu\text{m}$  excitation.<sup>26</sup> In the latter case, no pyridine was introduced into the electrochemical cell in order to avoid any possible increase in SHG associated with this adsorbate.

We shall now see how well these experimental results for the Raman and second-harmonic enhancements can be explained by our theory of macroscopic local fields. From electron micrographs, such as Fig. 1, the roughened silver surface is known to feature separated protrusions tens of nanometers in size. We model this topography by a perfectly conducting plane covered randomly with metal hemispheroids of varying dimensions. Interactions between the different protrusions are neglected, so the formulas of our previous analysis can be applied immediately. Since the spheroids have various aspect ratios, some of them should be appropriately shaped to exhibit a localized surface plasmon resonance and the accompanying large local-field enhancement at the frequency of the pump

laser. Scattering from these structures should be dominant. (Structures resonant at the harmonic frequency for SHG should make a much smaller contribution; those resonant at the Stokes-shifted frequency for Raman scattering should give a comparable contribution, which will be neglected.) The dimensions of the resonant protrusions can be determined in the following manner. According to Eq. (17), the criterion for resonance is  $\text{Re}[\epsilon + (\epsilon_m - \epsilon)A] = 0$ . For our case,  $\epsilon_m(\omega) = -22 + i0.4$ ,  $\epsilon_m(2\omega) = -1.3 + i0.3$  (Ref. 47), and  $\epsilon = \epsilon_{\text{water}} = 1.77$ , whence a resonance occurs at  $\omega$  for  $A = 0.074$ . This value of the depolarization factor corresponds to a hemispheroid with aspect ratio  $a/b = 4.1$  (Ref. 45). In the simple theory of Sec. II, the overall scale of the resonant structure does not affect the local-field enhancement. In reality, radiation damping limits the enhancement for large structures, and surface scattering increases the imaginary part of the dielectric constant for small structures, again limiting the enhancement. According to the work of Wokaun et al.,<sup>15</sup> the optimal enhancement for excitation of wavelength  $\lambda$  occurs for spheroids of volume  $V \sim 10^{-4} \lambda^3$ . With an effective radiating volume of  $V = \frac{4\pi}{3} ab^2$ , we then infer a semimajor axis  $a \sim 50$  nm and a semiminor axis  $b \sim 12$  nm.

For a hemispheroid of the specified dimensions, we can evaluate the macroscopic local-field factors of Eq. (17). Setting  $\epsilon' = \epsilon$  here and below and including radiation damping and small size effects as in Ref. (15), we obtain  $L(\omega) = 120$ ,  $L(\omega) = 9$ , and  $L(2\omega) = 1.0$ . In order to estimate  $\eta_{\text{SH}}$ , we must also evaluate the local-field correction factors for the flat silver surface. From Eq. (7), we find with the specified dielectric constants,  $L(\omega) = 1.9$ ,  $L^P(\omega) = 0.7$ , and  $L^P(2\omega) = 1.7$ . The surface enhancement is now given directly by Eq. (21) as  $\eta_{\text{SH}} = 1.0 \times$



$10^5$ , which exceeds the experimental value by a factor of 1000. We must consider, however, that on our electrolytically roughened silver surface, the protrusions of tens of nanometers in size are separated from one another by hundreds of nanometers and that only a fraction of these structures will be in resonance. Hence, the theoretically predicted enhancement should be reduced by the fractional surface area  $f$  of the structures resonant at the laser frequency. In order to make theory agree with experiment,  $f$  should be 0.10%, which seems reasonable.

In this analysis, we have supposed that the SH response of the silver can be described by a surface nonlinear susceptibility  $\chi^{\leftrightarrow(2)} = N\alpha^{\leftrightarrow(2)}$  [as defined by Eq. (5) of Ch. II] with only a significant  $\parallel\perp\parallel$ -component. As we have discussed in Ch. II C, experimental results indicate that  $S_{\perp\perp\perp}^{(2)} - S_{\perp\parallel\parallel}^{(2)}$  is negligible and that the so-called magnetic-dipole term (which is, strictly speaking, proportional to  $\gamma - S_{\perp\parallel\parallel}^{(2)}$ ) accounts for a comparable or smaller contribution to the SHG by p-polarized excitation than does the  $S_{\parallel\perp\parallel}^{(2)}$  surface term. Thus, for the flat surface, we introduce an error of less than a factor of 4 by overlooking the magnetic-dipole source polarization. In the limiting case where the significant resonant structures of the roughened surface are much smaller than a wavelength of the optical field, the surface terms will predominate over the bulk ones. Given the variation of experimental results and the crudeness of our model of the roughened surface, we shall not attempt to correct for the magnetic-dipole contribution further, but shall simply neglect it.<sup>46</sup>

In the case of Raman scattering, we shall apply the theory in which only the  $\perp\perp$ -component of the Raman polarizability is important. This approximation is justified since  $L_{\perp}(\omega)/L_{\parallel}(\omega) \sim 10$  at the laser

frequency. The anticipated Raman enhancement, according to Eq. (19), is then  $\eta_R = 6 \times 10^6$ . The local-field correction factors entering this calculation are  $L_{\perp}(\omega) = 120$  and  $L_{\perp}(\omega_s) = 75$ ; the broadness of the strong resonant enhancement can be attributed to the radiation damping and small size effects. Taking the value of  $f$  deduced above, we predict an average enhancement of  $f\eta_R = 6 \times 10^3$ . This is  $\sim 200$  times less than the observed enhancement. The discrepancy can be understood as an additional enhancement arising from microscopic local-field effects and chemical interactions of the adsorbed pyridine with the silver surface, which have not been included in our theory. The enhancement not treated by our theory is essentially that exhibited Raman scattering of adsorbates on a planar surface, in which case the macroscopic local-field corrections are comparatively minor. Udagawa et al.<sup>9</sup> have recently made measurements of the surface enhancement in ultrahigh vacuum for the same  $1005 \text{ cm}^{-1}$  mode of pyridine adsorbed on a (100) face of crystalline silver which was considered smooth. They report a value of  $\lesssim 440$  for the enhancement with excitation at  $0.514 \text{ }\mu\text{m}$ .

Consider now the surface enhancement for excitation at  $1.06 \text{ }\mu\text{m}$ . The relevant dielectric constants<sup>47</sup> are  $\epsilon_m(\omega) = -58 + i0.6$  and  $\epsilon_m(2\omega) = -12 + i0.4$ . The local surface plasmon resonance at  $\omega$  occurs for  $A = 0.030$ , i.e., for a structure with  $a/b = 7.7$ . Following the same procedure as above, we deduce  $a \sim 120 \text{ nm}$  and  $b \sim 16 \text{ nm}$  for those hemispheroids with maximal local-field correction factors of  $L_{\perp}(\omega) = 190$ ,  $L_{\parallel}(\omega) = 6$ , and  $L_{\parallel}(2\omega) = 1.4$ . We observe that here the local-field factor  $L_{\perp}$  assumes a larger value than was previously deduced for excitation at  $0.683 \text{ }\mu\text{m}$ . This behavior can be understood in terms of the lightning rod effect manifested by the very slender structures that are resonant

at the longer wavelength. The local-field factors for the flat surface are  $L_{\perp}(\omega) = 1.9$ ,  $L_{\parallel}^P(\omega) = 0.5$ ,  $L_{\parallel}^P(2\omega) = 0.8$ , yielding  $\eta_{SH} = 7 \times 10^5$ . The predicted enhancement agrees with the experimental value of  $1 \times 10^4$  for a fractional surface coverage of resonant structures of  $f \sim 1.4\%$ . [Because of the highly elongated shape of the resonant structures,  $f = 1.4\%$  corresponds to a coverage of just 0.11% for the projected (as opposed to the surface) area of the hemispheroids.] With this value for  $f$ , we can predict the average local-field enhancement of SERS. For a  $1005 \text{ cm}^{-1}$  Stokes shift,  $L_{\perp}(\omega_s) = 120$  and Eq. (19) gives an average enhancement of  $f\eta_R = 8 \times 10^4$  for a p-polarized pump incident at  $45^\circ$ . Microscopic local-field and chemical effects may further augment the signal. Using the same 200-fold increase deduced for the  $0.683 \mu\text{m}$  excitation, we expect to observe a total enhancement of  $\sim 2 \times 10^7$  in the Raman scattering of  $1.06 \mu\text{m}$  light by pyridine adsorbed on our electrolytically reformed silver surface. To our knowledge, SERS has not been observed with a  $1.06 \mu\text{m}$  pump laser. Our estimate, however, indicates that the expected enhancement is actually somewhat larger than for excitation in the visible.

#### D. Concluding Remarks

Our treatment of the macroscopic local-field enhancement relied on a simple model of noninteracting hemispheroids on a conducting plane. Nonetheless, this model was capable of predicting the local-field correction factors, the surface enhancement, the dispersion of this enhancement, and the fractional coverage of resonant structures, all of which were fairly reasonable from the experimental point of view.

The general formalism of local-field enhancement presented in this

paper should be applicable not only to local fields near a surface, metal or dielectric, but also to effects in the bulk. We shall not pursue this matter further, other than to give one additional example for a surface. Relying on our previously developed model for an electrochemically treated silver sample, we can calculate the emitted power for any surface optical process immediately. Here we consider the case of coherent anti-Stokes Raman scattering (CARS). We shall assume that only the  $\alpha_{\perp\perp\perp\perp}^{(3)}$  term of the relevant third-order nonlinear polarizability for the adsorbed molecular layer is significant. The radiated power at the anti-Stokes frequency  $\omega_a = 2\omega - \omega_s$  from a highly elongated hemispherical boss is found in the manner of Sec. II to be

$$\begin{aligned} \mathcal{P}_{\text{CARS}}(\omega_a) = & (2^{11} \pi^2 c \sqrt{\epsilon} / 3) (\omega_a / c)^4 (b/a)^8 N^2 a^4 \times \\ & \times |\alpha_{\perp\perp\perp\perp}^{(3)} L_{\perp}(\omega_a) L_{\perp}(\omega_s) L_{\perp}^2(\omega)|_{\text{spheroid}}^2 E^2(\omega_s) E^4(\omega) \sin^6 \theta. \end{aligned} \quad (24)$$

It is assumed here that both pump beams (frequencies  $\omega_s$  and  $\omega$ ) are p-polarized and incident on the base plane at angle  $\theta$ . The local-field factors are those of Eq. (17) and all other symbols are as defined before. By way of comparison, the CARS output from an area  $\mathcal{A}$  of a smooth surface is

$$\begin{aligned} \mathcal{P}_{\text{CARS}}(\omega_a) = & (2\pi c / \sqrt{\epsilon}) (\omega_a / c)^2 N^2 \mathcal{A} |\alpha_{\perp\perp\perp\perp}^{(3)} L_{\perp}(\omega_a) L_{\perp}(\omega_s) L_{\perp}^2(\omega)|_{\text{plane}}^2 \times \\ & \times \sec \theta \sin^8 \theta. \end{aligned} \quad (25)$$

Here the local-field factors are given by Eq. (7). Forming the ratio of

these expressions, we then deduce the surface enhancement of the CARS process:

$$\eta_{\text{CARS}} = (2^{11}/3\pi)(b/a)^7 (k_a a)^2 \cos\theta \csc^2\theta \frac{|L_{\perp}(\omega_a)L_{\perp}(\omega_s)L_{\perp}^2(\omega)|^2_{\text{spheroid}}}{|L_{\perp}(\omega_a)L_{\perp}(\omega_s)L_{\perp}^2(\omega)|^2_{\text{plane}}}, \quad (26)$$

with  $k_a = \sqrt{\epsilon} \omega_a / c$ . For a rough surface with only a fractional surface area  $f$  occupied by structures with large enhancements, the predicted enhancement must be reduced proportionately.

Let us now make a numerical estimate of the surface enhancement of CARS in the case of a silver sample with pump excitation ( $\omega$ ) at 0.683  $\mu\text{m}$ . For the optimally sized hemispheroid of  $a \sim 50$  nm and  $b \sim 12$  nm,  $L_{\perp}(\omega) = 120$  and  $L_{\perp}(\omega_a) \approx L_{\perp}(\omega_s) = 75$  for a  $1005 \text{ cm}^{-1}$  Stokes shift. Then taking  $f = 0.10\%$  and  $\theta = 45^\circ$ , as before, we deduce  $f\eta_{\text{CARS}} = 3 \times 10^8$ . Earlier we estimated that the microscopic local-field effects and the molecule-silver interaction enhanced the Raman cross-section  $\sigma_R$  of the  $1005 \text{ cm}^{-1}$  mode of pyridine by a further factor of  $\sim 200$ . Since  $\alpha^{(3)} \propto \sigma_R$ , the total surface enhancement for CARS should be on the order of  $(200)^2 f\eta_{\text{CARS}} = 1.2 \times 10^{13}$ . The absolute signal strength is predicted by Eq. (23) increased by the average enhancement of  $(200)^2 f\eta_{\text{CARS}}$ . For a  $1 \text{ cm}^2$  silver surface covered by an adsorbate with a nonlinearity  $^{48} \text{Na}_{\text{IIII}}^{(3)} = 10^{-20}$  esu, we expect emission of  $3 \times 10^5$  photons/pulse for pump excitation of 10 ns duration and a modest fluence of  $1 \text{ mJ/cm}^2$ . This anti-Stokes output should be readily observable if not overwhelmed by a background from the silver substrate. In this connection, it should be noted that although surface CARS is obviously a coherent process, the presence of the roughened surface needed for a macroscopic local-field enhancement may cause the anti-Stokes output to be angularly diffused

and potentially difficult to distinguish from incoherently scattered light.

## References

1. M. Fleischmann, P. J. Hendra, and A. J. McQuillan, Chem. Phys. Lett. 26, 163 (1974); D. L. Jeanmaire and R. P. van Duyne, J. Electroanal. Chem. 84, 1 (1977); M. G. Albrecht and J. A. Creighton, J. Am. Chem. Soc. 99, 5215 (1977).
2. For a recent review see Surface Enhanced Raman Scattering, edited by R. K. Chang and T. E. Furtak (Plenum, New York, 1982).
3. R. R. Smardzewski, R. J. Colton, and J. S. Murday, Chem. Phys. Lett. 68, 53 (1979).
4. P. N. Sanda, J. M. Warlaumont, J. E. Demuth, J. C. Tsang, K. Christmann, and J. A. Bradley, Phys. Rev. Lett. 45, 1519 (1980).
5. H. Seki and M. R. Philpott, J. Chem. Phys. 73, 5376 (1980).
6. T. H. Wood, D. A. Zwemer, C. V. Shank, and J. E. Rowe, Chem. Phys. Lett. 82, 5 (1981) and references therein.
7. J. C. Tsang, J. R. Kirtley, and T. N. Theis, Solid State Commun. 35, 667 (1980) and references therein.
8. C. A. Murray, D. L. Allara, and M. Rhinewine, Phys. Rev. Lett. 46, 57 (1981)
9. M. Udagawa, C.-C. Chou, J. C. Hemminger, and S. Ushioda, Phys. Rev. B 23, 6843 (1981).
10. D. A. Weitz, T. J. Gramila, A. Z. Genack, and J. I. Gersten, Phys. Rev. Lett. 45, 355 (1980).
11. A. Girlando, M. R. Philpott, D. Heitmann, J. D. Swalen, and R. Santo, J. Chem. Phys. 72, 5187 (1980).
12. C. Y. Chen, E. Burstein, and S. Lundquist, Solid State Commun. 32, 63 (1979); C. Y. Chen, I. Davoli, G. Ritchie, and E. Burstein, Surf. Sci. 101, 363 (1980).

13. J. G. Bergman, D. S. Chemla, P. F. Liao, A. M. Glass, A. Pinczuk, R. M. Hart, and D. H. Olson, *Opt. Lett.* 6, 33 (1981).
14. P. F. Liao, J. G. Bergman, D. S. Chemla, A. Wokaun, J. Melngailis, A. M. Hawryluk, and N. P. Economou, *Chem. Phys. Lett.* 82, 355 (1981).
15. A. Wokaun, J. P. Gordon, and P. F. Liao, *Phys. Rev. Lett.* 48, 957 (1982).
16. H. Wetzel and H. Gerischer, *Chem. Phys. Lett.* 76, 460 (1980).
17. K. U. von Raben, R. K. Chang, and B. L. Laube, *Chem. Phys. Lett.* 79, 465 (1981) and references therein.
18. T. E. Furtak and J. Kester, *Phys. Rev. Lett.* 45, 1652 (1980).
19. M. Koskovits, *J. Chem. Phys.* 69, 4159 (1978).
20. C. Y. Chen and E. Burstein, *Phys. Rev. Lett.* 45, 1287 (1980).
21. M. Kerker, D.-S. Wang, and H. Chew, *Appl Opt.* 19, 4159 (1980); D.-S. Wang and M. Kerker, *Phys. Rev. B* 24, 1777 (1981).
22. S. L. McCall, P. M. Platzman, and P. A. Wolff, *Phys. Lett.* 77A, 381 (1980).
23. J. Gersten and A. Nitzan, *J. Chem. Phys.* 73, 3023 (1980); 75, 1139 (1981).
24. P. F. Liao and A. Wokaun, *J. Chem. Phys.* 76, 751 (1982)
25. B. J. Messinger, K. U. von Raben, R. K. Chang, and P. W. Barber, *Phys. Rev. B* 24, 649 (1981) and references therein.
26. C. K. Chen, A. R. B. de Castro, and Y. R. Shen, *Phys. Rev. Lett.* 46, 145 (1981).
27. A. Wokaun, J. G. Bergman, J. P. Heritage, A. M. Glass, P. F. Liao, and D. H. Olson, *Phys. Rev. B* 24, 849 (1981).
28. C. K. Chen, T. F. Heinz, D. Ricard, and Y. R. Shen, *Phys. Rev.*

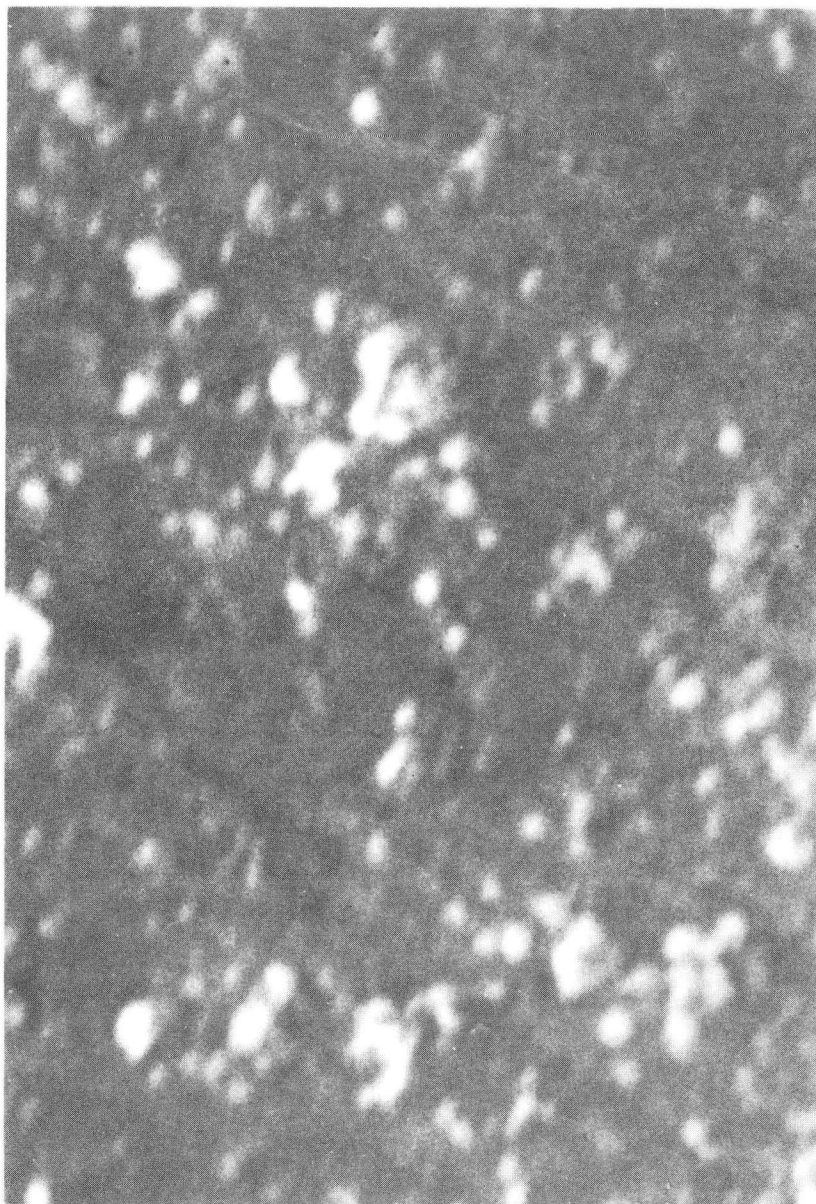


- Lett. 46, 1010 (1981) [Chap. III, Sec. A of this thesis].
29. T. F. Heinz, C. K. Chen, D. Ricard, and Y. R. Shen, Chem. Phys. Lett. 83, 180 (1981) [Chap. III, Sec. C of this thesis].
30. D. V. Murphy, K. U. von Raben, R. K. Chang, and P. B. Dorain, Chem. Phys. Lett. 85, 43 (1982).
31. A. Harstein, J. R. Kirtley, and J. C. Tsang, Phys. Rev. Lett. 45, 201 (1980).
32. A. M. Glass, A. Wokaun, J. P. Heritage, J. G. Bergman, P. F. Liao, and D. H. Olson, Phys. Rev. B 24, 4906 (1981).
33. G. Ritchie and E. Burstein, Phys. Rev. B 24, 4843 (1981) and references therein.
34. G. R. Erdheim, R. L. Birke, and J. R. Lombardi, Chem. Phys. Lett. 69, 495 (1980).
35. R. Dornhaus, M. B. Long, R. E. Benner, and R. K. Chang, Surf. Sci. 93, 240 (1980).
36. C. J. F. Böttcher and P. Bordewijk, Theory of Electric Polarization, 2nd ed. (Elsevier, Amsterdam, 1978).
37. A. Bagchi, R. G. Barrera, and B. B. Dasgupta, Phys. Rev. Lett. 44, 1475 (1980); A. Bagchi, R. G. Barrera, and R. Fuchs, Phys. Rev. B 25, 7080 (1982).
38. F. W. King, R. P. van Duyne, and G. C. Schatz, J. Chem. Phys. 69, 4472 (1978); G. C. Schatz and R. P. van Duyne, Surf. Sci. 101, 425 (1980).
39. S. Efrima and H. Metiu, J. Chem. Phys. 70, 1602 (1979); 70, 2297 (1979); T. Maniv and H. Metiu, J. Chem. Phys. 72, 1996 (1980).
40. W. H. Weber and G. W. Ford, Phys. Rev. Lett. 44, 1774 (1980); G. W. Ford and W. H. Weber, Surf. Sci. 109, 451 (1981).

41. J. A. Armstrong, N. Bloembergen, J. Ducuing, and P. S. Pershan, *Phys. Rev.* 127, 1918 (1962).
42. While we have not established the general conditions for the validity of this expression, we have verified its correctness in each case considered in this paper by a full solution of Maxwell's equations for the incoming and outgoing fields.
43. For a calculation of SHG by a small sphere with a free electron response, see G. S. Agarwal and S. S. Jha, *Solid State Commun.* 41, 499 (1982).
44. J. A. Stratton, *Electromagnetic Theory* (McGraw-Hill, New York, 1941), Ch.3.
45. Generally,  $A = [1 - \xi Q_1'(\xi)/Q_1(\xi)]^{-1}$  with Legendre function of the second kind  $Q_1(\xi) = (\xi/2) \ln[(\xi + 1)/(\xi - 1)] - 1$  and  $\xi = [1 - (b/a)^2]^{1/2}$ . For this formula and explicit tabulations of A, see J. A. Osborn, *Phys. Rev.* 67, 351 (1945) and E. C. Stoner, *Philos. Mag.* 36, 803 (1945). We can rewrite  $L_{||} = (\epsilon'/\epsilon_m)L = [Q_1(\xi) - \xi Q_1'(\xi)]/[\epsilon_m/\epsilon Q_1(\xi) - \xi Q_1'(\xi)]$ .
46. We shall use the same approximation in the case of 1.06  $\mu\text{m}$  excitation, for which the given term and the bulk polarization are believed to contribute approximately equally to SHG from a planar silver surface under p-polarized excitation. In our discussion, we shall neglect any possible variation in the coefficient  $\beta$  as a function of the surface structure on an atomic scale. Both of these points are treated in J. Rudnick and E. A. Stern, *Phys. Rev. B* 4, 4274 (1971).
47. P. B. Johnson and R. W. Christy, *Phys. Rev. B* 6, 4370 (1972).
48. P. D. Maker and R. W. Terhune, *Phys. Rev.* 137, A801 (1965).

Figure Caption

Fig. 1: Surface structure of a silver sample prepared by the specified cycling procedure as viewed with a scanning electron microscope.



↑ | 1 μm | ↓

XBB 820-9056

Fig. 1

## APPENDIX III: COUNTING STATISTICS

For signal strengths so weak as to generate less than one primary photoelectron in the photomultiplier tube, it is convenient to analyze the output with counting rather than analog techniques. Here we present a useful relation between the average number of primary photoelectrons emitted per pulse  $\lambda$  and the easily measurable fraction of pulses  $\Lambda$  for which at least one primary photoelectron is produced. The intensity of the optical signal is, of course, proportional to  $\lambda$ , while the quantity  $\Lambda$  is convenient from the experimental standpoint, since it can be found simply by counting all pulses from the photomultiplier above the noise level.

The emission of photoelectrons obeys Poisson statistics. Thus, denoting by  $P(n)$  the probability of the generation of  $n$  photoelectrons, we can write

$$P(n) = (\lambda^n/n!)e^{-\lambda}. \quad (1)$$

Whence,

$$\Lambda = \sum_{n=1}^{\infty} P(n) = 1 - P(0) = 1 - e^{-\lambda}, \quad (2)$$

or

$$\lambda = -\ln(1 - \Lambda) = \Lambda + \frac{1}{2}\Lambda^2 + \dots \quad (3)$$

Although this relation is valid for all values of  $\lambda$ , it is only an ef-

fective way to collect data for  $\lambda \ll 1$ . In this case, it allows one to correct for the few multiple-photoelectron events without the need to discriminate between differing pulse heights. This scheme also has the advantage of not requiring an accurate determination of the baseline to obtain accurate results, in contrast to the method of integrating the pulse height distribution.

This report was done with support from the Department of Energy. Any conclusions or opinions expressed in this report represent solely those of the author(s) and not necessarily those of The Regents of the University of California, the Lawrence Berkeley Laboratory or the Department of Energy.

Reference to a company or product name does not imply approval or recommendation of the product by the University of California or the U.S. Department of Energy to the exclusion of others that may be suitable.

TECHNICAL INFORMATION DEPARTMENT  
LAWRENCE BERKELEY LABORATORY  
UNIVERSITY OF CALIFORNIA  
BERKELEY, CALIFORNIA 94720